UNIVERSIDADE DE SÃO PAULO
ESCOLA DE ENGENHARIA DE SÃO CARLOS
DEPARTAMENTO DE ENGENHARIA ELÉTRICA E DE COMPUTAÇÃO
PROGRAMA DE PÓS-GRADUAÇÃO EM ENGENHARIA ELÉTRICA

Single and Multirate FFH-OCDMA Networks Based on PSK Modulation Formats

Anderson Leonardo Sanches

São Carlos
2015

ANDERSON LEONARDO SANCHES

Single and Multirate FFH-OCDMA Networks Based on PSK Modulation Formats

Thesis submitted to the São Carlos School of Engineering as part of the requirements to obtain the degree of Doctor of Science, Electrical Engineering Program, with emphasis on Telecommunications.

Concentration Area: Telecommunications.

Supervisor: Prof. Dr. Ben-Hur Viana Borges.

São Carlos
2015

Sanches, Anderson Leonardo

D722s Redes FFH-OCDMA Convencionais e de Múltiplas Taxas Baseadas em Formatos de Modulação PSK = Single and Multirate FFH-OCDMA Networks Based on PSK Modulation Formats / Anderson Leonardo Sanches; orientador Ben-Hur Viana Borges. São Carlos, 2015.

Tese (Doutorado) - Programa de Pós-Graduação em Engenharia Elétrica e Área de Concentração em Telecomunicações -- Escola de Engenharia de São Carlos da Universidade de São Paulo, 2015.

1. Acesso Múltiplo por Divisão de Código Óptico. 2. Formatos de Modulação. 3. Redes Coerentes 4. Codificação com Saltos Rápidos em Frequencia. 5. Interferência de Acesso Múltiplo 6. Múltiplas Taxas de Transmissão. 7. Taxa de Erro de Bit. I. Título

FOLHA DE JULGAMENTO

Candidato: Engenheiro **ANDERSON LEONARDO SANCHES.**

Título da tese: "Redes FFH-OCDMA convencionais e de múltiplas taxas de transmissão baseadas em formatos de modulação PSK".

Data da defesa: 13/05/2015

Comissão Julgadora:	**Resultado:**
Prof. Associado **Ben-Hur Viana Borges (Orientador)** (Escola de Engenharia de São Carlos/EESC)	Aprovado
Profa. Dra. **Mônica de Lacerda Rocha** (Escola de Engenharia de São Carlos/EESC)	Aprovado
Prof. Dr. **Aldario Chrestani Bordonalli** (Universidade Estadual de Campinas/UNICAMP)	Aprovado
Prof. Dr. **Fabio Renan Durand** (Universidade Tecnológica Federal do Paraná/UTFPR)	Aprovado
Prof. Dr. **Luiz Henrique Bonani do Nascimento** (Universidade Federal do ABC/UFABC)	Aprovado

Coordenador do Programa de Pós-Graduação em Engenharia Elétrica:
Prof. Associado **Luis Fernando Costa Alberto**

Presidente da Comissão de Pós-Graduação:
Prof. Associado **Paulo César Lima Segantine**

To my beloved wife, Paola.

ACKNOWLEDGEMENTS

Firstly, I would like to thank God for everything in life. I would like to thank my parents, Antonio Leonardo Sanches and Vilma da Silva Sanches, for their constant support, love, encouragement, and total comprehension.

I would like to thank specially my beloved wife Paola Andréia Pallaretti Sanches, for her understanding and endless love, unceasing encouragement, support, and attention through the duration of my studies.

I would like to show my gratitude to my uncles Conceição Aparecida Sanches and Luiz Antonio Rozelli, for all the support offered. It was fundamental to the conclusion of this important step in my life.

I would also like to thank my friend and father-in-law João Gonçalo Pallaretti, who has supported me throughout the entire process.

I wish to express my eternal love and gratitude to my beloved grandparents, Angelina and Sebastião.

I also wish to express my love and gratitude to my beloved relatives, Aldrin, Ana Beatriz, Cecília, Fábio, Fred, Giovanni, Isabelle, Juliana, Marcelo, Natália, Nayara, Pablo, Patrícia, Ramon, Saulo, Suelen, and also to Vanessa, for the good moments together.

I would like to thank my friends Breno Guilherme Olivares, Bruna Vicentim Nobre, Carlos Eduardo Forni, Evandro Rodrigues Ferreira, Marcela Farjani, and Suelen de Mello Maschio for companionship and the good times.

I would like to express my appreciation to my supervisor, Dr. Ben-Hur Viana Borges, for his continuous guidance, helpfulness, confidence, advices, and for giving me the opportunity to accomplish this research.

I would like to express my gratitude to all the Department members for their help and support, especially my friends: Achiles, Alex, Arturo, Clenilson, Daniel Marchesi, Daniel Mazulquim, Getúlio, Heinz, Israel, Larissa, Leone, Lídia, Luiz, Marcel, Marcelo, Mariana, Pedro, Rafael, Tany, Thiago Campos, Ulysses, Valdemir, Willian, and Yang.

I would like to express my deepest gratitude to my friends and work colleagues, professors Érico Gonçalves de Figueiredo, Jarbas Alves Fernandes, Renê Medeiros de Souza, and Tiago Oliveira Mota.

I would like to thank my friend and work colleague Thiago R. Raddo, for all useful remarks and discussions about OCDMA.

Finally, I also want to thank CAPES for the financial support, and the Federal University of the Recôncavo of Bahia, UFRB, for all support offered.

Let the future tell the truth, and evaluate each one according to his work and accomplishments. The present is theirs; the future, for which I have really worked, is mine.

Nikola Tesla

ABSTRACT

SANCHES., A. L. **Single and Multirate FFH-OCDMA Networks Based on PSK Modulation Formats.** 2015. Thesis (DSc) – São Carlos School of Engineering, University of São Paulo, São Carlos, 2015.

Aiming to achieve the better efficiency in the use of bandwidth (spectral efficiency), as well as a compromise with the energy utilized in the process (power efficiency), the service operators are obliged to change the way in which the information is conveyed. The simplicity of the OOK modulation format has always been the main reason for using it in optical communications. Hence, once the coherent technologies had reached the maturity from a commercial point of view, they have become real alternatives to extend the capacity of networks.

In this thesis, the performance of single and multirate FFH-OCDMA networks based on coherent modulation formats is addressed. The following modulation formats are assumed: binary and quadrature phase shift keying (BPSK and QPSK). For single rate networks, BPSK or QPSK are used as the modulation format for all users. For multirate networks, on the other hand, BPSK and QPSK modulation formats are employed for low and high rate transmission users, respectively. For both networks, new bit error rate (BER) formalisms regarding the main deleterious source in OCDMA are derived, namely multiple-access interference (MAI). The mathematical formalism developed here accounts for any kind of users' signal waveforms (which are accurately accounted for at the desired user's receiver). As a result, it can be successfully used to carry out performance analysis of any OCDMA network. Moreover, it is shown that both low and high rate users can surprisingly achieve similar BER levels. In addition, it is demonstrated that incoherent OOK-based networks are not good candidates for future single and multirate FFH-OCDMA implementations in this interference limited scenario. On the other hand, our results pave the way for BPSK- and QPSK-based networks, which are seen as potential candidates for next generation passive optical networks (NG-PON2), where higher data rates and a vast amount of users will be major network requirements.

Key-words: optical code division multiples access, modulation formats, coherent networks, fast frequency hopping, multiple access interference, multirate, bit error rate.

RESUMO

SANCHES., A. L. **Redes FFH-OCDMA Convencionais e de Múltiplas Taxas Baseadas em Formatos de Modulação PSK.** 2015. Tese (Doutorado) – Escola de Engenharia de São Carlos, Universidade de São Paulo, São Carlos, 2015.

No intuito de alcançar uma melhor eficiência no uso da largura de banda (eficiência espectral), bem como um compromisso com a energia utilizada no processo de transmissão de informações (eficiência em potência), as operadoras de serviços estão sendo obrigadas a alterar o modo em que a informações estão sendo transmitidas. Neste sentido, a simplicidade do formato de modulação OOK sempre foi a principal razão para a sua utilização em sistemas de comunicações ópticas. Assim, uma vez que a tecnologia coerente tem alcançado a maturidade do ponto de vista comercial, estas são reais alternativas para aumentar a capacidade das redes de comunicação ópticas.

Nesta tese, são avaliados os desempenhos de redes FFH-OCDMA convencionais e de múltiplas taxas baseadas em formatos de modulação coerentes. Os seguintes formatos de modulação assumidos são: modulação por chaveamento de fase binário e por quadratura (BPSK e QPSK). Para redes convencionais, BPSK e QPSK são utilizados como formatos de modulação para todos os usuários. Por outro lado, para redes de múltiplas taxas de transmissão, os formatos de modulação BPSK e QPSK são empregados para baixas e altas taxas, respectivamente. Para ambas as redes, foram derivados novos formalismos matemáticos considerando a principal fonte deletéria de desempenho em OCDMA, comumente chamada de MAI, no cálculo da BER. Os formalismos matemáticos desenvolvidos são generalizados para quaisquer tipos de formas de onda empregada nos sinais dos usuários (as quais são contabilizadas precisamente no receptor do usuário de interesse). Como resultados, o formalismo matemático pode ser utilizado com sucesso para realizar a análise de desempenho de qualquer rede OCDMA. Adicionalmente, é demonstrado que ambos os usuários em baixa ou alta taxa de transmissão podem surpreendentemente alcançar níveis similares de BER. Concomitantemente, é observado que redes incoerentes baseadas em OOK não são boas candidatas para implementações convencionais e de múltiplas taxas de transmissão considerando esse cenário limitado por interferência. Por outro lado, os resultados trilham o caminho para redes baseadas em BPSK e QPSK, as quais são potenciais candidatas para a próxima geração de redes ópticas passivas (NG-PON2),

onde os maiores requisitos são as altas taxas de transmissão e grande capacidade de inserção simultânea de usuários.

Palavras-chave: acesso múltiplo por divisão de código óptico, formatos de modulação, redes coerentes, codificação com saltos rápidos em frequência, interferência de acesso múltiplo, múltiplas taxas de transmissão, taxa de erro de bit.

LIST OF FIGURES

LIST OF TABLES

LIST OF ACRONYMS

ACF	Autocorrelation Function
ASK	Amplitude Shift Keying
BER	Bit Error Rate
BPSK	Binary-Phase-Shift-Keying
CCF	Cross-Correlation Function
CDMA	Code-Division Multiple-Access
CW	Continuous Wave
DFB	Distributed Feedback
DPSK	Differential Phase Shift Keying (DPSK)
DS	Direct-Sequence
DSP	Digital Signal Processing
EDFA	Erbium Doped Fiber Amplifiers
EQC-TS/WH	Extended Congruence Quadratic-Time Spreading/Wavelength Hopping
FBG	Fiber Bragg Grating
FE	Frequency Encoded
FE-OCDMA	Frequency Encoded Optical Code Division Muultiple Access
FFH	Fast Frequency Hopping
FH	Frequency-Hopping
FOOC	Folded Optical Orthogonal Coding
FTTH	Fiber To The Home
FWHM	Full Width at Half Maximum Width
Gb/s	Gigabits per Second
Gc/s	Gigachips per Second
G-PON	Gigabit PON
GVD	Group Velocity Dispersion
HDTV	High-Definition Television
IM-DD	Intensity-Modulation Direct-Detection
ITU-T	International Telecommunication Union - Telecommunication Standardization Sector
LAN	Local Area Networks
LO	Local Oscilator

LiNbO3	Lithium Niobate
MAI	Multiple-Access Interference
MAN	Metropolitan Area Networks
MBG	Multiple Bragg Grating
MMI	Multimode Interference
MWML-OOC	Multi-Weight Multi-Length OOC
MWOOC	Multiple-Wavelength Optical Orthogonal Code
MZI	Mach-Zehnder Interferometer
NG-PON	Next Generation Passive Optical Networks
OCDM	Optical Code-Division-Multiplexing
OCDMA	Optical Code-Division Multiple-Access
OCDMA-PON	Optical Code-Division Multiple-Access Passive Optical Network
OCFHC/OOC	One-Coincidence Frequency-Hopping Code/Optical Orthogonal Code
ODB	Optical Duobinary
ODL	Optical Delay Line
OFFH	Optical Fast Frequency Hopping
ONU	Optical Network Unit
OOC	Optical Orthogonal Code
OOK	On-Off Keying
PC/OOC	Prime Code/Optical Orthogonal Code
PDF	Probability Density Function
PMD	Polarization Mode Dispersion
PON	Passive Optical Network
PSK	Phase-Shift Keying
QPSK	Quadrature-Phase-Shift-Keying
QoS	Quality of Service
RTT	Round-Time Trip
SIR	Signal-to-Interference Ratio
TDM	Time-Division Multiplexing
TDMA	Time-Division Multiple-Access
T/S	Time and Space
TS/WS	Time Spreading/Wavelength Hopping
VoD	Video-on-Demand

WAN	Wide Area Networks
WDM	Wavelength-Division Multiplexing
WDMA	Wavelength-Division Multiple -Access
WDM/OCDMA	Wavelength-Division Multiplexing/Optical Code-Division Multiple-Access
WH/TS	Wavelength-Hopping/Time-Spreading
XG-PON	10-Gigabit PON
1-D	One-Dimensional
2-D	Two-Dimensional

LIST OF PUBLICATIONS

JOURNALS

SANCHES, A. L,REIS Jr, J. V.; RADDO, T. R.;. and BORGES, B.-H. V., "Single and Multirate FFH-OCDMA Networks Based on PSK Modulation Formats," *IEEE/OSA - Journal of Optical Communications and Networking*. (*Under review*: February, 2015).

CONFERENCES

A. L. SANCHES, T. R. RADDO, and B.H. V. BORGES, " BER Performance Improvement in FFH-OCDMA Networks with BPSK Modulation Format," *in IEEE Globecom*, 2015, submitted.

A. L. SANCHES, T. R. RADDO, REIS JR, J. V., and B.H. V. BORGES, "Multirate FFH-OCDMA Networks Based on Coherent Advanced Modulation Formats", In *IEEE - International Conference on Transparent Optical Networks*, Budapest, Hungary, 2015.

SANCHES, A. L.; RADDO, T. R.; REIS Jr, J. V. and BORGES, B.-H.V., "Highly Efficient FFH-OCDMA Packet Network with Coherent Advanced Modulation Formats".In *IEEE - International Conference on Transparent Optical Networks*, ICTON 2014, Graz, Austria, July, 2014.

CONTENTS

CHAPTER 1

1 INTRODUCTION

In order to meet clients' demands satisfactorily using a wider bandwidth, telecommunication service operators are obliged to migrate their access networks to technologies that are economically more viable and have a larger capacity for information traffic. It is expected that future telecommunication networks will be capable of providing a large number of broadband services to subscribers. However, in order to meet this demand, a substantial increase in the transmission rate is required. Conventional networks, which use twisted pair cables or coaxial cables as the transmission medium, are limited in bandwidth and are no longer considered viable alternatives for the near future. Technology advances over the last decades have used optical fiber as the appropriate medium of information transmission. There are innumerous advantages of optical fiber in relation to twisted pair cables or coaxial cables, such as: wider bandwidth, lower susceptibility to signal degradation, low weight and electromagnetic immunity [1]-[3]. Currently, optical fibers are used in communication systems that require multiple access to transmit data at high speeds. Multiple access is when a transmission medium is shared by several users in a given domain. Establishing unique channels enable different users to join and coexist in the network by multiplexing and demultiplexing signals.

The three best known schemes of access and multiplexing are illustrated in Figure. 1.1, namely time division multiple access (TDMA), wavelength or frequency division multiple access (WDMA or FDMA), and code division multiple access (CDMA). Optical systems based on TDMA and WDMA technologies have fixed channel allocations, characterizing them as deterministic systems. For the first scheme, the main advantage is that all encoders can operate using the same wavelength and the simpler structure of this receptor.

The main disadvantage is the fact that allocating time slots to users does not allow for statistical multiplexing gain, a desirable feature when burst data traffic occurs [4]. By taking this into account, bandwidth allocation algorithms need to be applied, adding complexity to the system.

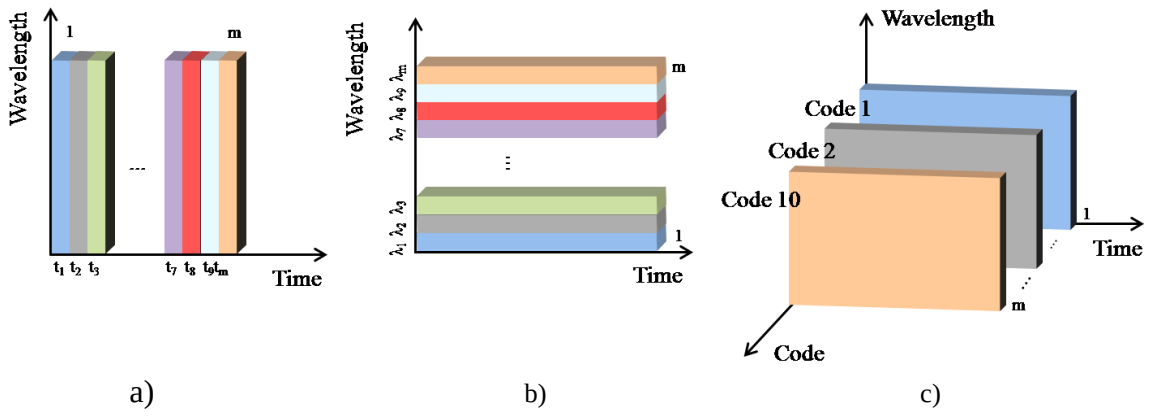

a) b) c)

Figure 1.1: Multiple access schemes for m users. a) TDMA, b) FDMA or WDMA and c) CDMA.

The advantage of the second scheme is that it is able to use virtual point-to–point topology, as well as dynamical optical routing based on wavelengths and traffic capacity reallocation. The main drawback of this network topology is the need to fine tune and monitor wavelengths emitted from each source, as well as the central wavelength of each filter to eliminate crosstalk among distinct wavelengths [5]. These two technologies are considered efficient alternatives and are viable in both metropolitan area networks (MAN) and wide area networks (WAN). However, local area networks (LAN) have requirements that are not easily met by TDMA and WDMA technologies. Hardware and additional protocols imposed by TDMA and WDMA technologies in the node distribution adds cost and complexity to the LAN [6]. The optical CDMA (or simply OCDMA), on the other hand, has greater flexibility in the available access bandwidth with the capacity of hiding (using codification) transmitted data.

By concerning the architecture used in networks, the passive optical network (PON) is one of the most promising solutions for fiber-to-the-home (FTTH) due to it being cost effective [7]. Moreover, equipment to implement the Gigabit PON (G-PON) standard has been commercialized all over the world. In order to increase network capacity, the International Telecommunication Union - Telecommunication Standardization Sector (ITU-T) has already found the specification of the standard capable of transmitting 10-Gigabits (XG-PON) [8] and has included it in the next generation of passive optical networks (NG-PON1). The NG-PON1 upgrade is based on time-division multiple-access (TDMA) and can transparently coexist with current G-PON technology, therefore offering a smooth transition path between both scenarios. Nonetheless, serious efforts are already being made to define

the future upgrade of NG-PON1 [9], namely the NG-PON2. NG-PON2 is currently under standardization, and has requirements such as: aggregate data ranging from 40 Gbps to 100 Gbps with ~1Gbps per user, 64 to 1000 optical network units (ONUs), extended reach of 60 km, and higher security level [9].

All of these requirements can be fully satisfied by joining the PON architectures with the OCDMA technique in order to constitute the passive optical code-division multiple-access (OCDMA-PON). OCDMA-PON networks also have several other remarkable attributes, such as asynchronous access, capacity on demand, lower cost/complexity for new users, the possibility of offering virtual point-to-point technology, high scalability, security, flexibility in code projects, and support for multiple data rate transmission at the physical layer [10]-[14].

Unfortunately, these networks are fundamentally dependent on the amount of simultaneously active codes (users). Concerning detection, the desired user code is identified by the autocorrelation peak (of significant amplitude), whereas the other users (interfering users) are seen by the system as background interference (due to cross-correlation). Thus, OCDMA-PON networks accept more degradation due to the amount of users accepted by the system, which characterizes it as a multiplexing statistical gain system. Therefore, using codification means an increase in security for the OCDMA-PON network related to user information when compared to other techniques. In addition, these networks can provide security at the physical layer level regardless of the data type transmitted since only the transmitted codes knowledge are necessary to retrieve the signals correctly [15]. Due to these comparative advantages, PON-OCDMA networks will be discussed in more detail later. Only for convenience sake, the term PON will be omitted after this point.

Starting with the code project, the utilized algorithms in the codification should meet some correlation properties, which can be defined in terms of orthogonality (ability to provide differentiation among the codes) and cardinality (ability to generate a larger number of codes with the highest orthogonality possible).

A good code project satisfies both properties and is of fundamental importance to reduce the main deleterious source of errors of this kind of network, namely multiple access interference (MAI) [16]-[24]. In OCDMA systems, MAI is directly proportional to the number of simultaneous users in the network; therefore, the MAI level increases as users are added simultaneously to the network. This interference source severely limits the overall performance of the system and should be minimized at all costs.

There is a large body of literature concerning codification alternatives, which provide different ways of dealing with the MAI. The most traditional codes available provide temporal spread utilizing only one wavelength and are known as unidimensional codes (1-D). A good example of this code family is optical orthogonal codes (OOC) [16]-[20]. These formulations use quite extensive code sequences, favoring the dispersive effects that result in temporal spread of pulses, thus limiting the applications that require high transmission rates. It should be mentioned that OCDMA systems based on 1-D codes experience low efficiency in bandwidth utilization and capacity.

There is also another group of codification algorithms capable of simultaneously providing spread in both time and wavelength domains. Codes with these characteristics are known as bi-dimensional codes (2-D) [21]-[24]. The 2-D codes are of particular interest, as they can reduce the temporal dimension of sequences in comparison with 1-D codes and increase the number of simultaneous users for the same bit error rate (BER) [25]. These optical codes are constructed in matrix form, whereby the rows represent wavelengths and the columns represent temporal displacements. The number of wavelengths and time slots are defined strictly by utilized code, whereby the code weight is defined by illuminated chips in a given code (signature). At the receiver side, the decoder should produce the "mirror" image of the codification matrix in order to correctly decipher the code incorporated in the desired information and, therefore, recover the desired user's transmitted data. All other codes are seen as interfering users, whereby the interference level is directly related to the code orthogonality.

There are many code schemes available in this family. For example, the time spreading/wavelength hopping (TS/WS) and the fast frequency hopping (FFH) proposed in [22] and [23], respectively. The low cardinality of these schemes was corrected afterwards by using a new approach based on extended congruence quadratic sequences for spreading and prime sequences (considering their cyclic shifts) for wavelength hopping (EQC-TS/WH) [26], [27]. However, the non ideal correlation properties of these codes make them unsuitable when a high number of simultaneous transmissions are required. In addition, both the code length and the number of wavelengths cannot be chosen independently. This limitation can be eliminated with OOC codes based on prime sequence permutations (PC/OOC), which present ideal correlation properties. Nevertheless, the requirement that the number of wavelengths is a prime number might be a problem in OCDMA systems because it directly affects the parameters related to the optical codes, such as cardinality and orthogonality, as explained in

detail in [23]. Later, this inconvenience was eliminated in [28] by using orthogonal codes based on multiple wavelengths (MWOOC) at the cost of higher complexity related to the algorithm generation. Another example of 2-D codes is the formulation introduced by Shurong et al. [29], whereby the code length can be chosen regardless of the number of wavelengths, without hindering the ideal properties of the correlation. These codes were based on one coincidence sequence for frequency hopping and OOC for time spreading (OCFH/OOC). However, these codes have a limited weight when few wavelengths are utilized. In addition, there are codes that can reuse wavelengths, therefore, making an increase of flexibility possible in the choice of code weight per wavelength and ideal correlation properties [30]. A good example of theses codes was proposed by Yang et al. [31], which besides the aforementioned benefits, have high cardinality. Such 2-D codes (called FOOC) are constructed by joining 1-D OOC codes to ideal correlation properties. In addition, other families of these codes can be found in [32]-[34]. As can be seen above, there are innumerous alternatives for performing encoding in OCDMA networks. It is worth mentioning that the mentioned codes were initially designed to support single rate transmissions (all users transmit at the same bit rate).

Nonetheless, diversified multimedia traffic (which creates the need for multirate transmissions) has encouraged communication companies to invest in access network architectures capable of offering bandwidth-hungry applications such as HDTV and 3D/4K video, as well as supporting the growing number of terminals (smartphones, tablets, e-reader). In OCDMA networks, the multirate transmission can be achieved by specific projects (while preserving the correlation properties) of multilength codes. In these cases, since the bit rate is inversely proportional to the code length (whereas the time chip is constant), the reducing/increasing factor in code length increases/reduces the bit rate proportionally.

The first proposal that supported multirate transmissions in OCDMA was based on unidimensional OOC codes [35]. In these networks, such codes offer support to two different user class rates and present non-ideal correlation properties (specifically cross-correlation of tree units, i.e., up to three hits can occur for each asynchronous time shift). Since this code family does not present ideal correlation properties, the deleterious effect of MAI also increases the BER. The strict multi-weight multi-length OOC (MWML-OOC) code family, which supports various rate transmissions and ideal correlation properties, was proposed in [36]. In this case, the different code lengths and code weights are assigned to the rate and quality of service (QoS) differentiation, respectively, among users.

It is also important to mention that all codes designed initially for single rate OCDMA can be utilized in multirate OCDMA networks when truncated. This only occurs due to the fact that truncation does not alter the code correlation properties. Nonetheless, the worst inconvenience of using this artifice is less control of the final parameter codes (code weight and/or number of wavelengths). However, in situations where the values of code weights and/or code wavelengths used in the final truncation are still significant for the considered network scenario, this method is very attractive because it does not need specially designed codes. The best case in terms of performance for truncated multirate codes occurs for the FFH algorithm, which can present the same code parameters for both especially designed and single rate truncated codes. In this thesis, 2-D codes based on fast frequency hopping (FFH) proposed in [37] and implemented experimentally in [38] are used as an alternative to encoding the users and carrying out the performance evaluation. The most attractive features that made us choose FFH codes are the possibility of obtaining the minimal code length dimension among all code families (considering both 1-D and 2-D kinds) and selecting few wavelengths of a group for code user composition. The first characteristics are desirable to reduce the linear dispersion (consequently, also the intersymbol interference) by maintaining the chip and the bit period comparable. On the other hand, the second characteristic has a greater distinction among the code users, thereby reducing MAI.

The first approach of OCDMA networks based on FFH codes (FFH-OCDMA) was proposed in [39]. Unfortunately, the performance analysis of the networks in terms of the BER was not investigated. Inaty et al. [40] have also proposed a version of the FFH-OCDMA network with multirate transmission and power control (for MAI mitigation) and showed its performance analysis.

Besides using the FFH coding scheme, a better network performance can be achieved if advanced modulation formats are utilized instead of the ordinary on-off keying (OOK). The simplicity of the OOK generation has always been the main reason for using it in optical communications. Previously, it was necessary for a modulation to maintain a commitment with the simplicity in detection. Consequently, OOK modulation format has been used, even in high rate transmissions ($\geq$10 Gb/s). However, high susceptibility to harmful fiber effects, such as group velocity dispersion (GVD) and polarization mode dispersion (PMD) makes some practical applications impossible as the data rate increases. Considering this, the project and practical implementation of high performance modulators contribute significantly to data rates above 10 Gb/s.

Afterwards, some attempts based on slightly more complex modulation techniques to exceed the 10 Gb/s data rate were carried out. In these implementations, optical duobinary (ODB) and differential phase shift keying (DPSK) modulation formats were used in order to transmit data rates in 40 Gb/s. However, commercial use has not been successful because requiring direct detection for both modulation techniques severely limits the reach of the optical signal [41]. In addition, the simultaneous decrease in the effective cost of OOK modulated transponders maintained this technique for transmissions of 40 Gb/s. The main technological breakthrough, which transmitted bit rates higher than 40 Gb/s, was coherent optical technology. Moreover, while developing coherent optical technology, the sufficient linewidth of distributed feedback (DFB) lasers (around 50 MHz) and erbium doped fiber amplifiers (EDFA) capable of extending the reach and capacity of legacy networks minimized the urgency to commercialize coherent technologies [42]. However, two main reasons were predominant and crucial for coherent technologies be adopted commercially. First, the greater spectral efficiency related to systems based on intensity modulation and direct detection (IM-DD). Second, the possibility of using digital signal processing (DSP) in order to minimize the impact of chromatic and polarization mode dispersions in IM-DD systems. Hence, once coherent technologies reached maturity from a commercial point of view, these technologies would greatly increase the capacity of transmitted information in comparison to IM-DD based networks.

Moreover, with the remarkable progress in optical device technology observed in the past few years, a large variety of devices targeting OCDMA applications has been proposed, such as encoders/decoders, source- (without a laser source) and color-less (non-wavelength specific), in-line dispersion-compensation-free using code bandwidth optimization, and also thresholding devices [43]-[45]. This has made coherent OCDMA networks a promising multiple access technique for PONs [46]. For example, phase-shift keying (PSK) modulation, such as single binary PSK (BPSK) and two bits per symbol quadrature PSK (QPSK), were implemented using all-optical modulation format conversion techniques (OOK to BPSK, and BPSK to QPSK) [47], [48]. Several researches perceive these techniques as potential candidates for symbol modulation in conventional and adaptive multirate networks [49].

In this thesis, two distinct single rate FFH-OCDMA networks based on BPSK and QPSK modulation formats are proposed. Also is proposed a new multirate FFH-OCDMA network through the simultaneous allocation of BPSK and QPSK modulation formats in order to support users with low- and high-data rate transmission, respectively.

For both single and multiple rate networks, new BER expressions are derived taking into account MAI. The mathematical formalism developed here assumes that the waveforms of the users' signals are accurately accounted for in the decision variable at the desired user's receiver. As a result, the developed formalism can be successfully applied to any OCDMA network. Moreover, the BER expressions can be further used to access the performance of both single rate and multirate FFH-OCDMA networks based also on the OOK modulation format. This is quite interesting not only for validation purposes, but also for future analysis of FFH-OCDMA networks based on the OOK modulation format, operating either in a MAI-limited scenario or with both MAI and several other deleterious sources (such as channel impairments and time jitter). It is further demonstrated that both single and multi rate PSK-based networks are more tolerant to MAI than OOK-based networks. In addition, concerning multirate PSK-based networks, it is shown that, unlike previous studies [35], [39], [40], [49]-[53] (which use OOK and different code lengths to achieve different rates), both low- and high-rate users can surprisingly achieve BER levels very close to the error-free region.

To the best of my knowledge, this is the first report on the performance of both single and multirate coherent PSK-based OCDMA networks.

This thesis is organized as follows. Chapter 2 revisited some usual configurations of OCDMA networks. Chapter 3 lays out the description of the sequential process carried out in the users' signals (from data/information source to data recovery) accomplished by the PSK-based FFH-OCDMA and presents the mathematical framework used to model the signal waveforms through these networks. The specific mathematical formalism for BER evaluations of single and multirate PSK-based FFH-OCDMA networks is presented in the Section 3.3. Chapter 4 presents relevant results regarding the proposed networks, describing the effects of MAI, and the effectiveness of the PSK modulation formats in the increase of signal-to-interference ratio (SIR). Finally, Chapter 5 presents some concluding remarks.

CHAPTER 2

2 OCDMA ENCODING, MAI AND MODULATION FORMATS

In this chapter, it is revisited some of most usual encoding techniques employed in OCDMA networks. In addition, it is presented a detailed description of several encoding and decoding techniques, including optical FFH, and its capacity of dealing with the MAI. Moreover, the structures and process involved in both optical BPSK and QPSK modulation of the users' signals are characterized.

2.1 OCDMA ENCODING

In OCDMA networks, the integrity and security of the users' signals is ensured by unique codes, i.e., codes attributed exclusively to each user. Currently, there are various options of codes in the literature, and each one has implementation requirements that should be fulfilled with respect to the availability of resources. The codes can be classified according to the domain where encoding occurs, i.e., time, wavelength, space, phase or a combination of them. When only one of these domains is adopted, these codes are classified as 1-D codes. On the other hand, when two or three domains are used for encoding, 2-D or 3-D codes are formed, respectively. The latter has a high degree of complexity considering its practical implementations and this is not the aim of the study here. The main features of 1-D and 2-D codes, often found in OCDMA applications, will be presented next.

2.1.1 TIME ENCODING (1-D ENCODING)

In conventional OCDMA-based transmission systems, one bit corresponds to one pulse with a much shorter duration than the generated data bit of duration T_b. The codification process consecutively creates L (code length) replicas of this pulse at different

time intervals. Each one of these pulses is called chip and its temporal width time is called T_c. Therefore, the initial pulse (before the encoding process) must have a period equal or less than T_b/L so that interferences within the sequence attributed to a given user do not occur. Figure 2.1 illustrates this case with the three uncoded a) and coded b) BPSK modulated bit {1 0 1} transmission sequence. The BPSK modulated representation will be used throughout this chapter for the sake of convenience only, as the OCDMA networks accept other modulation formats (as will be seen in the following sections) without changing the encoding process. As it can be observed, the generated data bits alternating between "0" and "1" create phase reversals, i.e., 180° degree phase shifts as the data bits shift state.

The first implementation of this type of codification used several optical delay lines (ODL) interconnected to pulse time allocation. The encoding process of data bit "1" using this technique is illustrated in Figure 2.2 a). In this scheme, the information data bit is represented by an optical pulse of high amplitude and a short duration, where the duration of each chip is related to the code weight adopted by the specific code algorithm. Therefore, the full width at half maximum width (FWHM) of a chip is given by $T_c = T_b/L$, where L is the

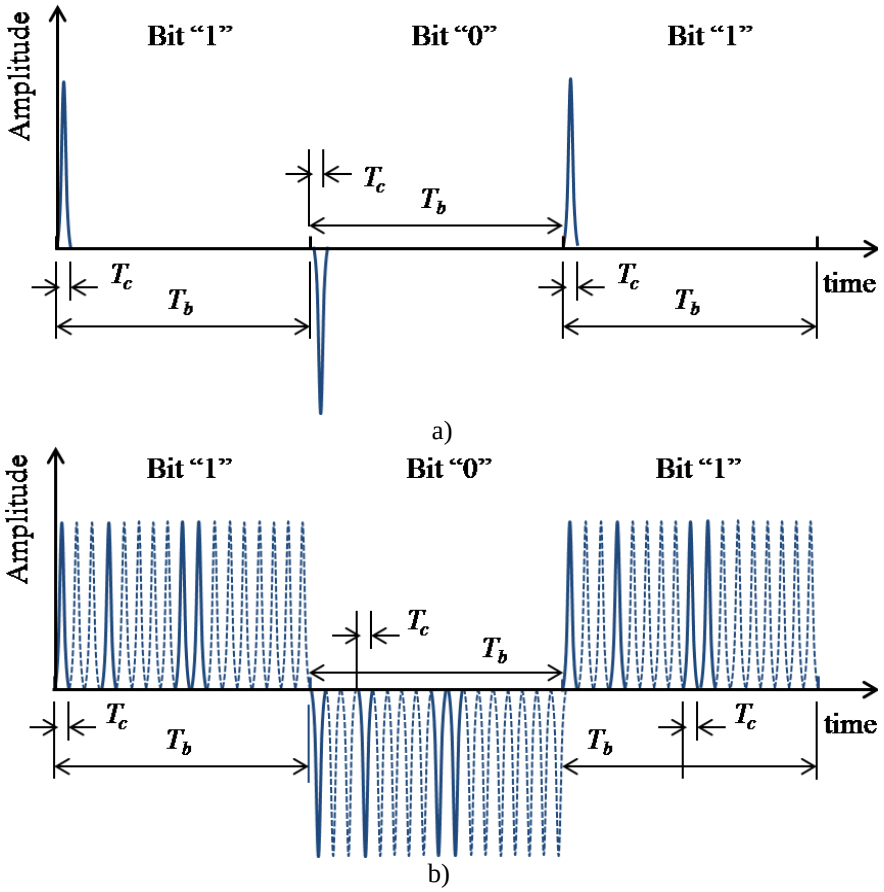

Figure 2.1: Generated pulse train for generated data bits {1,0,1}. a) Short pulses representing each generated bit data. b) Encoded short pulses representing each generated bit data.

code length (number of chips that fragments T_b).

The codification corresponds to sequences of short pulses, of a number proportional to the code weight (w), as shown in Figure 2.2 b). Signals from other users, represented by their specific sequence of chips (codes) are multiplexed in a star coupler. A set of similar delay lines (in the complementary configuration to be used in the encoder) is utilized to reconstruct the original pulse at the receiver, as can be seen in Figure 2.2 c). The decoding operation is carried out by intensity correlation.

Thus, if the pulses are positioned correctly, they form a defined pattern in the auto-correlation function (ACF). If they are not, they form a background signal (interfering signal), defined by a cross-correlation function (CCF). The outputs of the decodification process are shown in Figure 2.2 d).

In addition to traditional ODLs [54], other artifices which use photonic crystals [55] and integrated optics [56] have been suggested. Each data information bit is encoded in a waveform $s(t)$ that corresponds to a code signature. Furthermore, each receiver correlates the mask of this code, $f(t)$, with the transmitted signal, $s(t)$ [57]. The receiver output, $r(t)$, is a correlation operation which shows the similarity degree between them, and is given by

$$r(t) = \int_{-\infty}^{\infty} s(\tau)\, f(\tau - t) d\tau. \tag{1}$$

The algorithms generally seek to maximize the auto-correlation, $s(t) = f(t)$, and minimize the cross-correlation between codes, $s(t) \neq f(t)$, in order to extract the maximum in orthogonality (degree of differentiation between them) and cardinality (quantity of available codes). The general conditions for code orthogonality are [19]:

- ✓ Each version can be distinguished from the shifted version of itself;

- ✓ Each version (possibly a shifted version) can be distinguished from other sequences of the set of used codes.

Let us express the above statements in a mathematical form. For two sequences of length L, $X = \{x_0, x_1, x_2, \dots, x_{L-1}\}$ and $Y = \{x_0, x_1, x_2, \dots, x_{L-1}\}$, there are two results of discrete correlation that represent the interaction between them [17]

✓ For sequence $X = x(k)$

$$|Z_{x,x}| = \left| \sum_{i=0}^{L-1} x_i \, x_{i+k} \right| = \begin{Bmatrix} w, \text{ for } & k=0 \\ \leq \lambda_a, \text{ for } & 1 \leq k \leq L-1 \end{Bmatrix}. \tag{2}$$

✓ For each pair of sequences $X = x(k)$ and $Y = y(k)$

$$|Z_{x,y}| = \left| \sum_{i=0}^{L-1} x_i \, y_{i+k} \right| \leq \lambda_c, \quad for \quad 1 \leq k \leq L-1, \tag{3}$$

where $Z_{X,X}$ and $Z_{X,Y}$ correspond to the auto-correlation and cross-correlation, respectively, λ_a is the auto-correlation peak out of phase (lateral lobules corresponding to the shifted versions of the same sequence, $k \neq 0$) and λ_c is the cross-correlation peak (between different sequences). The strict orthogonality would achieve $\lambda_a = \lambda_c = 0$. However, if we consider

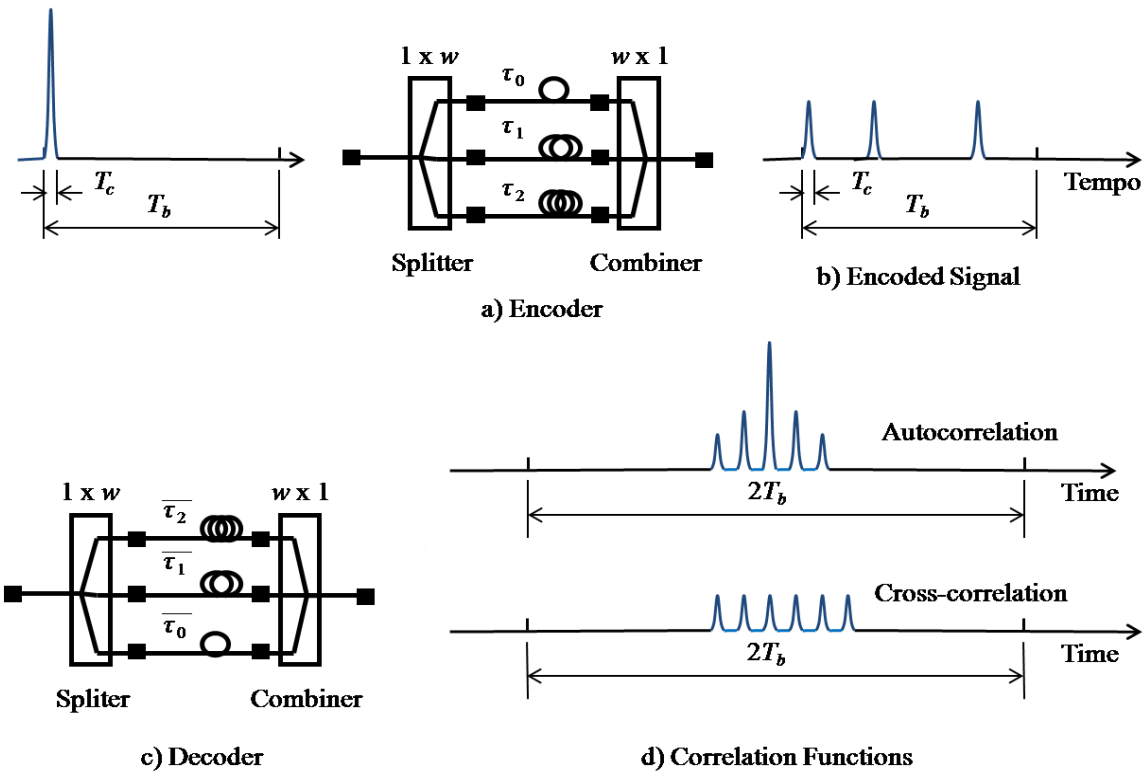

Figure 2.2: Time domain encoded with ODL: a) encoder; b) decoder (optical correlator); c) encoded signal; d) auto-correlation function (ACF) and cross-correlation function (CCF).

that the same modulated signal was sent from the users, this case would not be possible, as the manipulation of the optical pulses in the decoding process occurs using signal intensity. Therefore, there is a need to minimize λ_a and λ_c using encoding techniques.

The problem with this codification type is related to temporal duration of the chips when the data transmission rate becomes too high (hundreds of Mb/s or more). This problem becomes more critical when the number of simultaneous users is increased in the network.

2.1.2 SPECTRAL ENCODING (1-D ENCODING)

In the spectral domain, there is a possibility of manipulating signals of coherent or incoherent optical sources for phase or amplitude treatment of the optical signal (FE-OCDMA). The main motivation is the independence between the bandwidth signal and bandwidth source. Therefore, the parameters that define the code become independent from the information to be transmitted. The process is illustrated in Figure 2.3.

The frequency encoded process is similar to the phase coherent encoding in the sense that the spectral components of the broadband optical source are initially resolved [58], [59]. Each channel uses one amplitude spectral encoder in order to selectively transmit some wavelength components. In the receiver, two balanced photodetectors are used. Initially, the receiver filters the received signal with the same spectral amplitude filter used in the transmitter, $A(w)$, as well as its complementary filter, $\overline{A(w)}$. Next, the outputs of the

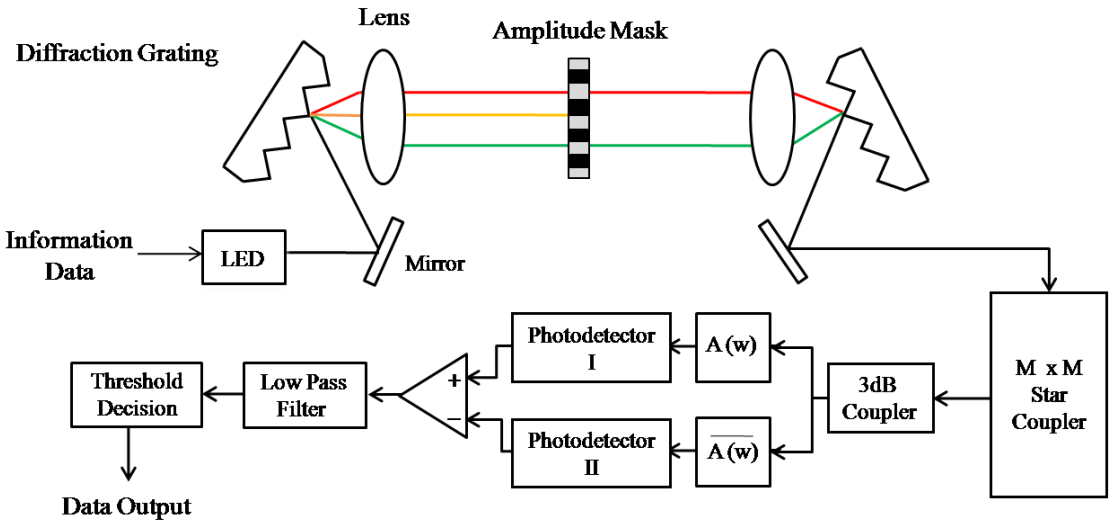

Figure 2.3: OCDMA Encoding system of incoherent spectral amplitude.

complementary filters are detected by two photodetectors connected at balanced mode. For a mismatched photodetector, half of the spectral components transmitted are related to the direct filter and the other half to the complementary filter. Once the output of the balanced receptor represents the difference between the outputs of the two photodetectors, mismatched signals will be cancelled, whereas matched signals will be correctly demodulated. Finally, the recovered signal is modulated by amplitude, specifically by amplitude shift keying (ASK), and a decision threshold device concludes the transmitted data bit.

2.1.3 SIMULTANEOUS TIME AND FREQUENCY ENCODING (2-D ENCODING)

Aiming at overcoming the problems concerning the inefficient bandwidth and power usage of the first encoding implementations using unipolar pseudo-orthogonal sequences, Mendez and Gagliardi, proposed ways to convert the 1-D sequences into 2-D sequences by manipulating time and space (T/S) [60], [61], and Lancevski and Andonovic [21] proposed the same for time and frequency.

Frequency and time encoding provides better flexibility in optical code choice, resulting in system capacity increase. Such flexibility allows for reduced code length design without hindering the code cardinality or the system performance in relation to one-dimensional codes. In addition, the frequency and time encoding can also reach longer transmissions at high rates to such an extent that the linear dispersion becomes less critical.

In addition, each simultaneous time and frequency OCDMA encoded signal can be seen as a combination of all OTDMA and OWDMA available resources (time slots and wavelengths). Figure 2.4 shows the relation between the TDMA and OWDMA systems with the OCDMA.

Accordingly, it has been proposed to add the wavelength dimension to the code design in order to construct codes with larger cardinality while maintaining good auto- and cross-correlation properties. In a 2-D coding technique, allocation of the chips is carried out simultaneously both in time and wavelength. In this case, the time and wavelength selections are decided according to a code construction algorithm, which not only increases the flexibility of the code design, but also improves the cardinality dramatically.

Furthermore, in this type of coding scheme, the code sequences are characterized by frequency hopping (FH). If a fast jumps occur at wavelengths that change for every pulse of a

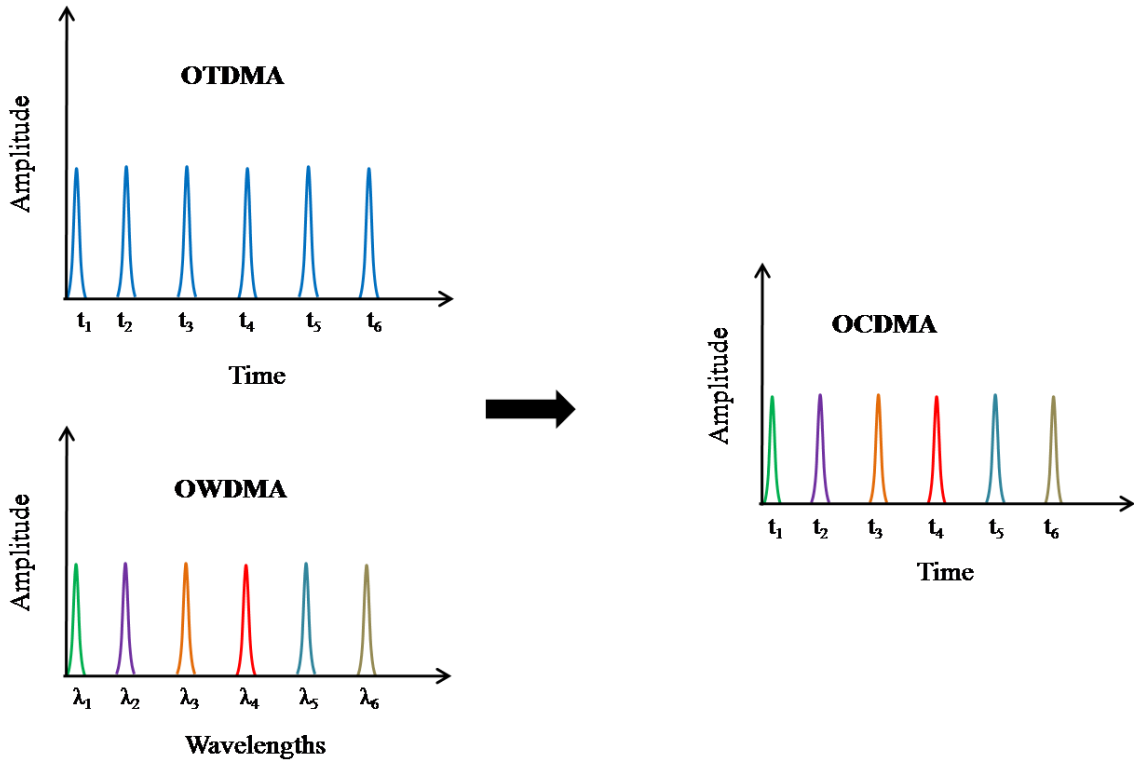

Figure 2.4: Relation between the TDMA and WDMA systems with OCDMA.

given temporal sequence, the process is defined as FFH. The difference between FH and FFH signals in terms of frequency hopping occupancy is depicted in Figure 2.5. It can be observed from this figure that, as time advances, the signal occupies a separate frequency band as determined by the pseudo-random hopping code sequence. It can be further observed that hops in FFH must be for an exclusive frequency, i.e., for a frequency different from the previous one used. Therefore, optical FFH (or OFFH) is a promising 2-D code to be implemented in multirate OCDMA systems. Both frequency hopping techniques are described in more detail in the next sub-sections.

The 2-D wavelength/time (W/T) codes have a matrix representation of $m \times n$, with the number of rows m associated with the available wavelengths, and the column number n related to the chip interval (code length). For instance, consider 2-D codes with x and y belonging to set C. By assuming orthogonality for different used wavelengths (neglecting interactions) implies that displacements will be considered only in time. Therefore, with $0 < \tau < n$, the results for the discrete binary correlation functions are given by [22]

✓ For the auto-correlation out of phase x

$$Z_{x,x}(\tau) = \sum_{i=0}^{m-1}\left(\sum_{j=0}^{n-1} x_{i,j}\, x_{i,(j+\tau)\mathrm{mod}(n)}\right) \leq \lambda_a. \tag{4}$$

✓ For the cross-correlation of x and y

$$Z_{x,y}(\tau) = \sum_{i=0}^{m-1}\left(\sum_{j=0}^{n-1} x_{i,j}\, y_{i,(j+\tau)\mathrm{mod}(n)}\right) \leq \lambda_c, \tag{5}$$

where $Z_{x,x}$ and $Z_{x,y}$ correspond to the auto-correlation and cross-correlation, respectively. The in-phase auto-correlation value is equal to the code weight, $Z_{x,x}(0) = w$. The cardinality

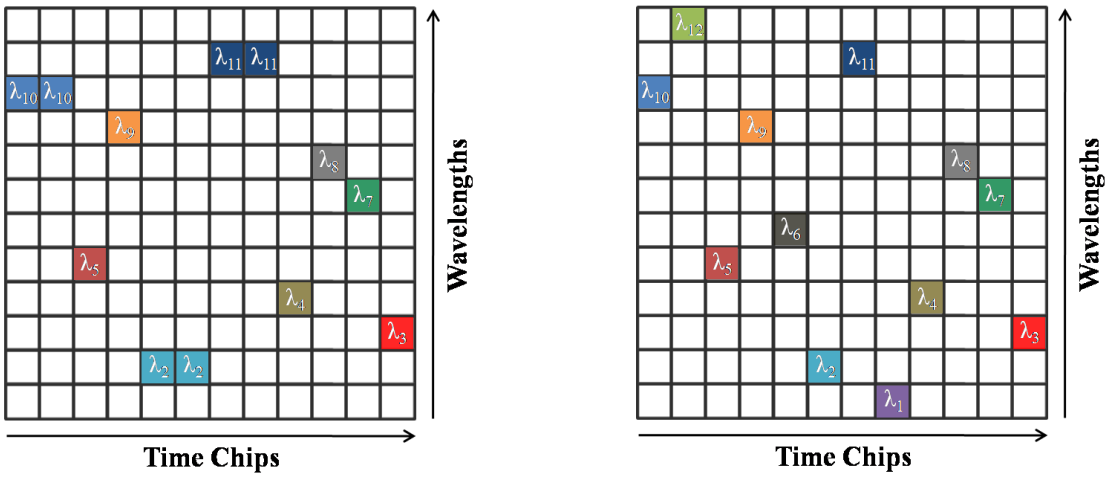

a)b)

Figure 2.5: Frequency hopping technique. a) Time and frequency occupancy of frequency-hopping (FH) signal; b) Time and frequency occupancy of fast frequency-hopping (FFH) signal.

depends on the utilized algorithm and the notation follows the identification standard ($m \times n, w, \lambda_a, \lambda_c$) or ($mn, w, \lambda_a, \lambda_c$), with the length given by $L = mn$. The correct decoding signal of a given user fundamentally depends on the proper implementation of this correlation function in the network.

2.1.3.1 *FREQUENCY HOPPING (FH-OCDMA)*

In frequency hopping, the carrier frequency of the transmitter hops an apparently random pattern. This pattern is, in fact, a pseudo-random code sequence. The order of the frequencies selected by the transmitter is taken from a predetermined set as dictated by the code sequence 2-D wavelength-hopping time-spreading (WH/TS), which was proposed [21], [22], [27] as an alternative to overcome the shortcomings of 1-D codes.

A 2-D WH/TS is a family of codes based on 2-D FH coding capable of performing frequency spreading in time and wavelength domains simultaneously. It is worth mentioning that this code family covers many coding schemes proposed in the literature, such as the prime code/optical orthogonal code (PC/OOC) [5], [62], multiple-wavelength optical orthogonal code (MWOOC) [23], and one-coincidence frequency-hopping code/optical orthogonal code (OCFHC/OOC) [29]. The OCFHC/OOC should receive special attention due to its good performance [11], [62] and good code generation features since the code length can be chosen regardless of the number of available wavelengths without forgoing good correlation properties. FH codes provide a significant increase in code cardinality, allowing for a larger number of active users in the system. In addition, it provides greater flexibility in the choice of code parameters.

In this encoding scheme, some chip positions are not filled and the same wavelength is used more than once (this never happens in FFH). Figure 2.6 illustrates a 2-D optical encoder/decoder suitable for WH/TS OCDMA [26]. The encoder in Figure 2.6 a) consists of a $1 \times W$ wavelength-division demultiplexer, W delay lines, and an $W \times 1$ wavelength-division multiplexer. Firstly, in the coding process, a short pulse corresponding to data bit “1” is separated by the wavelength-division demultiplexer into W pulses using a pre-established wavelength set. Next, the W pulses are delayed by their respective ODLs. Afterwards, the pulses are combined in the encoding output by a wavelength-division multiplexer. Similarly, the decoder in Figure 2.6 b) consists of a $1 \times W$ splitter, with W delay lines, and an $W \times 1$ wavelength-division multiplexer. Note that the time delays produced by the corresponding delay lines at the encoder and decoder are complementary to each other. When the decoder outputs an auto-correlation peak, the data bits are correctly restored after optical-to-electrical conversion and threshold decision. The performance of a 2-D WH/TS OCDMA system was investigated in [11], [62], [63].

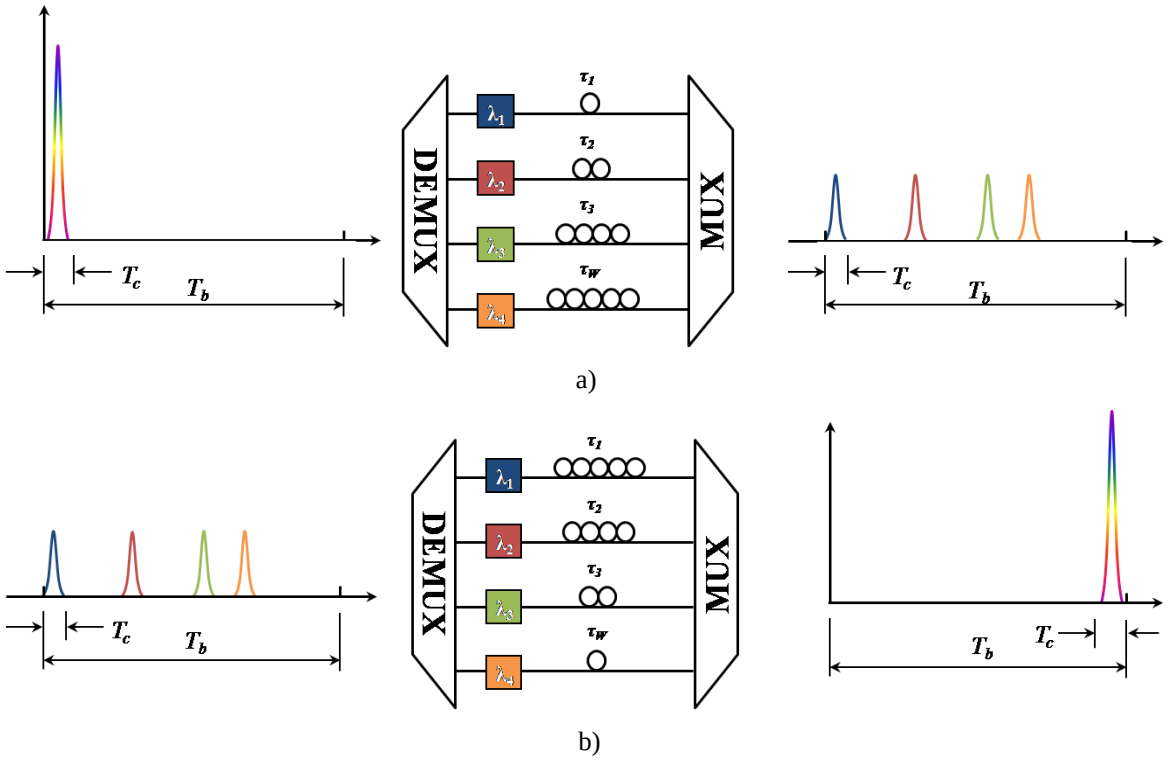

Figure 2.6: 2-D incoherent coding scheme based on time and frequency spreading, WH/TS OCDMA. a) Encoder using ODLs, multiplexer (MUX) and demultiplexer (DEMUX); b) Decoder using ODLs, MUX, and DEMUX.

2.1.3.2 Fast Frequency Hopping (FFH-OCDMA)

The FFH-CDMA system was originally proposed by Fathallah [64], [65], and is based on a series of multiple Bragg gratings (MBGs) [64] to generate fast hopping frequency patterns. These gratings spectrally and temporally slice an incoming broadband pulse into several components, thus generating optical frequency patterns, as can be seen in Figure 2.7. The passive all-optical signal coding, based on MBGs, implies in both low-cost and robust implementation of FFH-CDMA systems [64].

An inherent feature of FFH systems is that the frequency changes at a significantly higher rate than the information rate, which means that each pulse in a code sequence is transmitted at an exclusive wavelength. Thus, FFH systems are defined by several frequency hops within each data bit.

A possible architecture for FFH-CDMA systems depicting the desired user encoder with 12 gratings is illustrated in Figure 2.7. This figure illustrates the fiber Bragg grating (FBG) structures arranged in series to select 12 wavelengths.

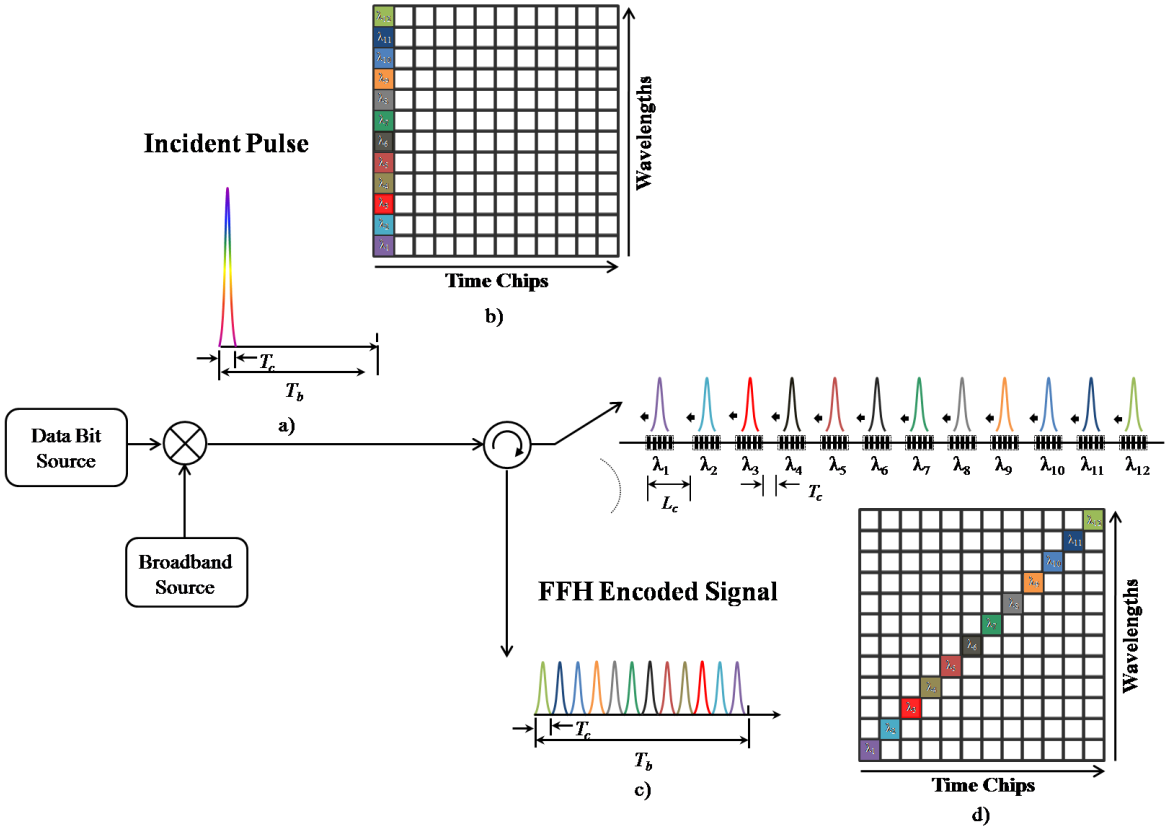

Figure 2.7: 2-D FFH-CDMA transmitter implementation scheme using MBG.a) Desired user incident broadband signal; b) Time-frequency hopping patterns matrix representation before encoding; c) and d) FFH pulses of desired user and FFH hopping patterns matrix representation , respectively, after encoding.

Initially, the users' data bits are modulated via coherent advanced modulation formats and then encoded with a low crosstalk code algorithm to guarantee the network quality of service. Assuming that the data bits have been modulated properly, the optical broadband short pulse is transmitted to the MBGs in the encoding process, shown in Figure 2.7 a). The time-frequency hopping patterns that compose the desired user's transmitted signals are formed by the time/wavelength matrix presented in Figure 2.7 b). The FFH encoded pulses are shown in Figure 2.7 c) for the desired user and the time-frequency hopping patterns that compose the transmitted signals from the wavelength subset matrix presented in Figure 2.8 d). Following this reasoning, the encoding technique will generate independent frequency pulses and places each of them in an appropriate time-frequency, as previously established by the FFH hopping sequence pattern [64].

It is worth mentioning that this coding scheme is based on a correlation of an incoherent short pulse modulated by the data source with the impulse response of each Bragg grating. This type of encoder can be considered as a logical combination of the first two 1-D

encoders previously described in Sections 2.1.1 and 2.1.2 of this chapter. As can be observed in Figure 2.7, while the Bragg gratings produce the frequency spectrum slicing, the Bragg grating positions produce the respective time delays in a similar fashion to that of the ODLs in 1-D coding. The response of each Bragg grating is defined as the inverse Fourier transform of the grating complex reflectivity and the incident pulses associated with the transmitted data are normally much narrower than the response duration of the grating.

In addition, the time frequency hopping pattern is determined by the order in which the wavelengths are tuned in the Bragg gratings [65], [66]. The time chip and the number of gratings in the encoder establishes the nominal data bit rate of the system, i.e., all reflected pulses of a data bit should leave the encoder before the next bit's pulses enter [67].

At the decoder, the gratings are placed in the reversed order in comparison to that of the encoder in order to accomplish the decoding function. This scheme is illustrated in Figure 2.8. Finally, the matched filter based-decoder removes the translation between the wavelengths and realigns all chips from the received signal into a single pulse, as shown in Figures 2.8 a) - b) and Figures 2.8 c) - d), respectively. As can be seen in Figure 2.8 c), if the pulses are positioned correctly, they form a defined pattern by the correlation property (similarity level between the transmitted and received desired signal). If they are not, the pulses would form an interfering background signal defined by the cross-correlation property (known as MAI).

In FFH coding, the available bandwidth is subdivided into contiguous frequency intervals, where the transmitted signal occupies a frequency range in each time chip $T_c = 2 \times n_{eff} \times L_s/c$, where L_s is the sum of one grating length plus one space distance between an adjacent grating, n_{eff} is the effective index, and c is the light speed [64], [66]. Since the Bragg gratings are equally spaced, i.e., T_c is constant, the pulses are correspondingly spaced at time intervals T_c seconds apart from each other, which corresponds to the round-trip time (RTT) between two consecutive gratings [65]. The bandwidth associated with the data rate is $B = 1/Tb$, and $T_b = 2 \times (L-1)n_{eff} \times L_s/c$, where L is equivalent to the number of gratings [64]. The gratings can be written at the wavelength λ_B (Bragg wavelength) and tuned to different wavelengths $(\lambda_1, \lambda_2, \ldots, \lambda_F)$, which are allocated in time intervals in accordance with the adopted algorithm. Parameter F accounts for the total number of available wavelengths. The Bragg wavelength of each grating $(\lambda_1, \lambda_2, \ldots, \lambda_F)$ should, thus, comply with the code needs and be allocated in time intervals according to the adopted algorithm.

As mentioned before, the fiber Bragg gratings also offer the possibility of tuning the Bragg wavelength, which is very attractive for reconfiguring the encoder/decoder [64]. Currently, each Bragg grating can be individually tuned using piezoelectric devices in order to adjust an intended wavelength from an available wavelength range [64]. The wavelengths tuned outside the bandwidth are not reflected by the FBGs, i.e. the FBGs become transparent to these wavelengths [64]-[66].

The tuning set of each pair of encoder-decoders will determine the code sequence used. Furthermore, each of these gratings contributes to a single reflected pulse. The number of available frequencies is limited by the tunability of the gratings, which establishes the system capacity. A possible way to implement FFH coding in practice is by using frequency-hopping patterns generated by the algorithm proposed by Bin [37]. This algorithm uses $F \geq L$ for the code set construction. Furthermore, the codes are classified as one-coincidence sequences [68] and characterized by the following three properties: 1) all the sequences have the same length; 2) each frequency is used at most once in each sequence; 3) the maximum number of hits between any pair of sequences for any time shift equals one.

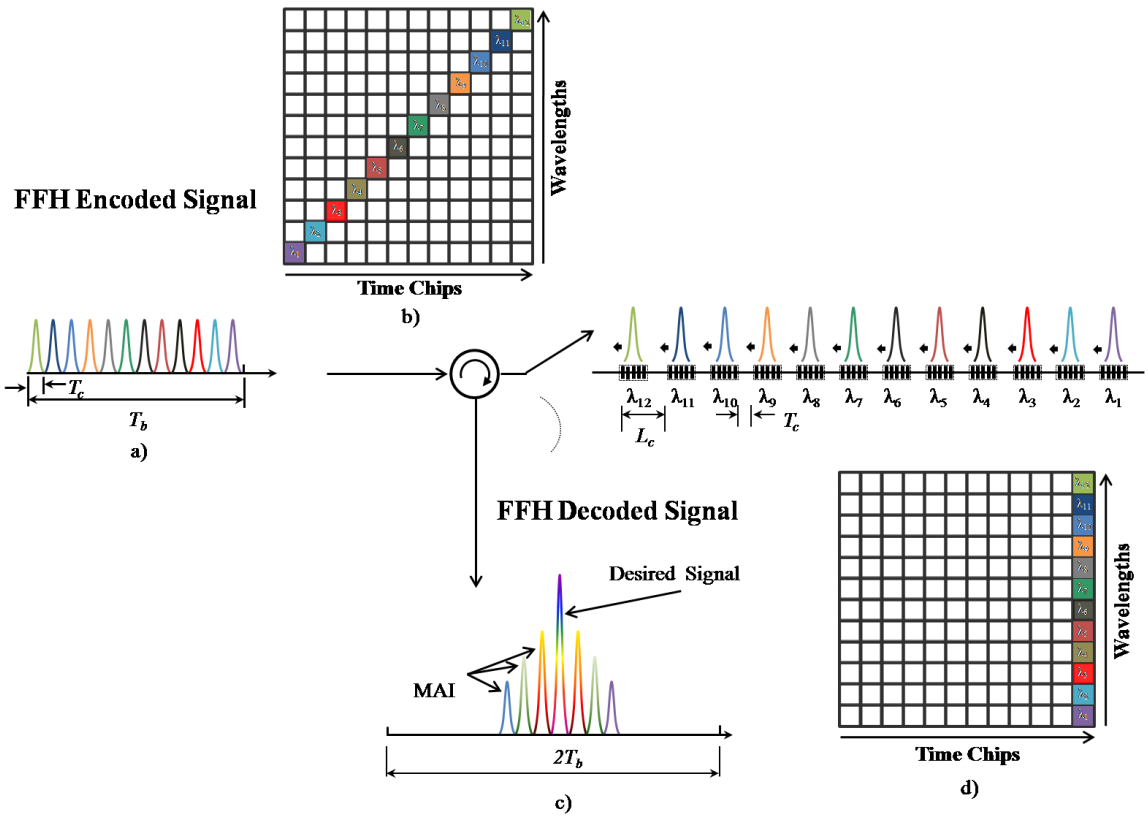

Figure 2.8: 2-D FFH-CDMA receiver implementation scheme using MBG. a) and b) Desired user signal and matrix representation, respectively, of the received FFH signal; c) Desired (high peak) and interfering (sidelobes) decoded signals and d) Matrix representation of the desired user decoded signal.

2.2 MULTIPLE ACCESS INTERFERENCE (MAI)

Using codes with good orthogonality does not ensure total differentiation between the users, as the manipulation of optical pulses occurs by signal intensity [69]-[77]. This can be understood as follows: consider an OCDMA 2-D system, which uses temporal displacements of optical pulses in several wavelengths, arranged according to a specific algorithm for the code that will be attributed to each user. The information of each user is encoded using a specific signature sequence, multiplexed and sent through the channel (optical fiber) to all the users simultaneously. Each receiver contains the replica of the code attributed to each user, which enables the information to be extracted from a correlation operation. At the decoder side, the pulses of different wavelengths overlap to form an auto-correlation peak of high intensity if the corresponding user to the code contained in the receiver sends some information. Otherwise, the pulses in different wavelength will remain far apart and low cross-correlation signals will be generated [73].

When the network accommodates many users simultaneously, the cross-correlation signals can accumulate and generate an interfering power comparable to the autocorrelation peak [16]-[19]. This interference, known as MAI, can cause a significant increase of the BER and severely limit the capacity of users to be served by the network. Figure 2.9 illustrates that the MAI of various simultaneous users influences the signal of the desired user. For this example, three users have their data bits encoded by specific codes based on FFH. The encoded signals use 12 of a larger number of available wavelengths, arranged in 12 time

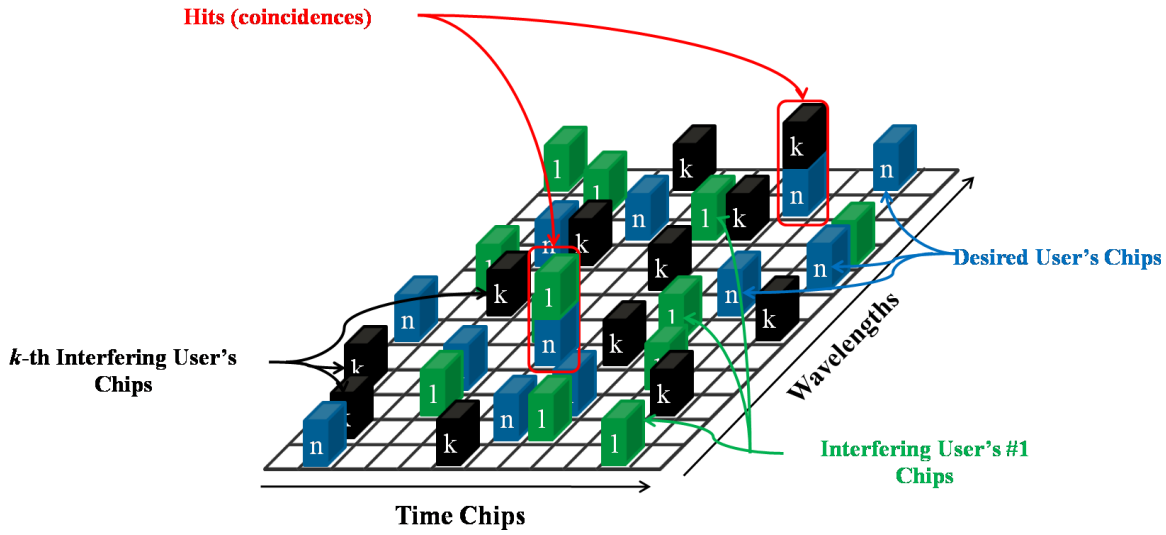

Figure 2.9: Time and Frequency of chip allocations in FFH-OCDMA.

chips in accordance with the generated FFH code. In addition, the encoded signals are shown in matrix form and the rows and columns represent the time and wavelength assigned to each chip, respectively. In addition, the matrix consists of chips from three users: the desired user (cyan boxes); the interfering user denoted by number 1 (green boxes) and the *k*-th interfering user (black boxes).

Note that there are hits from chips emitted by the users in time, wavelength and both dominions. Moreover, the FFH property of one coincidence code ensures that maximum one hit occurs (overlap of two chips at the same time and wavelength) between two encoded user signals for each asynchronous access in the network. The hits contribute to errors in the desired user receiver due to the fact that these additional contributions generated by MAI are allocated at the decision window after the autocorrelation of the desired user.

With the aim of showing the errors caused by MAI, Figure. 2.10 illustrates the transmission of 5 data bits $\{0, 1, 0, 0, 1\}$ by the user and the simultaneous asynchronous access of six interfering users. Asynchronous access is easily identified (observe that the

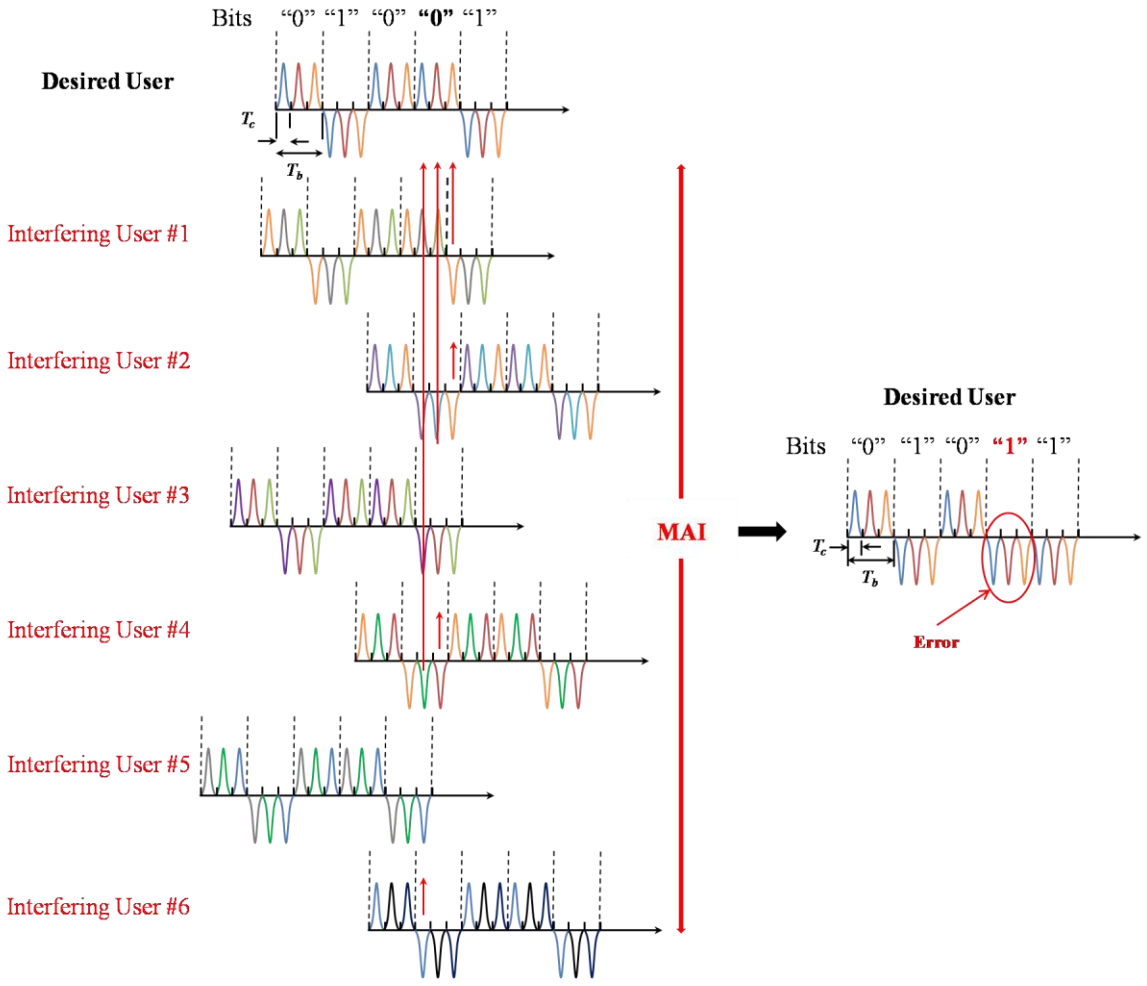

Figure 2.10: Contributions of MAI on the desired user in the BPSK- based FFH-OCDMA network.

start of each sequence of the users does not occur at the same time). Consequently, the hits among the chips of the users occur naturally after accessing the channel. As can be observed, the coincidence function of the FFH codes and the bipolar characteristics of the BPSK modulation ensures that the errors occur only when a minimum of $2w$ (w is the code weight) users are simultaneously active in the network. This happens because w users are needed to produce opposite polarity overlaps (eliminating the original signal of the desired user) and more w users to reproduce the pattern of chips with opposite polarity to the original (concerning the transmission of the other data bit).

2.3 MODULATION FORMATS

Modulation is the process of manipulating the signal waveform to accurately transmit information. Modulation formats refer to the technique used to apply information to a carrier. Two strategies are used to carry out modulation in optical domain. In the first option, commonly known as direct modulation, the dependence between the power at the output of a semiconductor laser and the current injected through the laser diode is used to convert the information from the electrical to optical domain. In practical terms, the output of the semiconductor laser is maintained without power until the current at its input reaches the threshold level. Then, the input current increment above the threshold level accomplishes the inversion of population and, as a result, increases proportionally the output power until a saturation value. Thus, the output current depends on the data bits in a way that the optical signal is emitted from a semiconductor laser only when the data bits are "1", whereas the "0" data bits transmissions are represented by the absence of the optical signal.

However, this is not a practical option due to various problems generally associated to non-ideality of the optical source. The main disadvantage of directly modulated lasers is the chirp, i.e., the residual phase modulation generated with the intensity modulation. Unfortunately, the chirp causes variations in the intensity, frequency and optical signal phase, even when submitted to negligible electric current fluctuations. This occurs due to spontaneous emission and recombination of carriers within the lasers.

In the second option, called external modulation, a laser that produces a continuous output beam or continuous wave (CW) can be used to emit optical signals. In this case, a

second device, known as a modulator, is used to switch the optical signal according to the data bits. A classical external modulator known as Mach-Zehnder interferometer (MZI) modulator based on litium niobate (LiNb03) is shown in Figure 2.11.

With appropriate orientation, an electro-optic crystal (the LiNb03 is the crystal more widely used for this application) provides phase modulation when excited by a voltage in a given direction. Here, for simplicity, the phase displacement in just one arm is shown, but this can be present in both arms.

The principle of the MZI is to divide the pulse amplitude and phase modulation of one part of the signal to produce constructive or destructive interferences after recombining it. This can be better understood by considering that the incoming optical signal is added to the input of the MZI, as illustrated in Figure. 2.11. Initially, the incoming signal is divided into two arms. In the lower arm, light experiences a phase delay (as a consequence, the effective velocity is changed) due to a change in the refractive index of the waveguide. Finally, when the two optical signals are combined, a series of phase changes are attributed to the input signal. After describing the MZI operation, it is interesting to analyze the mathematical formalism associated with the light in the device. After this point, it will be considered a practical MZI with modulation signals present in both arms. Furthermore, an equivalent circuit that has the phase modulation in both MZI branches will be considered.

Then, the combined signal in the ideal MZI output can be written as [74]

$$E_o(t) = \frac{E_i(t)}{2} e^{\left[\frac{j\pi v_1(t)}{V_\pi}\right]} + \frac{E_2(t)}{2} e^{\left[\frac{j\pi v_2(t)}{V_\pi}\right]}, \tag{6}$$

where $E_i(t)$ and $E_2(t)$ are the optical fields at the upper and lower arms of the MZI,

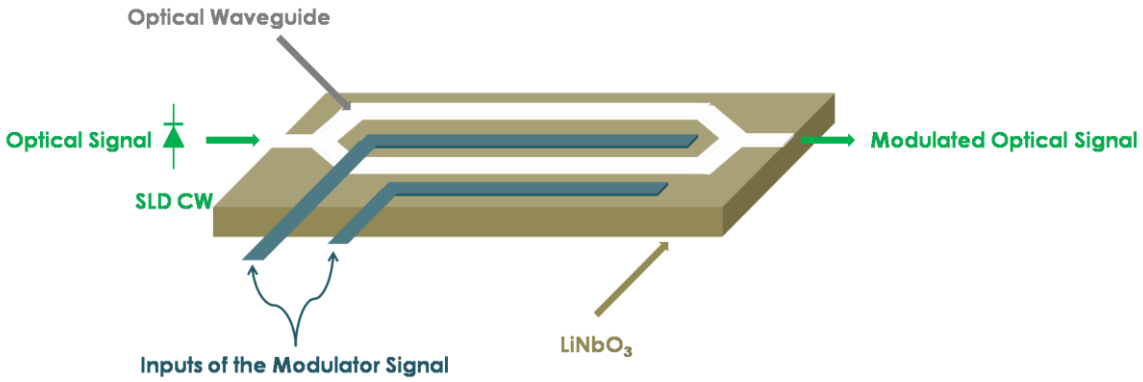

Figure 2.11: Structure and operating scheme of the MZI fabricated in LiNb0$_3$.

respectively, V_π is the parameter that causes a shift of π in the optical field phase in a given MZI arm (corresponding to a point of inflection in the transference curve of the optical field in the output) and, $v_1(t)$ and $v_2(t)$ are the applied phase modulation voltages.

2.3.1 ASK AND PSK MODULATION

The MZI structure can be used to implement basic to advanced modulation formats. A basic modulation format, which is widely used in networks is based on OOK. This signalizing technique is a specific case of ASK whereby the presence or absence of an optical field represents data bits "1" and "0", respectively. In this implementation, the representation of "1" data bits can be achieved without applying voltage to the MZI. Consequently, the relative phase of the signals in the MZI branches remains unchanged. Thus, after recombining the two signals that propagated in the branches, the wave added to the MZI input is restored. To represent the "0" data bits, in turn, the modulation voltages applied must produce a difference of phase π between the lower and upper MZI branches. The representations of OOK modulated data bits are shown in Figure 2.12.

For several years, the modulation format based on OOK has been the one used in optical communications. The main motivation for using it is the simplicity in both generation and detection, which is an intrinsic characteristic of IM-DD process. However, recent advances in photonic engineering have enabled the use of more sophisticated modulation formats than the ordinary OOK. Such techniques are classified as advanced modulation formats and can achieve simultaneously higher spectral and power efficiencies. There has been increasing interest in advanced modulation formats based on PSK to transmit one and several bits per symbol. For one bit per symbol, BPSK transmits the optical field signal for

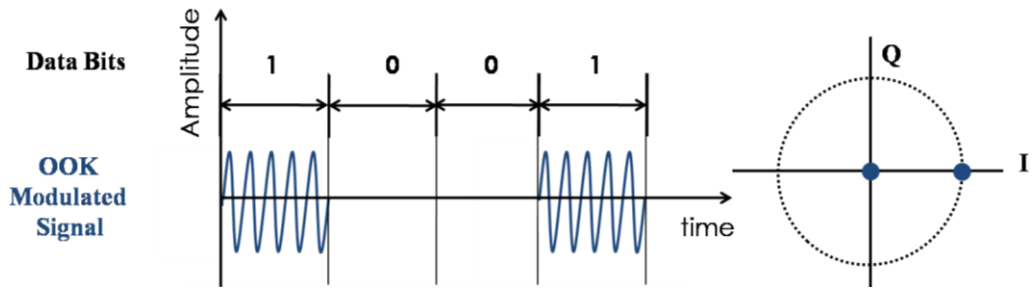

Figure 2.12: Representation of the OOK modulation format. a) Signal waveform of the modulated signal. b) Constellation diagram.

both the “1” and “0” data bits by changing the 0 and π phases, respectively. Considering this, the “1” data bits are represented by the constructive interference of the signals in the MZI arms when there is no difference of the relative phase, as in the above case. Nonetheless, the “0” data bit transmission is represented by the combination of the π phase shifted versions of

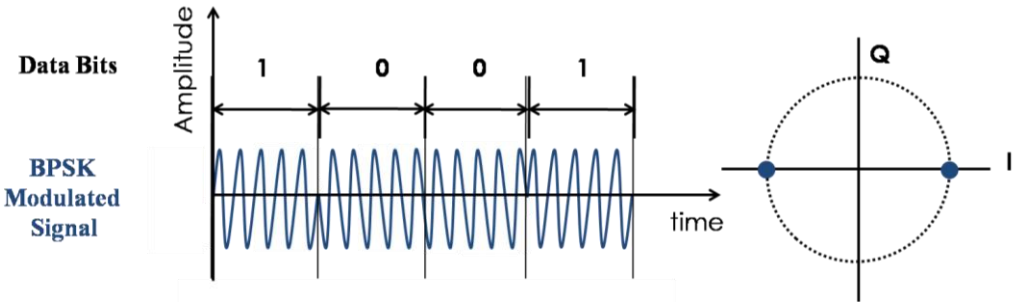

Figure 2.14: Representation of BPSK modulation format. a) Waveform of the modulated signal. b) Constellation diagram.

the signals in the branches. The BPSK modulated data bits are shown in Figure 2.13.

Another technique which also uses PSK modulation, but can represent the transmission of two bits with just one phase modulated waveform, is called QPSK. The modulator and its outputs waveforms are illustrated in Figure 2.14.

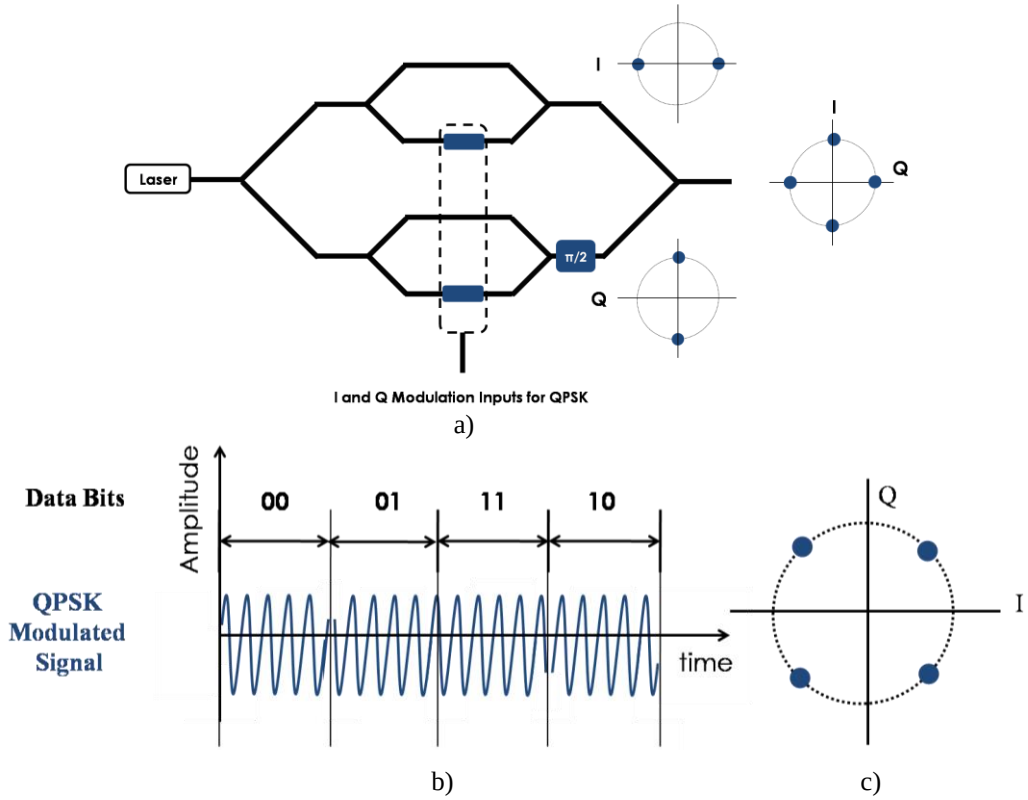

Figure 2.13: Structure of QPSK Modulator showing the In-Phase (I) and Quadrature-Channels (Q). a) QPSK modulator b) Data bits and their associated QPSK modulated signals c) Constellation diagram.

In this technique, each one of the four phases $\pi/4$, $3\pi/4$, $5\pi/4$ and $7\pi/4$ are assigned to represent the following pairs of bits 00, 01, 11 and 10, respectively.

Moreover, despite the $\pi/2$ phase difference between the signal waveforms, the amplitude of all the symbols is maintained constant (points on the circle in the constellation diagram). To implement, it requires a series of nested MZI components (known as super MZI), where the upper MZI forms the named in-phase (I) channel and the lower MZI (passing through a $\pi/2$ phase shifter) forms the quadrature (Q) channel.

2.3.2 ASK AND PSK DEMODULATION

The modifications carried out in signal waveforms by the modulation process must be removed at the receiver side in order to extract the data bit pattern of the sent information. There are several ways to carry out demodulation depending on how the baseband data signals are transmitted in the carrier signal. Moreover, the demodulation techniques can be either coherent or incoherent, according to whether the carrier phase information is needed or not, respectively. The ASK modulated signals can be demodulated using incoherent methods, since only is the comparison of the signal amplitude with the previously established threshold is required. In Figure 2.15, the demodulator for a network based on the OOK modulation format is shown. It should be remembered that OOK is a specific case of ASK when the optical field is not transmitted for "0" bit. In this case, a photodetector receives the optical signal and carries out the opto-electrical conversion, i.e., it generates an electrical current proportional to the optical field amplitude. Afterwards, the output level of the integrator is delivered to the optical decision device, which infers if the "0" or "1" data bits in its input are less or greater than the previously determined threshold, respectively. Finally, if the level in the input of the decision device is equal to the threshold, the decision concerning the sent bit

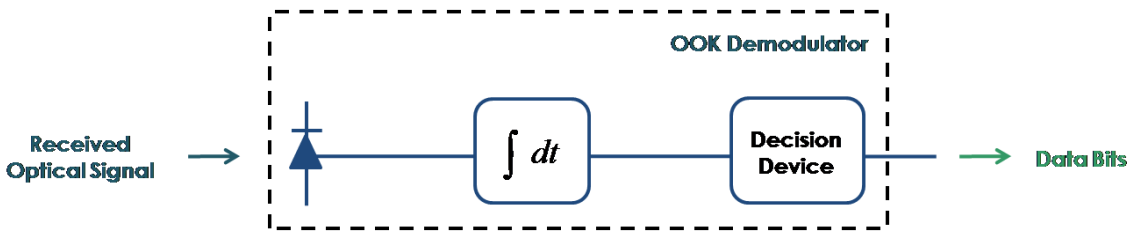

Figure 2.15: Demodulator for OOK symbols.

is made randomly. On the other hand, the coherent demodulation requires the phase information to be preserved to extract the data bits. Fortunately, there are some artifices to maintain the phase of the received signal after photodetection. One of the most used methods consists of using another signal to force the square detection followed by photodetection to carry out signal multiplication. In this simple scheme, shown in Figure 2.16, multiplication is carried out in a few steps. Firstly, the reference signal is generated and added to the phase modulated signal via a 3 dB coupler. Next, the sum of the optical signals is converted into the proportional electric current.

Then, the resultant electrical current in the photodetector can be written as

$$\begin{aligned} I_1(t) &= \Re \times \left\{ \left[\frac{E_{sig}(t)}{\sqrt{2}} + \frac{E_{LO}(t)}{\sqrt{2}} \right] \times \left[\frac{E_{sig}(t)}{\sqrt{2}} + \frac{E_{LO}(t)}{\sqrt{2}} \right]^* \right\} \\ &= \frac{\Re}{2} \times \left\{ \left| E_{sig}(t) \right|^2 + |E_{LO}(t)|^2 + Re\left[E_{sig}(t) {E_{LO}}^*(t) + {E_{sig}}^*(t) E_{LO}(t) \right] \right\}, \\ &= \frac{\Re}{2} \times \left[P_{sig}(t) + P_{LO}(t) + 2\sqrt{P_{sig}(t) P_{LO}(t)} \cos\left(2\pi \Delta_f + \Delta_\theta\right) \right] \end{aligned} \tag{7}$$

where $E_{sig}(t)$ and $E_{LO}(t)$ are the optical field of the modulated signal and LO signal, respectively, $P_{sig}(t)$ and $P_{LO}(t)$ are the instantaneous powers of the modulated signal and LO signal, respectively, $\Delta_f = f_{sig} - f_{LO}$ is the intermediary frequency, f_{sig} and f_{LO} are the frequency of the modulated signal and LO signal, respectively, $\Delta_\theta = \theta_{sig} - \theta_{LO}$ is the deviation of phase and, θ_{sig} and θ_{LO} are the phase of the modulated signal and LO signal, respectively. Note that the optical field amplitude $E(t)$ is normalized so that $|E(t)|^2$ gives the instantaneous power $P(t)$. Generally, the two first terms on the right hand side of (7) can be neglected, either because the LO signal is chosen to be much stronger than the signal or due to using balanced detection with the second port of a 3 dB coupler [75]. Balanced detection is preferred in practice due to its capacity of suppressing undesired signals (including possible

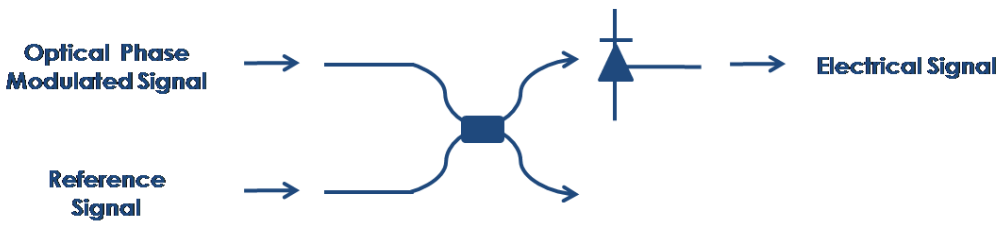

Figure 2.16: Demodulation of the phase modulated signal using a reference signal.

intensity noise generated by LO). For effective suppression of undesired signals, the second output port of the 3dB coupler should produce the difference between the modulated signal and the LO signal. Consequently, the photodetector located at the second port of the 3 dB coupler has the following electrical current in its output

$$\begin{aligned} I_2(t) &= \Re \times \left\{ \left[\frac{E_{sig}(t)}{\sqrt{2}} - \frac{E_{LO}(t)}{\sqrt{2}} \right] \times \left[\frac{E_{sig}(t)}{\sqrt{2}} - \frac{E_{LO}(t)}{\sqrt{2}} \right]^* \right\} \\ &= \frac{\Re}{2} \times \left\{ \left| E_{sig}(t) \right|^2 + |E_{LO}(t)|^2 - Re\left[E_{sig}(t) E_{LO}{}^*(t) + E_{sig}{}^*(t) E_{LO}(t) \right] \right\}, \\ &= \frac{\Re}{2} \times \left[P_{sig}(t) + P_{LO}(t) - 2\sqrt{P_{sig}(t) P_{LO}(t)} \cos\left(2\pi \Delta_f + \Delta_\theta \right) \right], \end{aligned} \tag{8}$$

Thus, the electrical current in the output of the balanced detection is given by

$$I(t) = I_1(t) - I_2(t) = \Re \times \left[2\sqrt{P_{sig}(t) P_{LO}(t)} \cos\left(2\pi \Delta_f + \Delta_\theta \right) \right], \tag{9}$$

Sequentially, as shown in Figure 2.17, the BPSK demodulator integrates the signal provided by the balanced detection, it compares the level obtained with the threshold and decides on the bit which is sent.

A similar scheme can be used to demodulate the QPSK signals which transport two bits simultaneously. In QPSK transmission, combinations of two bits are associated to phase modulated signals. These phase modulated signals can be represented by the sum of two orthogonal phase modulated signals, namely in- and quadrature signals. Moreover, each of the orthogonal signals is responsible for transporting one bit.

Consequently, demodulation is carried out using two independent channels identical to the BPSK demodulator, as shown in Figure. 2.18. As can be observed, the modulated

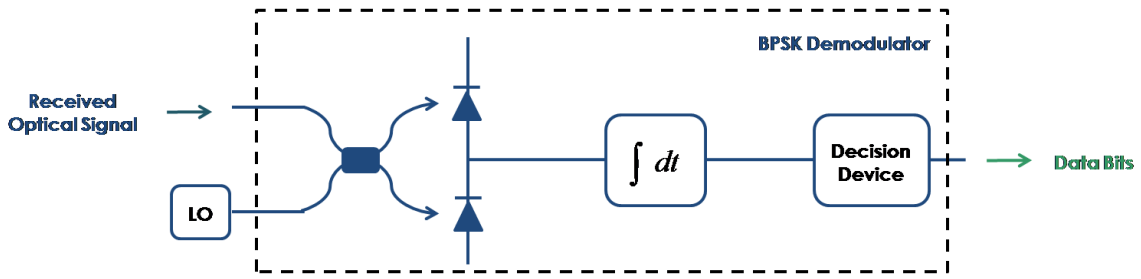

Figure 2.17 Demodulator for BPSK symbols.

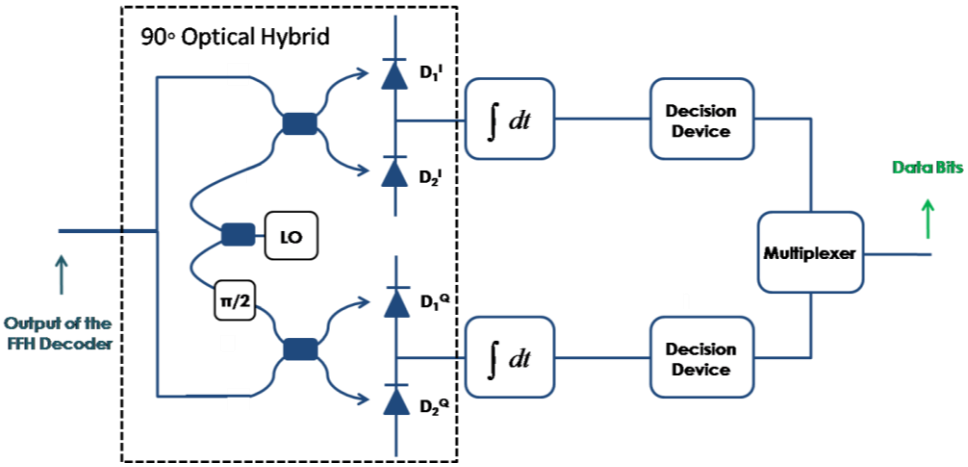

Figure 2.18: Demodulator for QPSK symbols.

phase signal is divided into two branches and multiplied by the LO signal. Note that due to the orthogonality between the components of the modulated phase signal, the LO signal should be added to the in-phase and quadrature in the upper and lower branches, respectively. Afterwards, the modulated phase signal and the two versions of the signal provided by LO are multiplied in the balanced detection of each branches. The operations are commonly achieved by 90°-hybrid devices (represented in the dashed square), couplers and fibers.

The electrical currents of the photodetectors (grouped in a balanced mode configuration) present in the in- and quadrature phase of transmitted signal, can be mathematically described as

$$\begin{bmatrix} I_1^I(t) \\ I_2^I(t) \\ I_1^Q(t) \\ I_2^Q(t) \end{bmatrix} = \begin{bmatrix} \Re \times \left| \frac{E_{sig}(t)}{2} + \frac{E_{LO}(t)}{2} \right|^2 \\ \Re \times \left| \frac{E_{sig}(t)}{2} - \frac{E_{LO}(t)}{2} \right|^2 \\ \Re \times \left| \frac{E_{sig}(t)}{2} + \frac{E_{LO}(t)}{2} e^{j\frac{\pi}{2}} \right|^2 \\ \Re \times \left| E_{sig}(t) - \frac{E_{LO}(t)}{2} e^{j\frac{\pi}{2}} \right|^2 \end{bmatrix}$$

$$= \begin{bmatrix} \frac{\Re}{4} \times \left\{ \left| E_{sig}(t) \right|^2 + |E_{LO}(t)|^2 + Re\left[E_{sig}(t) E_{LO}{}^*(t) + E_{sig}{}^*(t) E_{LO}(t) \right] \right\} \\ \frac{\Re}{4} \times \left\{ \left| E_{sig}(t) \right|^2 + |E_{LO}(t)|^2 - Re\left[E_{sig}(t) E_{LO}{}^*(t) + E_{sig}{}^*(t) E_{LO}(t) \right] \right\} \\ \frac{\Re}{4} \times \left\{ \left| E_{sig}(t) \right|^2 + |E_{LO}(t)|^2 + Im\left[E_{sig}(t) E_{LO}{}^*(t) e^{-j\frac{\pi}{2}} + E_{sig}{}^*(t) E_{LO}(t) e^{j\frac{\pi}{2}} \right] \right\} \\ \frac{\Re}{4} \times \left\{ \left| E_{sig}(t) \right|^2 + |E_{LO}(t)|^2 - Im\left[E_{sig}(t) E_{LO}{}^*(t) e^{-j\frac{\pi}{2}} + E_{sig}{}^*(t) E_{LO}(t) e^{j\frac{\pi}{2}} \right] \right\} \end{bmatrix}$$

$$= \begin{bmatrix} \frac{\Re}{4} \times \left[P_{sig}(t) + P_{LO}(t) + 2\sqrt{P_{sig}(t)P_{LO}(t)} \cos\left(2\pi\Delta_f + \Delta_\theta\right) \right] \\ \frac{\Re}{4} \times \left[P_{sig}(t) + P_{LO}(t) - 2\sqrt{P_{sig}(t)P_{LO}(t)} \cos\left(2\pi\Delta_f + \Delta_\theta\right) \right] \\ \frac{\Re}{4} \times \left[P_{sig}(t) + P_{LO}(t) + 2\sqrt{P_{sig}(t)P_{LO}(t)} \sin\left(2\pi\Delta_f + \Delta_\theta\right) \right] \\ \frac{\Re}{4} \times \left[P_{sig}(t) + P_{LO}(t) - 2\sqrt{P_{sig}(t)P_{LO}(t)} \sin\left(2\pi\Delta_f + \Delta_\theta\right) \right] \end{bmatrix}, \quad (10)$$

After the balanced detection, the electrical currents at the decision variable can be written as

$$I^I(t) = I_1^I(t) - I_2^I(t) = \Re \times \sqrt{P_{sig}(t)P_{LO}(t)} \cos\left(2\pi\Delta_f + \Delta_\theta\right), \quad (11)$$

and

$$I^Q(t) = I_1^Q(t) - I_2^Q(t) = \Re \times \sqrt{P_{sig}(t)P_{LO}(t)} \sin\left(2\pi\Delta_f + \Delta_\theta\right), \quad (12)$$

Finally, each channel takes a decision concerning the bit sent and the two generated bits are serially transmitted by the multiplexer.

CHAPTER 3

3 MATHEMATICAL FORMALISM

In this section, a detailed description of FFH-OCDMA networks based on coherent advanced QPSK or BPSK modulation formats, the two modulation formats considered in this thesis, is presented (see Figure 3.1).

3.1 DESCRIPTION OF THE PROPOSED FFH-OCDMA NETWORKS

At the transmitter side, the data information bits from each user (green blocks) are QPSK/BPSK modulated. Sequentially, the optical pulses are simultaneously encoded in sequential time slots and disjoint wavelength subbands by the FFH encoder (blue blocks).

Therefore, a unique code sequence, in which each chip signaling interval occupies one wavelength slot, is assigned to each user. After attributing code sequences to users, the next step is to access the fiber channel, which is provided by the passive combiner. Here, it is considered that all optical fiber impairments are appropriately compensated. Despite the ideal channel characteristics, the simple superposition of users' signals in the combiner produces MAI, which is delivered to each user by the splitter. As well known, MAI severely affects the data recovery at the receiver side. However, when the wavelength translation introduced at the transmitter is removed by the FFH decoder (blue blocks), only the additional energy

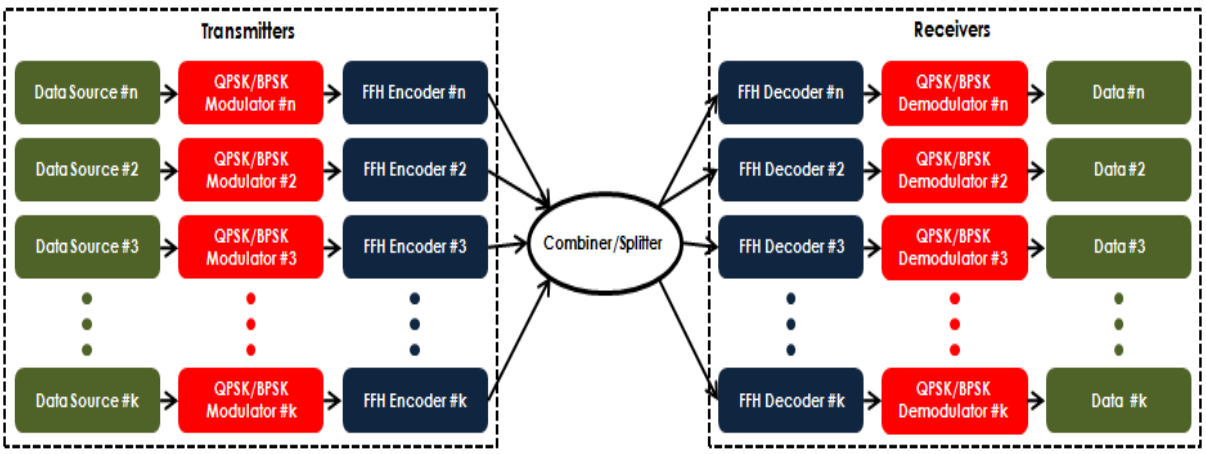

Figure 3.1: Block diagram of the proposed FFH-OCDMA based on the QPSK or BPSK modulation formats.

generated by the MAI within the chip period at which the autocorrelation peak is formed has an impact on the overall network performance. Then, the decoded information (along with MAI) is sent to the demodulation unit.

Finally, as well as the conventional function of detecting the transmitted information data bits, the proposed QPSK and BPSK demodulators (red blocks) also increase the SIR before recovering the data (green blocks). Such functions can be better understood by analyzing the QPSK and BPSK formats in modulation and demodulation processes, which will be addressed in the following sections.

3.1.1 QPSK MODULATED NETWORK

For the QPSK modulation format, the carrier phase is shifted of $\pi/2$. Four values are assigned to the carrier phase, namely $\pi/4$, $3\pi/4$, $5\pi/4$ and $7\pi/4$. In the demodulator unit shown in Figure 3.2, one reference signal is generated locally, which is the desired user signal in the demodulator. Specifically, the reference signal is a replica of the desired decoded user signal exempt from MAI, i.e., the autocorrelation signal of the desired user. It can be generated by adding one incoming broadband pulse sequentially to the desired user's FFH encoder and FFH decoder. Sequentially, the output signal of the FFH decoder and the reference signal provided by the LO are inserted into the 90° optical hybrid. A commercially available implementation of the optical hybrid consists of a photonic integrated circuit composed by one 2×4 multimode interference (MMI) structure and four photodetectors [78]-[80], as shown in the dashed box in Figure 3.2. The MMI circuit is composed by optical couplers interconnected in such a way to present four distinct vectorial additions of the received and LO signals. Moreover, the two MMI in-phase (I) outputs are proportional to the sum and subtraction between the signals, while the other two quadrature-phase (Q) outputs perform the same operations, but after the LO signal undergo a $\pi/2$ phase shift. Once the I and Q components of the received signal are discriminated, the balanced detection amplifies the desired signal (generated by the square-law detection) in each component while suppresses all other signals.

Next, the resulting signals are integrated. This sequence of operations amplifies significantly the SIR at the desired user receiver. As result, the combined interfering chip pulses are less likely to reproduce the auto-correlation signal (and thus to exceed the

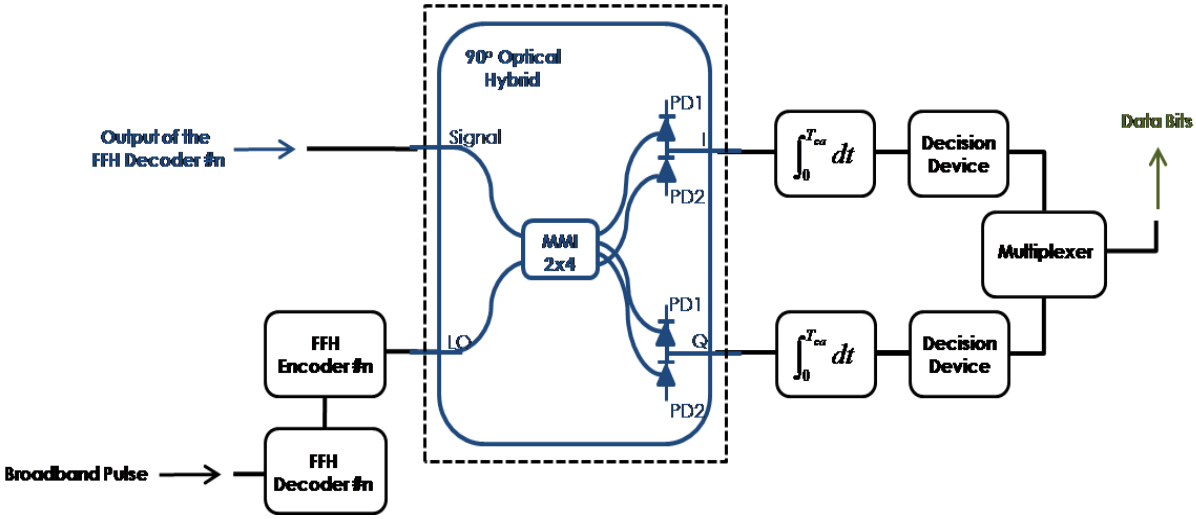

Figure 3.2: – Proposed QPSK demodulator for the FFH-OCDMA networks.

threshold for error detection) than in an OOK-based network. Therefore, this process accounts for increasing the SIR when compared with the legacy OOK-based FFH-OCDMA networks.

Afterwards, the bit decision in each channel is made based on the comparison between the integrator output level with a threshold level previously established. Finally, since each channel infers over only one bit, the multiplexer combines the bits serially to restore the original two bits sent by the transmitter.

3.1.2 BPSK Modulated Network

In the BPSK modulation format, the most basic form of PSK, the users transmit data bits "1" and "0" using carriers of phase 0 and π, respectively [47]. Information data bits can be detected using a demodulation scheme such as shown in Figure 3.3. Although the decision of a single bit does not require the *Q* components of the received signal, the same photonic integrated circuit (with one 90° optical hybrid and four balanced photodetectors) is also adopted here. In this case, the signal present in the output of the FFH decoder is mixed with a reference signal generated locally. As previously discussed, the reference signal is the desired user's auto-correlation signal generated by the sequential operation of encoding and decoding of the broadband pulse. Consecutively, with the mixing operation realized in the 90° optical

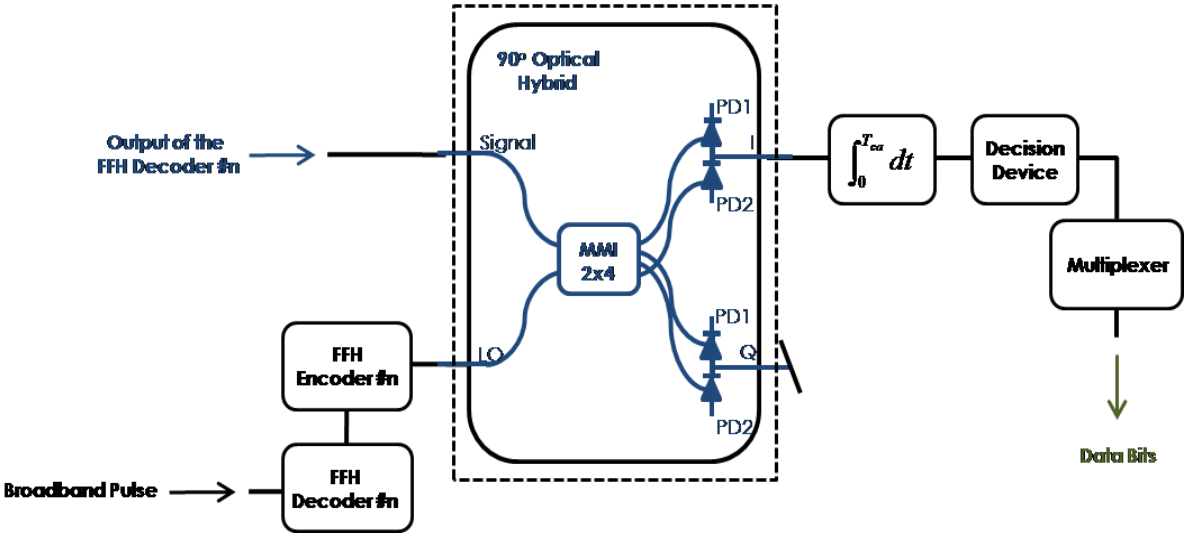

Figure 3.3:– Proposed BPSK demodulator for the FFH-OCDMA networks.

hybrid, the signal is integrated and further compared with the fixed threshold. Thus, if the integrator output remains below or exceeds the throughput level, the decision is made by data bit "0" or 1", respectively.

3.2 MODELING OF THE NETWORKS

3.2.1 QPSK MODULATION FORMAT

In QPSK modulation, the information bits are represented by $\pi/2$ phase shifts of the optical field. With four distinct phases, QPSK can transmit two information bits per symbol [48]. When the QPSK modulation format is applied to FFH-OCDMA, each information bit from *m* users is encoded into a code sequence as

$$c_{QPSK_m}(t,\theta_b) = \sum_{l=1}^{L} p\left(\frac{t-lT_c}{T_{c0}}\right) e^{j(\omega_l t+\theta_b)}, \tag{13}$$

where $\theta_b \in \{\pi/4, 3\pi/4, 5\pi/4, 7\pi/4\}$ is the phase associated to the data bit, L is the code length, $p(t)$ is the chip signaling waveform, T_c is the chip period, T_{c0}=T_c/f_c is the half width

of the pulse, f_c is the pulse compression factor, and ω_l is the $l-$th chip's wavelength. Here, the optical field amplitude $c_{QPSK_m}(t,\theta_b)$ is normalized so that $\left|c_{QPSK_m}(t,\theta_b)\right|^2$ gives the instantaneous power [81].

At the receiver side, the composed users' signal is applied to a matched filter with impulse response $h_n(t)$ given by the inverse Fourier transform of the reflectivity spectrum of the gratings. In all simulations, the encoders and decoders were modeled using multiple apodized fiber Bragg gratings ($sinc$ reflectivity profile) via the transfer matrix method [82]. Hence, the desired user decoder n outputs an optical autocorrelation signal given by

$$E_{ac\_QPSK_n}(t,\theta_b) = \int_{-\infty}^{\infty} c_{QPSK_n}(\tau,\theta_b) h_n(\tau - t)\, d\tau, \tag{14}$$

where $-L+1 \le \tau \le L-1$ is the chip delay.

A similar expression can be obtained for the optical cross-correlation signal between the n and k users, which reads as

$$E_{cc\_QPSK_{n,k}}(t,\theta_b) = \int_{-\infty}^{\infty} c_{QPSK_k}(\tau,\theta_b) h_n(\tau - t)\, d\tau. \tag{15}$$

Assuming that there are K interfering active users transmitting signals in the network, the received optical field at the decoder output of the desired user n is

$$E_{QPSK_n}(t,\theta_b) = E_{ac\_QPSK_n}(t,\theta_b) + \sum_{k=1\ (k\neq n)}^{K} E_{cc\_QPSK_{n,k}}(t-\tau_k,\theta_b), \tag{16}$$

where τ_k is the relative network transit delay of the k-th interferer.

After decoding, the demodulation process is initiated by inserting both received and LO signals into the 90° optical hybrid. Once in the optical hybrid (and assuming the received and the LO signals as co-polarized) the MMI produces the following signal combinations in the I outputs

$$E_{PD1_n}^{I}(t) = \frac{1}{2}\left[E_{QPSK_n}(t,\theta_b) + E_{LO_n}(t)\right] \tag{17}$$

and

$$E_{PD2_n}^{I}(t) = \frac{1}{2}\left[E_{QPSK_n}(t,\theta_b) - E_{LO_n}(t)\right], \tag{18}$$

The *Q* channel output, in turn, are given by

$$E_{PD1_n}^{Q}(t) = \frac{1}{2}\left[E_{QPSK_n}(t,\theta_b) + E_{LO_n}(t)e^{j\pi/2}\right] \tag{19}$$

and

$$E_{PD2_n}^{Q}(t) = \frac{1}{2}\left[E_{QPSK_n}(t,\theta_b) - E_{LO_n}(t)e^{j\pi/2}\right], \tag{20}$$

where

$$E_{LO_n}(t) = E_{ac\_QPSK_n}(t,0), \tag{21}$$

is the LO signal. Afterwards, each photodetector converts the optical field signals into electric currents. In this step, the square detection performs the mixing between the received and LO signals. Then, the electric current output of the square-law photodetectors at the *I* channel are given by

$$\begin{aligned} i_{PD1_n}^{I}(t) &= \Re \times \left[E_{PD1_n}^{I}(t) \times {E_{PD1_n}^{I}}^{*}(t)\right] \\ &= \frac{\Re}{4} \times \left\{P_{QPSK_n} + Re\left[{E_{QPSK_n}}^{*}(t,\theta_b)E_{LO_n}(t)\right.\right. \\ &\quad \left.\left. + E_{QPSK_n}(t,\theta_b){E_{LO_n}}^{*}(t)\right] + P_{LO_n}\right\} \end{aligned} \tag{22}$$

and

$$
\begin{aligned}
i_{PD2_n}^{I}(t) &= \Re \times \left[E_{PD2_n}^{I}(t) \times {E_{PD2_n}^{I}}^{*}(t)\right] \\
&= \frac{\Re}{4} \times \Big\{P_{QPSK_n} - Re\Big[{E_{QPSK_n}}^{*}(t,\theta_b) E_{LO_n}(t) \\
&+ E_{QPSK_n}(t,\theta_b) {E_{LO_n}}^{*}(t)\Big] + P_{LO_n}\Big\}
\end{aligned} \tag{23}
$$

Analogously, the electric current output of the square-law photodetectors at the *Q* channel are given by

$$
\begin{aligned}
i_{PD1_n}^{Q}(t) &= \Re \times \left[E_{PD1_n}^{Q}(t) \times {E_{PD1_n}^{Q}}^{*}(t)\right] \\
&= \frac{\Re}{4} \times \Big\{P_{QPSK_n} + Im\Big[{E_{QPSK_n}}^{*}(t,\theta_b) E_{LO_n}(t) e^{j\pi/2} \\
&+ E_{QPSK_n}(t,\theta_b) {E_{LO_n}}^{*}(t) e^{-j\pi/2}\Big] + P_{LO_n}\Big\},
\end{aligned} \tag{24}
$$

and

$$
\begin{aligned}
i_{PD2_n}^{Q}(t) &= \Re \times \left[E_{PD2_n}^{Q}(t) \times {E_{PD2_n}^{Q}}^{*}(t)\right] \\
&= \frac{\Re}{4} \times \Big\{P_{QPSK_n} - Im\Big[{E_{QPSK_n}}^{*}(t,\theta_b) E_{LO_n}(t) e^{j\pi/2} \\
&+ E_{QPSK_n}(t,\theta_b) {E_{LO_n}}^{*}(t) e^{-j\pi/2}\Big] + P_{LO_n}\Big\},
\end{aligned} \tag{25}
$$

where $\mathcal{R}e[\cdot]$ and $Im[\cdot]$ denote the real and the imaginary part, respectively, $\Re$ is the photodetector responsivity, P_{QPSK_n} and P_{LO_n} are the received and LO instantaneous signal powers, respectively. However, the interaction between the signals also creates undesired signals, which can be overcome with the balanced detection arrangement. Finally, the electric current of the mixed signal after balanced detection at the *I*- and *Q* channels are given, respectively, by

$$
\begin{aligned}
i_n^I(t) &= i_{PD1_n}^{I}(t) - i_{PD2_n}^{I}(t) \\
&= \mathcal{R}e\left\{\frac{\Re}{2} \times \left[{E_{QPSK_n}}^{*}(t,\theta_b) E_{LO_n}(t) + E_{QPSK_n}(t,\theta_b) {E_{LO_n}}^{*}(t)\right]\right\}
\end{aligned} \tag{26}
$$

and

$$i_n^Q(t) = i_{PD1_n}^Q(t) - i_{PD2_n}^Q(t)$$
$$= Im\left\{\frac{\Re}{2} \times \left[{E_{QPSK_n}}^*(t,\theta_b)E_{LO_n}(t)e^{j\pi/2} + E_{QPSK_n}(t,\theta_b){E_{LO_n}}^*(t)e^{-j\pi/2}\right]\right\} \quad (27)$$

Thus, the signal phase is implicitly maintained in this expression as long as the LO and the received optical field are multiplied at the decoder output. After this operation the integration and comparison of the resulting signal can occur.

Therefore, the decision variables at the *I* and *Q* channels in the desired user's receiver are denoted by

$$Z_{QPSK_n}^I = \int_{T_{ca}} i_n^I(t)dt$$
$$= \mathcal{R}e\left\{\frac{\Re}{2} \times \left[\int_{T_{ca}} \left({E_{ac\_QPSK_n}}^*(t,\theta_b)E_{LO_n}(t) + E_{ac\_QPSK_n}(t,\theta_b){E_{LO_n}}^*(t)\right)dt\right.\right.$$
$$+ \frac{1}{2}\sum_{k=1\ (k\neq n)}^{K} \int_{T_{ca}} \left({E_{cc\_QPSK_{n,k}}}^*(t-\tau_k,\theta_b)E_{LO_n}(t)\right.$$
$$\left.\left.\left. + E_{cc\_QPSK_{n,k}}(t-\tau_k,\theta_b){E_{LO_n}}^*(t)\right)dt\right]\right\} \quad (28)$$

and

$$Z_{QPSK_n}^Q = \int_{T_{ca}} i_n^Q(t)dt$$
$$= Im\left\{\frac{\Re}{2} \times \left[\int_{T_{ca}} \left({E_{ac\_QPSK_n}}^*(t,\theta_b)E_{LO_n}(t)e^{j\pi/2}\right.\right.\right.$$
$$\left. + E_{ac\_QPSK_n}(t,\theta_b){E_{LO_n}}^*(t)e^{-j\pi/2}\right)dt$$
$$+ \frac{1}{2}\sum_{k=1\ (k\neq n)}^{K} \int_{T_{ca}} \left({E_{cc\_QPSK_{n,k}}}^*(t-\tau_k,\theta_b)E_{LO_n}(t)\,e^{j\pi/2}\right.$$
$$\left.\left.\left. + E_{cc\_QPSK_{n,k}}(t-\tau_k,\theta_b){E_{LO_n}}^*(t)e^{-j\pi/2}\right)dt\right]\right\}. \quad (29)$$

The $1/2$ factor in the second term of both (28) and (29) is necessary to eliminate the redundancy of the negative frequency components in the decision variable, once that the frequency of MAI emitted by each interfering user is always lower than the frequency of the signal. Note that in both (28) and (29), the first integral is the desired user's signal while the second integral is the MAI.

3.2.2 BPSK MODULATION FORMAT

In BPSK modulation, the simplest form of PSK modulation, the information bits are represented by π phase shifts of the optical field. When the BPSK modulation format is applied to FFH-OCDMA, each information bit from the m users is encoded into a code sequence as

$$c_{BPSK_m}(t,\theta_b) = \sum_{l=1}^{L} p\left(\frac{t-lT_c}{T_{c0}}\right) e^{j(\omega_l t+\theta_b)}, \tag{30}$$

where $\theta_b \in \{0, \pi\}$ is the phase associated to the information bit. In addition, due to the $\pi/2$ offset between two adjacent QPSK symbols, both *I* and *Q* channels can be regarded as BPSK signals. Thus, without any loss of generality, the BPSK mathematical formalism is written by modifying only the QPSK *I* channel equations (presented in the previous section). For convenience sake, the acronym *I* will be omitted. Yet, the same waveform parameters, encoders and decoder impulse response (transfer functions) of the previous scenario are maintained. At the receiver's side, assuming *K* interfering active users transmitting signals in the network, the received optical field at the decoder output of the desired user n will be

$$E_{BPSK_n}(t,\theta_b) = E_{ac\_BPSK_n}(t,\theta_b) + \sum_{k=1\ (k\neq n)}^{K} E_{cc\_BPSK_{n,k}}(t-\tau_k,\theta_b), \tag{31}$$

where the decoder of the desired user n outputs an auto-correlation optical signal given by

$$E_{ac\_BPSK_n}(t,\theta_b) = \int_{-\infty}^{\infty} c_{BPSK_n}(\tau,\theta_b)h_n(\tau - t)\,d\tau, \tag{32}$$

A similar expression can be obtained for the optical cross-correlation signal between the n and k users, which reads

$$E_{cc\_BPSK_{n,k}}(t,\theta_b) = \int_{-\infty}^{\infty} c_{BPSK_k}(\tau,\theta_b)h_n(\tau - t)\,d\tau. \tag{33}$$

Similarly, as in previous section, the output current after the balanced detection is

$$\begin{aligned} i_n\,(t) &= i_{PD1_n}(t) - i_{PD2_n}(t) \\ &= \mathcal{R}e\left\{\frac{\Re}{2} \times \left[{E_{BPSK_n}}^*(t,\theta_b)E_{LO_n}(t) + E_{BPSK_n}(t,\theta_b){E_{LO_n}}^*(t)\right]\right\}. \end{aligned} \tag{34}$$

Therefore, the detection of the BPSK system produces the following decision variable

$$\begin{aligned} Z_{BPSK_n} &= \int_{T_{ca}} i_n\,(t)dt \\ &= \mathcal{R}e\left\{\frac{\Re}{2} \times \left[\int_{T_{ca}} \left({E_{ac\_BPSK_n}}^*(t,\theta_b)E_{LO_n}(t) + E_{ac\_BPSK_n}(t,\theta_b){E_{LO_n}}^*(t)\right)dt\right.\right. \\ &+ \frac{1}{2}\sum_{k=1\ (k\neq n)}^{K} \int_{T_{ca}} \left({E_{cc\_BPSK_{n,k}}}^*(t-\tau_k,\theta_b)E_{LO_n}(t)\right. \\ &\left.\left. + E_{cc\_BPSK_{n,k}}(t-\tau_k,\theta_b){E_{LO_n}}^*(t)\right)dt\right]\Bigg\}, \end{aligned} \tag{35}$$

where the LO signal is given by

$$E_{LO_n}(t) = E_{ac\_BPSK_n}(t,0), \tag{36}$$

Again, the $1/2$ factor is necessary to eliminate the redundancy of the negative frequency components in the decision variable since the frequency of MAI emitted by each interfering user is always lower than the frequency of the signal. In addition, note that in (35) the first integral is the desired user's signal while the second integral is the MAI.

3.2.3 OOK MODULATION FORMAT

The OOK is a particular case of ASK modulation format which represents the data as the presence or absence of optical field. When the OOK modulation format is applied to FFH-OCDMA network, each information bit from the m users is encoded into a code sequence as

$$c_{OOK_m}(t) = b_m \sum_{l=1}^{L} p\left(\frac{t - lT_c}{T_{c0}}\right) e^{j\,\omega_l t}, \tag{37}$$

where $b_m \in \{0, 1\}$ is the value associated to the information bit. In addition, once each waveform represents one bit transmission, the OOK mathematical formalism can be written by modifying the BPSK equations (presented in the previous section). Also, the same waveform parameters, encoders and decoder impulse response (transfer functions) of the previous scenario are maintained. At the receiver's side, assuming *K* interfering active users transmitting signals in the network, the received optical field at the decoder output of the desired user n will be

$$E_{OOK_n}(t) = E_{ac\_OOK_n}(t) + \sum_{k=1\ (k\neq n)}^{K} E_{cc\_OOK_{n,k}}(t - \tau_k), \tag{38}$$

where the decoder of the desired user n outputs an auto-correlation optical signal given by

$$E_{ac\_OOK_n}(t) = \int_{-\infty}^{\infty} c_{OOK_n}(\tau) h_n(\tau - t)\, d\tau, \tag{39}$$

A similar expression can be obtained for the optical cross-correlation signal between the n and k users, which reads

$$E_{cc\_OOK_{n,k}}(t) = \int_{-\infty}^{\infty} c_{OOK_k}(\tau) h_n(\tau - t)\, d\tau. \tag{40}$$

In this case, it is realized the conventional detection from received optical field at the decoder output. Therefore, the output current after the decoding operation is

$$i_n\,(t) = \mathcal{R}e\{\Re \times [E_{OOK_n}(t, \theta_b) {E_{OOK_n}}^*(t, \theta_b)]\} \tag{41}$$

Therefore, the detection of the OOK system produces the following decision variable

$$\begin{aligned} Z_{OOK_n} &= \int_{T_{ca}} i_n\,(t) dt \\ &= \mathcal{R}e\Bigg\{\Re \times \Bigg[\int_{T_{ca}} E_{ac\_OOK_n}(t) {E_{ac\_OOK_n}}^*(t) dt \\ &+ \sum_{k=1\ (k\neq n)}^{K} \int_{T_{ca}} E_{cc\_OOK_{n,k}}(t-\tau_k) {E_{cc\_OOK_{n,k}}}^*(t-\tau_k) dt \\ &+ \frac{1}{2} \int_{T_{ca}} \big(E_{ac\_OOK_n}(t) {E_{cc\_OOK_{n,k}}}^*(t-\tau_k) \\ &+ {E_{ac\_OOK_n}}^*(t) E_{cc\_OOK_{n,k}}(t-\tau_k) \big)\, dt \Bigg] \Bigg\} \end{aligned} \tag{42}$$

Again, the $1/2$ factor is necessary to eliminate the redundancy of the negative frequency components in the decision variable since the frequency of MAI emitted by each interfering user is always lower than the signal frequency. Also, note in (42) that the first term is the desired user's signal, and the other terms accounts for the MAI.

3.3 BIT ERROR RATE (BER)

In this section, the mathematical framework for assessing the performance of both single and multirate FFH-OCDMA networks illustrated in Figure 3.1 is presented. Note that the block diagram shown is generalized enough to consider both scenarios: 1) the same modulation format is assigned to all users (single rate network) and 2) a different modulation format is assigned to each users' group or class (multirate network).

For convenience sake, only the full detailed expressions for the QPSK are shown. Nonetheless, the new equations and necessary substitutions in the *I* and *Q* channel equations for performance evaluation of BPSK-based networks are clearly given and indicated.

Remarkably, the proposed formalism can also be used to evaluate legacy FFH-OCDMA networks based on OOK modulation formats through appropriate parameter substitutions. In addition, such substitutions are made and explicitly given to the reader in this section.

3.3.1 SINGLE RATE NETWORKS

3.3.1.1 QPSK MODULATION FORMAT

The BER formalism explicitly requires the decision variables of the desired user to be defined in terms of auto- and cross-correlation signals. Therefore, both (28) and (29) can be rewritten as

$$\mu_{QPSK_n}^{I,Q} = \mu_{QPSK_{ac}}^{I,Q} + \mu_{QPSK_{MAI}}^{I,Q}, \tag{43}$$

where the equations associated to the *I* channel are given by

$$\mu_{QPSK_{ac}}^{I} = \mathcal{R}e\left\{\frac{\Re}{2} \times \left[\int_{T_{ca}} \left(E_{ac\_QPSK_n}{}^{*}(t,\theta_b)E_{LO_n}(t) + E_{ac\_QPSK_n}(t,\theta_b)E_{LO_n}{}^{*}(t)\right) dt\right]\right\}, \tag{44}$$

and

$$\mu_{QPSK_{MAI}}^{I} = \mathcal{R}e\left\{\frac{\Re}{4}\times\left[\sum_{k=1\ (k\neq n)}^{K}\int_{T_{ca}}\left(E_{cc\_QPSK_{n,k}}{}^{*}(t-\tau_k,\theta_b)E_{LO_n}(t)\right.\right.\right.$$
$$\left.\left.\left.+E_{cc\_QPSK_{n,k}}(t-\tau_k,\theta_b)E_{LO_n}{}^{*}(t)\right)dt\right]\right\}, \tag{45}$$

The equations associated to the *Q* channel, by their turn, can be expressed as

$$\mu_{QPSK_{ac}}^{Q} = Im\left\{\frac{\Re}{2}\times\left[\int_{T_{ca}}\left(E_{ac\_QPSK_n}{}^{*}(t,\theta_b)E_{LO_n}(t)e^{j\pi/2}\right.\right.\right.$$
$$\left.\left.\left.+E_{ac\_QPSK_n}(t,\theta_b)E_{LO_n}{}^{*}(t)e^{-j\pi/2}\right)dt\right]\right\}, \tag{46}$$

and

$$\mu_{QPSK_{MAI}}^{Q} = Im\left\{\frac{\Re}{4}\times\left[\sum_{k=1\ (k\neq n)}^{K}\int_{T_{ca}}\left(E_{cc\_QPSK_{n,k}}{}^{*}(t-\tau_k,\theta_b)E_{LO_n}(t)e^{j\pi/2}\right.\right.\right.$$
$$\left.\left.\left.+E_{cc\_QPSK_{n,k}}(t-\tau_k,\theta_b)E_{LO_n}{}^{*}(t)e^{-j\pi/2}\right)dt\right]\right\}, \tag{47}$$

with $\mu_{QPSK_n}^{I,Q}$ representing the decision variable, and $\mu_{QPSK_{ac}}^{I,Q}$ and $\mu_{QPSK_{MAI}}^{I,Q}$ representing the contributions of the autocorrelation and cross-correlation signals to decision variable, respectively.

In addition, as the interfering users are statistically independent, it is convenient to express the cross-correlation signal level when only two interfering users transmit simultaneously. Thus, the instantaneous MAI power in the *j* interfering user's receiver when the *k* interfering user transmits data at the *I* and *Q* channels are given, respectively, by

$$\mu_{QPSK_{MAI}{}_{j,k}}^{I} = \mathcal{R}e\left\{\frac{\Re}{4}\times\left[\int_{T_{ca}}\left(E_{cc\_QPSK_{j,k}}{}^{*}(t-\tau_k,\theta_b)E_{LO_j}(t)\right.\right.\right.$$
$$\left.\left.\left.+E_{cc\_QPSK_{j,k}}(t-\tau_k,\theta_b)E_{LO_j}{}^{*}(t)\right)dt\right]\right\}, \tag{48}$$

and

$$\mu_{QPSK_{MAI}\,j,k}^{Q} = Im\left\{\frac{\Re}{4}\times\left[\int_{T_{ca}}\left(E_{cc\_QPSK_{j,k}}{}^{*}(t-\tau_k,\theta_b)E_{LO_j}(t)e^{j\pi/2}\right.\right.\right.$$
$$\left.\left.\left.+\,E_{cc\_QPSK_{j,k}}(t-\tau_k,\theta_b)E_{LO_j}{}^{*}(t)e^{-j\pi/2}\right)dt\right]\right\}, \tag{49}$$

First, since it is not known which coded symbols will be active at any given time, an average calculation ($\overline{\mu_{QPSK_{MAI}\,j,k}^{I,Q}}$) considering all possible coded symbols and random-access delay of every user is required [65]. Therefore, the interference variance becomes,

$$\sigma^{2}_{QPSK_{MAI}\,j,k}{}^{I,Q} = \left(\mu_{QPSK_{MAI}\,j,k}^{I,Q} - \overline{\mu_{QPSK_{MAI}\,j,k}^{I,Q}}\right)^{2}. \tag{50}$$

Similarly, the average interference variance of all users is denoted by $\overline{\sigma^{2}_{QPSK_{MAI}}{}^{I,Q}} = \overline{\sigma^{2}_{QPSK_{MAI}\,j,k}{}^{I,Q}}$. By considering the occurrence of data bits "0" and "1" to be independent variables and that their probability density functions (*pdfs*) can be represented by Gaussian functions, the error probabilities conditioned to decision variables of the desired user in QPSK networks are given, respectively, by

$$Pr\left(Z_{QPSK_n}^{I,Q} = 1 \geq \gamma/0\right) = \int_{\gamma}^{\infty}\frac{1}{\sqrt{2\pi}\sigma_0^{I,Q}}e^{\left[-\frac{\left(Z_{QPSK\,n}^{I,Q}-\mu_0^{I,Q}\right)^2}{2\sigma_0^{2\,I,Q}}\right]}dZ_{QPSK_n}^{I,Q} \tag{51}$$

and

$$Pr\left(Z_{QPSK_n}^{I,Q} = 0 < \gamma/1\right) = \int_{-\infty}^{\gamma}\frac{1}{\sqrt{2\pi}\sigma_1^{I,Q}}e^{\left[-\frac{\left(Z_{QPSK\,n}^{I,Q}-\mu_1^{I,Q}\right)^2}{2\sigma_1^{2\,I,Q}}\right]}dZ_{QPSK_n}^{I,Q}, \tag{52}$$

where γ is the general threshold level, $\mu_0^{I,Q}$ and $\sigma_0^{2\,I,Q}$ are, respectively, the mean and variance associated to bit "0" transmission, and $\mu_1^{I,Q}$ and $\sigma_1^{2\,I,Q}$ are, respectively, the mean and variance associated to bit "1" transmission. Consequently, the BER can be written as

$$BER_{QPSK_n}^{I,Q} = P(0)Pr\left(Z_{QPSK_n}^{I,Q} = 1 \geq \gamma/0\right) + P(1)Pr\left(Z_{QPSK_n}^{I,Q} = 0 < \gamma/1\right), \quad (53)$$

where $P(0)$ and $P(1)$ are the transmission probabilities of bits "0" and "1", respectively. As usual, these probabilities are considered equiprobable, so (53) can be rewritten as

$$BER_{QPSK_n}^{I,Q} = \frac{1}{2}\int_{\gamma}^{\infty} \frac{1}{\sqrt{2\pi}\sigma_0^{I,Q}} e^{\left[-\frac{\left(Z_{QPSK_n}^{I,Q} - \mu_0^{I,Q}\right)^2}{2\sigma_0^{2\,I,Q}}\right]} dZ_{QPSK_n}^{I,Q}$$
$$+ \frac{1}{2}\int_{-\infty}^{\gamma} \frac{1}{\sqrt{2\pi}\sigma_1^{I,Q}} e^{\left[-\frac{\left(Z_{QPSK_n}^{I,Q} - \mu_1^{I,Q}\right)^2}{2\sigma_1^{2\,I,Q}}\right]} dZ_{QPSK_n}^{I,Q}. \quad (54)$$

Next, the value of γ that minimizes the BER causing $\frac{\partial \mathrm{BER}}{\partial \gamma} = 0$ is required. Solving the above equation for γ and observing that the desired user signal is much larger than the MAI signal, the optimum threshold is

$$\gamma_o^{I,Q} = \frac{\mu_1^{I,Q}\sigma_0^{I,Q} + \mu_0^{I,Q}\sigma_1^{I,Q}}{\sigma_0^{I,Q} + \sigma_1^{I,Q}}. \quad (55)$$

Finally, it can be observed in [83] that the *pdfs* related to the MAI limited network are symmetrical at the optimum threshold level, which implies in $\sigma_0^{I,Q} = \sigma_1^{I,Q} = \overline{\sigma_{QPSK_{MAI}}^{2\,I,Q}}$. As a result, the optimum threshold level is reduced to

$$\gamma_o^{I,Q} = \frac{\mu_1^{I,Q} + \mu_0^{I,Q}}{2}. \quad (56)$$

Hence, the "0" and "1" bit contributions in the decision variable are given, respectively, by

$$\mu_1^{I,Q} = \mu_{QPSK_{ac}}^{I,Q} \quad (57)$$

and

$$\mu_0^{I,Q} = -\mu_{QPSK_{ac}}^{I,Q}. \tag{58}$$

After substituting (57) and (58) into (56), it can be observed that the bipolar signal characteristics pushes the optimal threshold level to zero, i.e., $\gamma_o^{I,Q} = 0$. Then, after simple algebraic substitutions, and assuming that the K interfering users are statistically independent, the average interference variance for K interfering users can be expressed as the minimal BER for QPSK based networks as

$$BER_{QPSK}^{I,Q} = Q\left(\sqrt{SIR_{QPSK}^{I,Q}}\right) \tag{59}$$

where

$$SIR_{QPSK}^{I,Q} = \frac{\left(\mu_{QPSK_{ac}}^{I,Q}\right)^2}{K\overline{\sigma_{QPSK_{MAI}}^{2\ I,Q}}} \tag{60}$$

is the SIR in the FFH-OCDMA network based on the QPSK modulation format. Note that each channel takes an independent decision on the bit that represents the transmitted symbol.

Consequently, the mean BER resulting from the combined actions of the two channels can be calculated as

$$BER_{QPSK} = 1 - \left(1 - BER_{QPSK}^{I}\right)\left(1 - BER_{QPSK}^{Q}\right) \tag{61}$$

3.3.1.2 BPSK MODULATION FORMAT

As in the previous section, it is necessary to express explicitly the desired user's decision variables in terms of auto- and cross-correlation signals. Therefore, (35) should be rewritten as

$$\mu_{BPSK_n} = \mu_{BPSK_{ac}} + \mu_{BPSK_{MAI}}, \tag{62}$$

where

$$\mu_{BPSK_{ac}} = \mathcal{R}e\left\{\frac{\Re}{2} \times \left[\int_{T_{ca}} \left(E_{ac\_BPSK_n}{}^{*}(t,\theta_b)E_{LO_n}(t) + E_{ac\_BPSK_n}(t,\theta_b)E_{LO_n}{}^{*}(t)\right)dt\right]\right\} \tag{63}$$

and

$$\mu_{BPSK_{MAI}} = \mathcal{R}e\left\{\frac{\Re}{4} \times \left[\sum_{k=1\ (k\neq n)}^{K} \int_{T_{ca}} \left(E_{cc\_BPSK_{n,k}}{}^{*}(t-\tau_k,\theta_b)E_{LO_n}(t) + E_{cc\_BPSK_{n,k}}(t-\tau_k,\theta_b)E_{LO_n}{}^{*}(t)\right)dt\right]\right\}, \tag{64}$$

where μ_{BPSK_n} representing the decision variable and, $\mu_{BPSK_{ac}}$ and $\mu_{BPSK_{MAI}}$ representing the contributions of the autocorrelation and cross-correlation signals to decision variable, respectively.

By considering the same steps and assumptions adopted to obtain (47)-(50), the user's interference variance can be expressed as $\overline{\sigma^2_{BPSK_{MAI}}} = \overline{\sigma^2_{BPSK_{MAI_{j,k}}}}$. Due to the distance of BPSK symbols also being symmetrical to the origin, the optimum threshold for this modulation format is also zero. Therefore, proceeding with the same steps as for (51)-(58), the minimal BER for BPSK based network can be expressed as

$$BER_{BPSK} = Q\left(\sqrt{SIR_{BPSK}}\right) \tag{65}$$

where

$$SIR_{BPSK} = \frac{\left(\mu_{BPSK_{ac}}\right)^2}{K\overline{\sigma^2_{BPSK_{MAI}}}}, \tag{66}$$

is the SIR of the FFH-OCDMA network based on the BPSK modulation format.

3.3.1.3 OOK MODULATION FORMAT

As in the above sections, it is necessary to express explicitly the desired user's decision variables in terms of auto- and cross-correlation signals. Therefore, (42) should be rewritten as

$$\mu_{OOK_n} = \mu_{OOK_{ac}} + \mu_{OOK_{MAI}}, \tag{67}$$

where

$$\mu_{OOK_{ac}} = \mathcal{R}e\left\{\Re \times \left[\int_{T_{ca}} E_{ac\_OOK_n}(t) {E_{ac\_OOK_n}}^*(t)dt\right]\right\} \tag{68}$$

and

$$\begin{aligned}\mu_{OOK_{MAI}} = \mathcal{R}e\Bigg\{\Re \times \Bigg[&\sum_{k=1\ (k\neq n)}^{K} \int_{T_{ca}} E_{cc\_OOK_{n,k}}(t-\tau_k) {E_{cc\_OOK_{n,k}}}^*(t-\tau_k)dt \\ &+\frac{1}{2}\int_{T_{ca}} \Big(E_{ac\_OOK_n}(t) {E_{cc\_OOK_{n,k}}}^*(t-\tau_k) \\ &+ {E_{ac\_OOK_n}}^*(t,\theta_b) E_{cc\_OOK_{n,k}}(t-\tau_k)\Big)dt\Bigg]\Bigg\},\end{aligned} \tag{69}$$

where μ_{OOK_n} representing the decision variable and, $\mu_{OOK_{ac}}$ and $\mu_{OOK_{MAI}}$ representing the contributions of the autocorrelation and cross-correlation signals to decision variable, respectively.

By considering the same steps and assumptions adopted to obtain (47)-(50), the user's interference variance can be expressed as $\overline{\sigma^2_{OOK_{MAI}}} = \overline{\sigma^2_{OOK_{MAI}{}_{j,k}}}$. Due to the distance of BPSK symbols also being symmetrical when related to the origin, the optimum threshold for this modulation format is also zero. Therefore, proceeding with the same steps performed in (51)-(58), the minimal BER for OOK based network can be expressed as

$$BER_{OOK} = Q\left(\sqrt{SIR_{OOK}}\right), \tag{70}$$

where

$$SIR_{OOK} = \frac{\left(\mu_{OOK_{ac}}\right)^2}{K\overline{\sigma^2_{OOK_{MAI}}}}, \tag{71}$$

is the SIR of the FFH-OCDMA network based on the OOK modulation format.

3.3.2 MULTI RATE NETWORKS

3.3.2.1 PSK MODULATION FORMATS

The multirate scenario also requires the decision variables of the desired user (also defined in terms of the auto- and cross-correlation signals) to be rewritten. However, the BER formalism must account separately for the MAI from the high- and low-rate user classes [40], [49]-[53]. Recall that the QPSK and BPSK modulated users transmit their data bits at high- and low-rates, respectively. Then, the variance associated to high-rate users is the same one derived for the QPSK modulation format, but restricted to the number of users in this class. Thus, considering that K_{hr} interfering users are active in a high-rate class, the average interference from these users is given by $\overline{\sigma^2_{QPSK^{I,Q}_{MAI,hr}}}$.

Similarly, the variance associated to low-rate users is the same one derived for the BPSK modulation format, but restricted to the number of users in this class. Thus, considering that K_{lr} interfering users are active in low-rate classes, the average interference from these users is given by $\overline{\sigma^2_{BPSK_{MAI,lr}}}$.

Now, it is necessary to express the variance for the cases where the interfering users of a given class are demodulated by the receiver of the desired user that is active in another class. Therefore, consider first that the interfering users transmit data bits at a low-rate and their signals are demodulated in the receptor of the desired user, which is designed for high-

rates. Consequently, the MAI at the I and Q channels in the receiver of the desired user n_Q when K_{lr} interfering users transmit are given by

$$\mu^{I}_{QPSK/BPSK_{MAI}} = \mathcal{R}e\left\{\frac{\mathfrak{R}}{4}\times\left[\sum_{k_B=1}^{K_{lr}}\int_{T_{ca}}\left(E_{cc\_BPSK_{n_Q,k_B}}{}^{*}(t-\tau_k,\theta_b)E_{LO_{n_Q}}(t)\right.\right.\right.$$
$$\left.\left.\left.+E_{cc\_BPSK_{n_Q,k_B}}(t-\tau_k,\theta_b)E_{LO_{n_Q}}{}^{*}(t)\right)dt\right]\right\} \quad (72)$$

and

$$\mu^{Q}_{QPSK/BPSK_{MAI}} = Im\left\{\frac{\mathfrak{R}}{4}\times\left[\sum_{k_B=1}^{K_{lr}}\int_{T_{ca}}\left(E_{cc\_BPSK_{n_Q,k_B}}{}^{*}(t-\tau_k,\theta_b)E_{LO_{n_Q}}(t)\,e^{j\pi/2}\right.\right.\right.$$
$$\left.\left.\left.+\,E_{cc\_BPSK_{n_Q,k_B}}(t-\tau_k,\theta_b)E_{LO_{n_Q}}{}^{*}(t)e^{-j\pi/2}\right)dt\right]\right\}. \quad (73)$$

Again, following the same steps and assumptions to obtain (47)-(50), the average interference among active users of different classes is given by $\overline{\sigma^{2\ I,Q}_{QPSK/BPSK_{MAI}}} = \overline{\sigma^{2\ I,Q}_{QPSK/BPSK_{MAI}{}_{j_Q,k_B}}}$, where j_Q and k_B are active interfering users in high- and low-classes, respectively.

Next, the case where the interfering users transmit data at a high-rate and their signals are demodulated in the receptor of the desired user, which is designed for a low-rate, is considered. Then, the MAI in the receiver of the desired user n_B when K_{hr} interfering users transmit is given by

$$\mu_{BPSK/QPSK_{MAI}} = \mathcal{R}e\left\{\frac{\mathfrak{R}}{4}\times\left[\sum_{j_Q=1}^{K_{hr}}\int_{T_{ca}}\left(E_{cc\_QPSK_{n_B,j_Q}}{}^{*}(t-\tau_k,\theta_b)E_{LO_{n_B}}(t)\right.\right.\right.$$
$$\left.\left.\left.+E_{cc\_QPSK_{n_B,j_Q}}(t-\tau_k,\theta_b)E_{LO_{n_B}}{}^{*}(t)\right)dt\right]\right\} \quad (74)$$

In a similar fashion, the average interference among users of different classes can be denoted as $\overline{\sigma^2_{BPSK/QPSK_{MAI}}} = \overline{\sigma^2_{BPSK/QPSK_{MAI}{}_{k_B,j_Q}}}$.

Hence, the BER of multirate networks can be adapted from [39] and [40] based on the specific features of the here-proposed network, where users achieve different rates via QPSK and BPSK modulation formats. Now, by considering that the desired user is active in the high-rate class, the BER of this user is given by

$$BER_{QPSK\_MR} = 1 - \left(1 - BER^{I}_{QPSK\_MR}\right)\left(1 - BER^{Q}_{QPSK\_MR}\right), \tag{75}$$

where

$$BER^{I,Q}_{QPSK\_MR} = Q\left(\sqrt{SIR^{I,Q}_{QPSK\_MR}}\right) \tag{76}$$

and

$$SIR^{I,Q}_{QPSK\_MR} = \frac{\left(\mu^{I,Q}_{QPSK_{ac}}\right)^2}{K_{hr}\overline{\sigma^2_{QPSK^{I,Q}_{MAI,hr}}} + K_{lr}\overline{\sigma^2_{BPSK/QPSK_{MAI}}}} \tag{77}$$

is the BER and SIR measured in each channel of the users' demodulator, respectively. Finally, when the desired user is active at the low-rate class, the BER of this user class can be expressed as

$$BER_{BPSK\_MR} = Q\left(\sqrt{SIR_{BPSK\_MR}}\right) \tag{78}$$

where

$$SIR_{BPSK\_MR} = \frac{\left(\mu_{BPSK_{ac}}\right)^2}{K_{lr}\overline{\sigma^2_{BPSK_{MAI,lr}}} + K_{hr}\overline{\sigma^2_{QPSK^{I,Q}/BPSK_{MAI}}}}, \tag{79}$$

is the SIR measured in the desired user demodulator.

3.3.2.2 OOK MODULATION FORMAT

As in the previous sections, the decision variables of the desired user (also defined in terms of auto- and cross-correlation signals) should be rewritten. However, the BER formalism must separately account for the MAI from high- and low-rate user classes [40], [49]-[53]. Recall that in legacy FFH-OCDMA multirate networks all users are OOK modulated and for high and low rate users are allocated small and large code length, respectively.

With this, the variance associated to high-rate users is the same one derived for the single rate OOK modulation format, but restricted to the number of users in this class. Thus, considering that K_{hr} interfering users are active in a high-rate class, the average interference from these users is given by $\overline{\sigma^2_{OOK_{MAI,hr}}}$.

Similarly, the variance associated to low-rate users is the same one derived for the BPSK modulation format, but restricted to the number of users in this class. Thus, considering that K_{lr} interfering users are active in low-rate classes, the average interference from these users is given by $\overline{\sigma^2_{OOK_{MAI,lr}}}$.

Now, it is necessary to express the variance for the cases where the interfering users of a given class are demodulated by the receiver of the desired user that is active in another class. Therefore, consider first that the interfering users transmit data bits at a low-rate and their signals are demodulated in the receptor of the desired user, which is designed for high-rates. Consequently, the MAI at the receiver of the desired user n_Q when K_{lr} interfering users transmit is given by

$$\begin{aligned}\mu_{High/Low_{MAI}} &= \mathcal{R}e\{\Re \\ &\times\left[\sum_{k_B=1}^{K_{lr}}\int_{T_{ca}} E_{cc\_OOK_{n_Q,k_B}}(t-\tau_k)E_{cc\_OOK_{n_Q,k_B}}{}^{*}(t-\tau_k)dt\right. \\ &+\frac{1}{2}\int_{T_{ca}}\Big(E_{ac\_OOK_{n_Q}}(t)E_{cc\_OOK_{n_Q,k_B}}{}^{*}(t-\tau_k) \\ &\left.+E_{ac\_OOK_{n_Q}}{}^{*}(t)E_{cc\_OOK_{n_Q,k_B}}(t-\tau_k)\Big)dt\right]\Big\},\end{aligned} \tag{80}$$

when j_Q and k_B interfering users are active in high- and low-classes, respectively. Again, following the same steps and assumptions to obtain (47)-(50), the average interference among active users of different classes is given by $\overline{\sigma^2_{High/Low_{MAI}}} = \overline{\sigma^2_{High/Low_{MAI_{j_Q,k_B}}}}$.

Next, the case where the interfering users transmit data at a high-rate and their signals are demodulated in the receptor of the desired user, which is designed for a low-rate, is considered. Then, the MAI at the receiver of the desired user n_B when K_{hr} interfering users transmit is given by

$$\begin{aligned}\mu_{Low/High_{MAI}} &= \mathcal{R}e\{\Re \\ &\times\left[\sum_{j_Q=1}^{K_{hr}}\int_{T_{ca}} E_{cc\_OOK_{n_B j_Q}}(t-\tau_k)E_{cc\_OOK_{n_B j_Q}}{}^{*}(t-\tau_k)dt\right. \\ &+\frac{1}{2}\int_{T_{ca}}\Big(E_{ac\_OOK_{n_B}}(t)E_{cc\_OOK_{n_B,j_Q}}{}^{*}(t-\tau_k) \\ &\left.+E_{ac\_OOK_{n_B}}{}^{*}(t)E_{cc\_OOK_{n_B,j_Q}}(t-\tau_k)\Big)dt\right]\Big\},\end{aligned} \tag{81}$$

In a similar fashion, the average interference among users of different classes can be denoted as $\overline{\sigma^2_{Low/High_{MAI}}} = \overline{\sigma^2_{Low/High_{MAI_{k_B,j_Q}}}}$.

Hence, the BER of multirate networks can be adapted from [39] and [40] based on the specific features of the here-proposed generalized formalism. Now, considering that the desired user is active in the high-rate class, the BER of this user is given by

$$BER_{High\_MR} = Q\left(\sqrt{SIR_{High\_MR}}\right), \tag{82}$$

where

$$SIR_{High\_MR} = \frac{\left(\mu_{High_{ac}}\right)^2}{K_{hr}\overline{\sigma^2_{High_{MAI,lr}}} + K_{lr}\overline{\sigma^2_{Low/High_{MAI}}}}, \tag{83}$$

is the SIR measured in desired user demodulator at the high rate class.

Finally, when the desired user is active at the low-rate class, the BER of this user class can be expressed as

$$BER_{Low\_MR} = Q\left(\sqrt{SIR_{Low\_MR}}\right), \tag{84}$$

where

$$SIR_{Low\_MR} = \frac{\left(\mu_{Low_{ac}}\right)^2}{K_{lr}\,\overline{\sigma^2_{Low_{MAI,lr}}} + K_{hr}\,\overline{\sigma^2_{High/Low_{MAI}}}}, \tag{85}$$

is the SIR measured in the desired user demodulator.

3.4 DECISION VARIABLES COMPARISON

In this section, the differences between the power amount of signal and MAI that impact on the bit detection are demonstrated and discussed. To do so, it is compared the signal waveforms related to decision variables at the desired user receiver of PSK- and legacy OOK-based networks. Only for convenience sake, the analysis will be carried out for single rate networks. Nonetheless, the similarity of the transceivers allows the same considerations and the formalism can be easily modified in order to consider the particularities of multirate demodulation. Moreover, it is utilized the BPSK modulation and demodulation for this comparison. The results for QPSK demodulator, in turn, are the same because its receiver can be considered as two BPSK demodulators working in parallel configuration.

Initially, it is convenient to reproduce the decision variable of the OOK modulation format described in (42) disregarding the negative frequencies. Thus, the decision variable for FFH-OCDMA based on OOK modulation formats can be rewritten as

$$Z_{OOK_n} = \mathcal{R}e\left\{\Re \times \left[\int_{T_{ca}} P_{ac\_OOK_n}\,dt + \sum_{k=1\ (k\neq n)}^{K} \int_{T_{ca}} \left(P_{cc\_OOK_{n,k}} + E_{ac\_OOK_n}(t)E_{cc\_OOK_{n,k}}{}^{*}(t-\tau_k)\right)dt\right]\right\}, \tag{86}$$

where the first term is the desired user signal, the second and third terms are the MAI contribution. The spectral power as a function of angular frequency related to this decision variable is illustrated in Figure 3.4.

Sequentially, it is described the decision variable of the network based on BPSK modulation format. Moreover, in order to clearly show the differences between the decision variables, let's substitute the LO signal as the autocorrelation signal expressed in (36) and also disregarding the negative frequencies in (35).

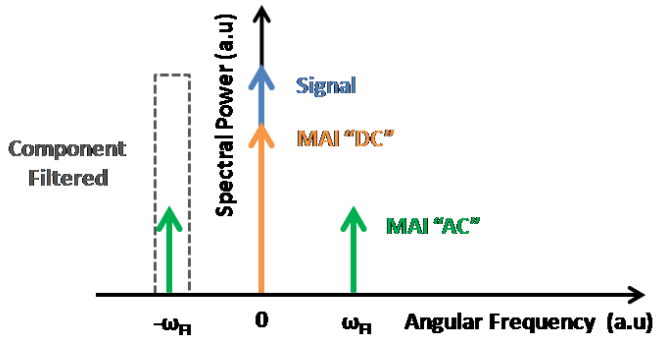

Figure 3.4: – Spectral representation of the signals that compose the decision variable for FFH-OCDMA networks based on OOK modulation format.

Thus, the spectral power as function of angular frequency for FFH-OCDMA networks based on BPSK modulation formats can be rewritten as

$$Z_{BPSK_n} = \mathcal{R}e\left\{\Re \times \left[\int_{T_{ca}} P_{ac\_BPSK_n} e^{j\Delta\theta_b}\, dt + \sum_{k=1\ (k\neq n)}^{K} \frac{1}{2}\int_{T_{ca}} E_{ac\_BPSK_n}(t) E_{cc\_BPSK_{n,k}}{}^{*}(t-\tau_k)\, dt\right]\right\}, \quad (87)$$

where $\Delta\theta_b$ is the phase difference between auto- and cross-correlation signals. In this case, Figure 3.5 illustrates the spectral distribution of the decision variable.

Further, it is interesting to note the differences between the decision variables and then infer on the mechanism that increases the network performance. As can be observed, the BPSK demodulation maintains the auto-correlation signal, whereas suppresses and reduces by half the "dc" and "ac" levels of the cross-correlation signal, respectively. As a matter of

fact, the balanced detection in the demodulation eliminates the desired signal because of the electric conversion in each photodetector.

Then, the reconstruction and amplification of the desired user signal occur by homodyne demodulation (multiplication with signal of the same wavelength) provided from the LO. Nonetheless, the difference between the wavelengths of LO and cross-correlation signals does not allow recovery of the MAI "dc" level.

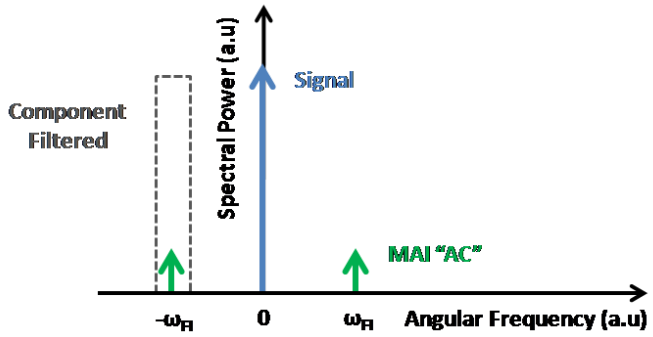

Figure 3.5: – Spectral representation of the signals that compose the decision variable for FFH-OCDMA networks based on BPSK modulation format.

CHAPTER 4

4 NUMERICAL RESULTS

The formalism developed in the previous section is now applied to the FFH-OCDMA network illustrated in Figure 3.1 for both QPSK and BPSK modulation formats. Further, it is carried out a validation procedure of the proposed formalism where the BPSK or QPSK convergence towards conventional OOK is assumed as the validation criteria. Moreover, the network performance is investigated considering distinct encoding schemes, namely, ideal and nonideal.

Before starting the network performance analyses, it is interesting to define the common encoding parameters adopted for both ideal and nonideal schemes. Then, the average power per symbol is maintained constant regardless of the modulation format adopted (in order to make a fair comparison between them). Further, only for the sake of simplicity, it is assumed that the photodetector responsivity is unitary and that the optical field amplitude (taken as a basis to maintain the same average power between the proposed PSK networks) of each individual chip is normalized to the chip peak amplitude of the OOK-based network. Thus, once there is power transmitted in all PSK symbols, the encoded BPSK/QPSK-modulated chips have their individual amplitudes reduced by $1/\sqrt{2}$ relative to OOK amplitude. Bragg gratings with a *sinc* apodization profile are utilized to achieve nearly disjoint and high density wavelength slices [65], [66]. It is also considered chip synchronization, a situation that does not take advantage of the OCDMA concept where completely asynchronous traffic, either of bits or chips, is possible. Nonetheless, this assumption greatly simplifies the formalism, and the obtained expression for the BER reflects the worse possible scenario [11], [40], [49]-[53], [57]-[66]. In addition, it is assumed the desired user transmits at 10 Gbps, which is compatible with an eventual NG-PON2 standardization.

With all common network configuration parameters properly described, the waveforms associated to the desired user can now be discussed. Nonetheless, it is worth mentioning that the present formalism can be successfully applied to any code family, pulse waveforms, wavelength range and spacing between them.

Next, before we proceed with the networks analysis itself, it becomes necessary to define the network scenarios of interest. The first and second scenarios refer to the ideal and

nonideal encoding schemes, respectively. Once they have been laid out, we will move to the performance comparison between them.

a) First Scenario: Ideal Encoding

In the ideal encoding scheme, the pulsed chips are spaced perfectly in both time and spectral domains. In this sense, the pulsed chips are compressed when compared to the chip time slot, and also the Bragg gratings support bandwidth sufficient for self-containing each chip of the encoded spectrum.

Initially, it is interesting to analyze the signal evolution from generation until detection for the ideal scenario. For convenience sake, it is shown solely the waveforms of the desired user in the FFH-OCDMA network based on the QPSK modulation. Moreover, 12 of the available 29 wavelengths in the range of 1.205 μm – 1.625 μm (0.015 μm spacing) are used, arranged in 12 time chips (code length) in accordance with the generated FFH code. Furthermore, the chip pulse shape is assumed to be Gaussian, compressed by a factor of ten when compared to the chip period. Consequently, the effective transmission rate is proportional to this compression factor with chip rate transmission at 1200 Gc/s (Giga chips per second). The current configuration is chosen exclusively to avoid interchip interference, which enables the validation procedure (reproducing idealized results in [11], [40], [49]-[53], [57]-[66]) to be carried out. For convenience sake, only the resulting signals for the *I* channel will be shown. The *Q* channel differs only by a 90° shift from the reference signal generated within the demodulator.

First, the normalized absolute value of the encoded pulse amplitudes (black curves) superposed by the impulse response of the encoder (blue curves) of the desired user signal as function of time is shown in Figure 4.1. The adopted modulation index depth of 1.25×10^{-2} and grating length of 1 mm allow for the spectral distribution of the transfer function to fully confine the pulse bandwidth [84]-[86]. As a result, the grating response approaches that of an ideal band pass filter.

The normalized absolute value of the encoded spectral representation (black curves) superposed by the transfer function (blue curves) of the desired user encoder is shown in Figure 4.2. Once more, this approximation is chosen solely to reproduce the idealized results found in the literature [40], [49]-[53], [57]-[66]. Next, following the flow of the encoded signal in the network shown in Figure 3.1, the chips are regrouped according to the desired user decoder resulting in a high level autocorrelation peak when the data bit is transmitted.

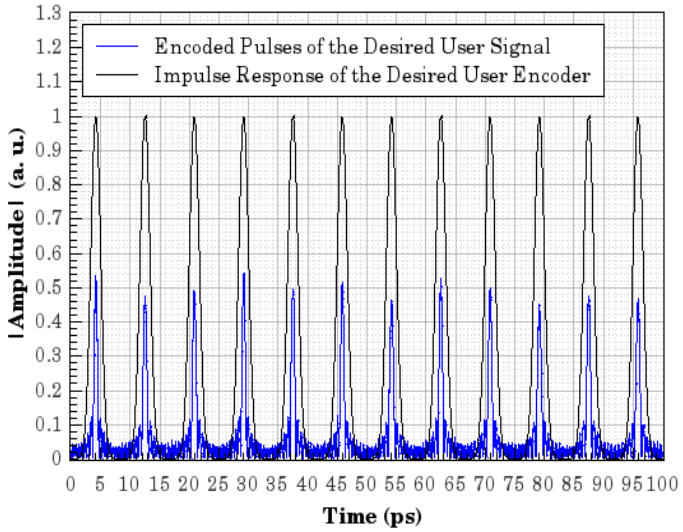

Figure 4.1: – Time representation of the desired encoded pulses (black curves) and impulse response of the desired encoder (blue curves).

In a situation in which the desired user does not send data bits, only the interfering users that exactly coincide in time and wavelength at the autocorrelation peak effectively contribute with errors. This statement can be more easily understood by analyzing the highlighted codes in Table 1. In this table, code #23, shown in black bold letters, is randomly assigned to the desired user (any other choice would produce the same result). The interfering users #24 and #25 (shown in orange and olive bold letters), despite having chips in the same wavelength, never contribute to errors when they access the network in bit synchronism with the desired user. This occurs because the chips with identical wavelengths do not coincide temporally and, therefore, are not detected at the autocorrelation window decision.

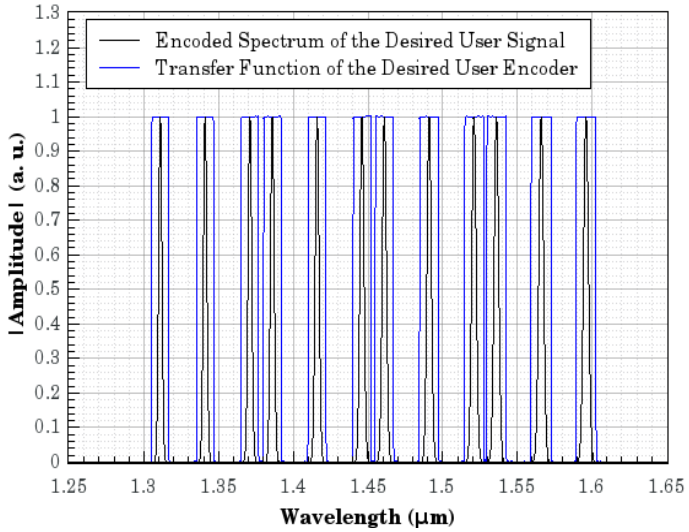

Figure 4.2: – Spectral representation of the desired user encoded pulses (black curves) and transfer function of the desired encoder (blue curves).

Codes	Chips / Wavelengths											
#1	17	1	25	15	22	20	3	19	24	5	27	0
#2	18	2	26	16	23	21	4	20	25	6	28	1
#3	19	3	27	17	24	22	5	21	26	7	0	2
#4	20	4	28	18	25	23	6	22	27	8	1	3
#5	21	5	0	19	26	24	7	23	28	9	2	4
#6	22	6	1	20	27	25	8	24	0	10	3	5
#7	23	7	2	21	28	26	9	25	1	11	4	6
#8	24	8	3	22	0	27	10	26	2	12	5	7
#9	25	9	4	23	1	28	11	27	3	13	6	8
#10	26	10	5	24	2	0	12	28	4	14	7	9
#11	27	11	6	25	3	1	13	0	5	15	8	10
#12	28	12	7	26	4	2	14	1	6	16	9	11
#13	0	13	8	27	5	3	15	2	7	17	10	12
#14	1	14	9	28	6	4	16	3	8	18	11	13
#15	2	15	10	0	7	5	17	4	9	19	12	14
#16	3	16	11	1	8	6	18	5	10	20	13	15
#17	4	17	12	2	9	7	19	6	11	21	14	16
#18	5	18	13	3	10	8	20	7	12	22	15	17
#19	6	19	14	4	11	9	21	8	13	23	16	18
#20	7	20	15	5	12	10	22	9	14	24	17	19
#21	8	21	16	6	13	11	23	10	15	25	18	20
#22	9	22	17	7	14	12	24	11	16	26	19	21
#23	**10**	**23**	**18**	**8**	**15**	**13**	**25**	**12**	**17**	**27**	**20**	**22**
#24	11	24	19	9	16	14	26	**13**	**18**	28	21	**23**
#25	**12**	**25**	**20**	**10**	**17**	**15**	**27**	14	19	0	**22**	24
#26	13	26	21	11	18	16	28	15	20	1	23	25
#27	14	27	22	12	19	17	0	16	21	2	24	26
#28	15	28	23	13	20	18	1	17	22	3	25	27
#29	16	0	24	14	21	19	2	18	23	4	26	28

TABLE 1: FFH User codes generated from 29 available wavelengths

This can be seen in Figure 4.3, where the normalized amplitude is plotted as a function of time after the decoding. In this decoding process, it is considered that only three users should access the channel in a bit-synchronous manner. Such a low number of simultaneous users (three users) in the channel are only to show the interfering users' chips after the correlation procedure.

As can be observed from Figure 4.3, the desired user is successfully decoded so that the delays introduced by the encoder for each wavelength element have a complementary delay in the decoder leading to a single cumulative delay for all elements (black curves within the red window decision). The interfering users, on the other hand, are illustrated as the background signal in Figure 4.3 (orange and olive curves). Finally, in the demodulation unit shown in the diagram of Figure 3.1, the decoded FFH-OCDMA signal is added to the 90° optical hybrid and the indication of the phase transmitted with the user data bit is carried out after the mixed detection, i.e, multiplication with the broadband pulse of the autocorrelation peak. For convenience sake, only the resulting signal of the above mentioned multiplication is shown in Figure 4.4, where the absolute normalized power is plotted as a function of time. Moreover, regarding Figure 4.4, the black curve is maintained within the decision window, but it has been amplified by the multiplication with the reference signal.

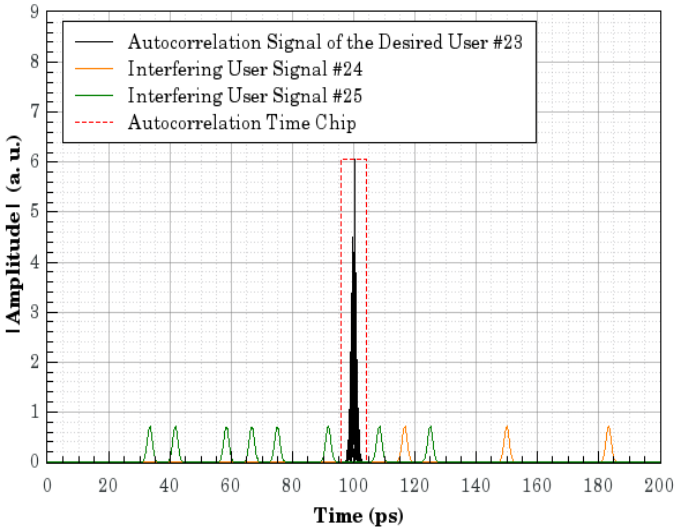

Figure 4.3: Time representation of the FFH decoder output showing the desired user #23 autocorrelation (black curves) in decision window (red curves) superposed by interfering users pulses #24 (green) and #25 (orange).

It is noteworthy that the lateral side lobes are eliminated due to multiplication with the zero amplitude LO optical field outside the decision window (i.e., outside the red dotted rectangle). Once more, this type of MAI elimination does not alter the bit error occurrences because the threshold level is compared only to the power within the decision window. Therefore, the PSK modulation formats cannot be seen as MAI mitigators, but rather as an artifice to increase the SIR.

Next, before proceeding with the PSK performance analysis itself, it is necessary to compare the results with those published in the literature. By considering that, it is defined a

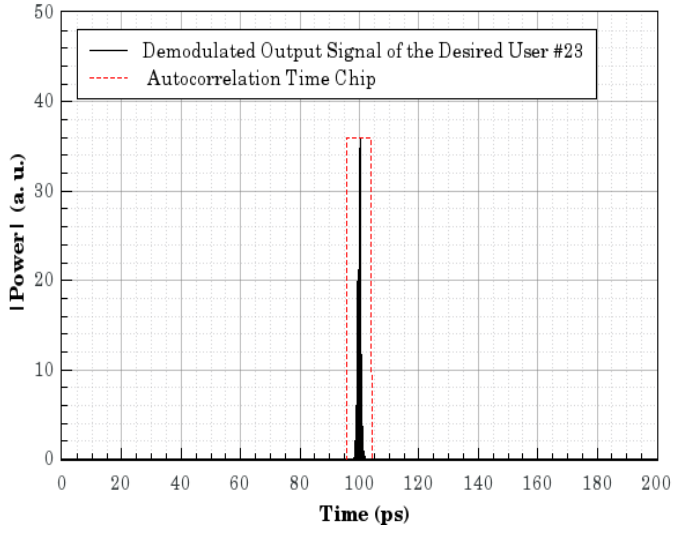

Figure 4.4: Time representation of the QPSK demodulator output showing the desired user #23 autocorrelation (black curves) in decision window (red curves).

validation criterion for the proposed PSK-based formalisms as to guarantee convergence towards the OOK modulation format. It is noteworthy that the proposed BPSK or QPSK-based FFH-OCDMA network converge to the OOK-based FFH-OCDMA when the addition of the LO signal at the input of the 90° optical hybrid does not occur and conventional detection (instead of balanced detection) is employed. In order to prove the above statement, the networks analyzed by Fathallah et al. [65] are simulated with the proposed formalism. The performance evaluation is carried out by using FFH codes with 17 to 29 wavelength subbands. The results of the BER as a function of the number of simultaneous users are shown in Figure 4.5. The close agreement between the results in [65] and those obtained with the proposed formalism (Figure 4.5) proves the ability of this formalism to correctly evaluate the performance of legacy OOK-based FFH-OCDMA networks. Nonetheless, these results show that OOK-based networks only support a restricted number of users in acceptable BER levels, particularly if error-free networks are desired (BER~10^{-12}). For example, the maximum number of simultaneous users that can be served technically error-free is 14 when 19 wavelength slots (cross symbols) are available for FFH encoding. Up to roughly 19 simultaneous users can be supported when 29 wavelength slots (circle symbols) are available for FFH encoding.

The application of the PSK modulation formats allows the BER to be drastically reduced, making it possible error-free transmissions even when few wavelength sub bands are used. The results of the BER as a function of the number of simultaneous users for the PSK-based FFH-OCDMA networks are shown in Figure. 4.6. As the BER difference

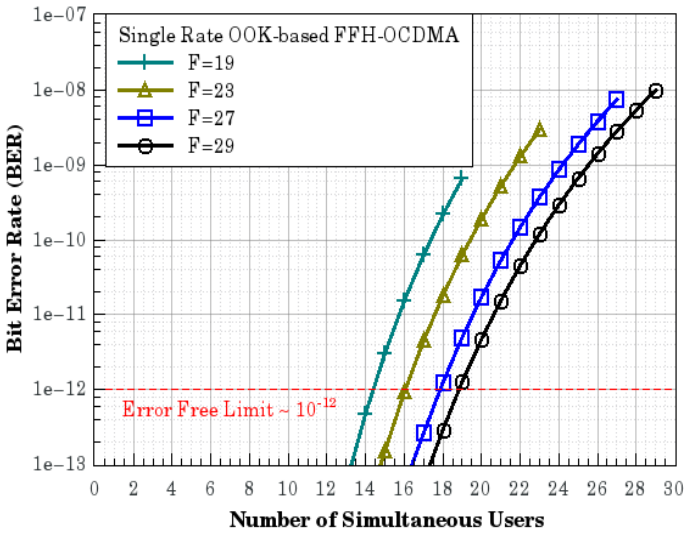

Figure 4.5: BER for legacy FFH-OCDMA based on OOK modulation formats using the following number of available wavelengths: 19 (cross), 23 (triangles), 27 (squares) and 29 (circles).

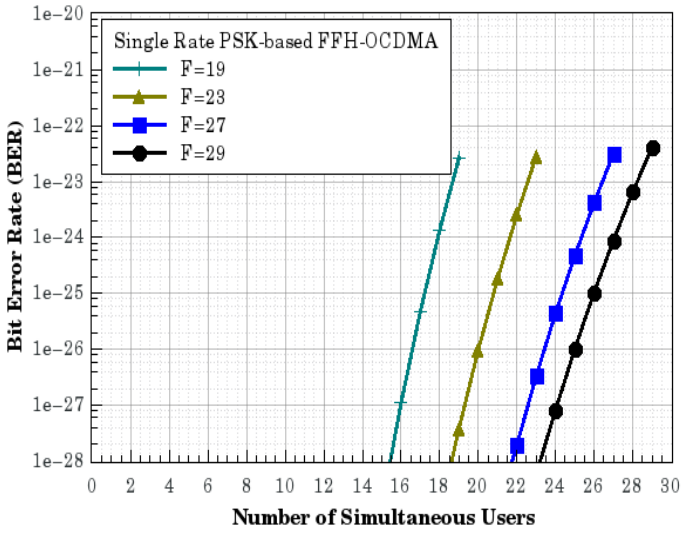

Figure 4.6: BER for proposed FFH-OCDMA based on BPSK/QPSK modulation formats using the following available wavelengths: 19 (cross), 23 (triangles), 27 (squares) and 29 (circles).

between these PSK formats is considerably small (the BER of QPSK is approximately twice that of BPSK), the BPSK results were omitted to avoid making the figure too dense.

As can be observed in this figure, error-free transmissions are obtained even when a reduced number of 19 wavelengths (cross symbols) are used. As expected, this behavior is further improved as the number of wavelengths is increased. The best performance of PSK networks occurs, in fact, due to the demodulation process, which provides outputs proportional to the auto-correlation peak if the desired user code is transmitted. Moreover, it helps reduce the MAI contribution in the chip decision window due to reduction of cross correlation signals. Furthermore, note that even though all the curves presented in Figure 4.6 show that the transmission of data bits occurs error-free, regardless of the number of simultaneous users, these curves are intended only to express the trends.

Next, the performances of the proposed multirate PSK-based FFH-OCDMA networks is investigated. The BER as function of the number of simultaneous users for a two-class network using QPSK for high-rate user classes and BPSK for low-rate user classes is plotted in Figure 4.7. The proposed formalism is also applied to a conventional multirate OOK-based FFH-OCDMA as proposed in [40] for validation purposes. As previously mentioned, the proposed formalism is robust and shows a close agreement with the performance prediction of OOK-based networks (hollow symbols).

Finally, it can also be observed from Figure 4.7 that the performance of high-rate users in the proposed multirate PSK-based network is not significantly penalized in terms of BER (or quality of service) as previous studies show [40], [49]-[52]. It should also be

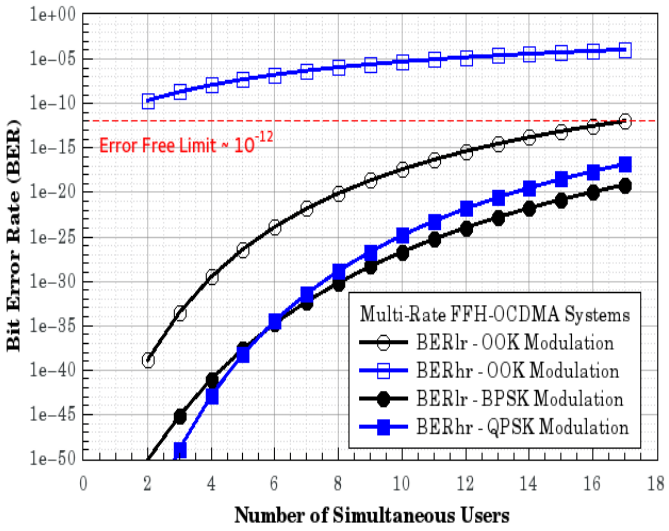

Figure 4.7: BER for the proposed multirate FFH-OCDMA based on PSK modulation formats (solid symbols) and legacy FFH-OCDMA based on OOK modulation format (hollow symbols). Circles refer to low-rate users and squares to high-rate users.

mentioned that even when all the 23 simultaneous users (17 low rate users plus 6 high rate users) are active in the network, the BER is still within the error-free limit.

Once the ideal scenario has been fully considered, it will be discuss in the next section how the nonideal encoding scheme impacts the overall networks performance.

b) Second Scenario: Nonideal Encoding

As discussed in the first scenario, several factors are not favorable to the ideal encoding adoption in OCDMA networks. These requirements impose three constraints to the design of practical networks. Firstly, it implies the use of ultrashort pulses for encoding (higher chip rate), which degrades the user's waveforms due to dispersive effects in the channel. Secondly, the encoders and decoders design may be impracticable as the Bragg gratings require a very wide bandwidth. Finally, the wide wavelength spacing employed in the code design can exceed the spectrum width available in the C-band (L-band should also be used).

In the nonideal encoding scheme, on the other hand, the requirements previously mentioned are minimized allowing then a practical adoption of OCDMA networks. In this sense, the nonideal scenario includes an encoded pulse width equals to the time chip, feasible broadband Bragg gratings, and sufficient wavelengths within the C-band for users' code design.

The FFH codes are designed to present 12 chips and, consequently, a chip transmission rate of 120 Gc/s. Moreover, 29 wavelengths are employed in the users' code design in the spectral range of 1530 nm – 1630.8 nm (3.6 nm spacing). For convenience sake, the optical field amplitude of each chip is normalized to the unity.

Once all the parameters were described accordingly, it is interesting to discuss the waveforms associated to the users' signal before starting the network performance analysis itself.

For convenience sake, only the resulting signal of the desired user in the FFH-OCDMA network based on the QPSK modulation is shown, since the main purpose is to evaluate the influence of the desired signal at the autocorrelation waveform and, consequently, on the bit decision. Also, as it was done previously, only will the resulting signals for the *I* channel be shown.

Initially, the normalized absolute value of the encoded pulses amplitudes of the temporal chips (black curves) superposed by the impulse response of the encoder (blue curves) as a function of time is shown in Figure 4.8. Note that it is impossible to distinguish the individual chips signals in the waveform of encoded signal due to the temporal superposition.

Next, the normalized absolute value of the encoded spectral representation (black curves) superposed by the transfer function (blue curves) of the desired user encoder is shown in Figure 4.9. Bragg gratings are designed to present a high modulation index depth of 2.6×10^{-3} with 1mm length in order to operate in large bandwidths [13], [14]. Moreover, the

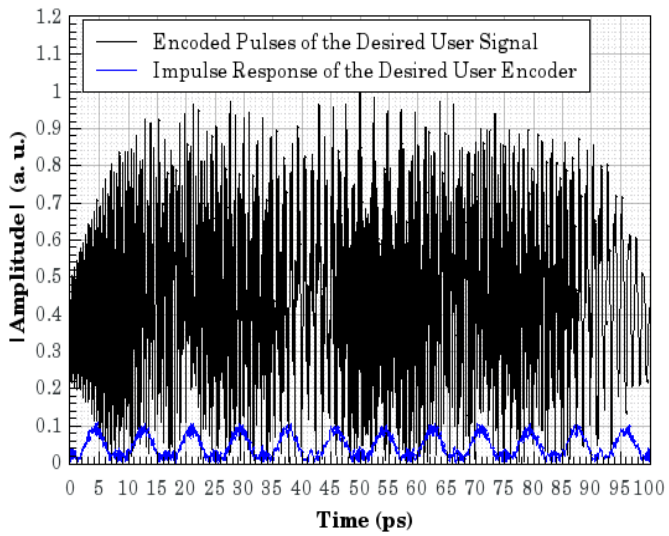

Figure 4.8: Time representation of the desired encoded pulses (black curves) and impulse response of the desired encoder (blue curves).

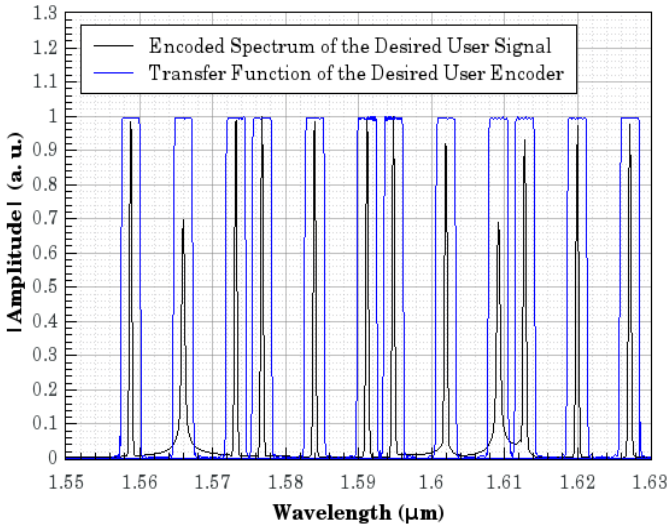

Figure 4.9: Spectral representation of the desired user encoded pulses (black curves) and transfer function of the desired encoder (blue curves).

3.6 nm Bragg bandwidth (equal the minimum spacing among the wavelengths in order to not have the same wavelength reflection by different gratings) still maintains the 29 wavelengths employed in the FFH codes within the C-band.

As the main objective is to evaluate the network performance under a MAI limited scenario, it is again adopted a back-to-back network configuration, neglecting noises in the detector. Sequentially, the FFH decoder removes the wavelength translation introduced in the encoder. Then, the chips of the desired user are combined by superposition to form a high auto-correlation pulse. All the other interfering chips that do not coincide simultaneously in time and wavelength, but only coincide in wavelength, have their energy mostly presented aside the autocorrelation pulse. On the other hand, the remaining small part of the interfering chips energy is within the decision window and contributes to bit errors. It is worth pointing out that this error contribution does not happen in the ideal scenario. The hits from interfering users' chips that coincide in both time and wavelength, in turn, are present at the auto-correlation time window and, consequently, contribute most effectively to bit errors. Both kind of interfering chips are known as cross-correlation signals.

This statement can be better understood if the FFH-OCDMA is analyzed with some users accessing simultaneously the network. Only for convenience sake, it is considered that three users share the network in a bit synchronous manner. Here, the highlighted codes in Table 1 are used again to make it clear the error contribution occurrence. In this table, code #23, shown in black bold letters, is randomly assigned to the desired user (any other choice would produce the same result). The interfering users, in turn, are also assigned by #24 and #25 codes (shown in orange and olive bold letters). In this case, the chips of interfering users

with identical wavelengths do not coincide temporally when related to desired user sequence. Thus, at the same time as the decoding operation regroups the desired user chips to produce the autocorrelation signal, the interfering chips in same wavelengths are displaced and a small part of their energy is present at the decision window. This can be seen in Figure 4.10, where the normalized absolute value of the amplitudes is plotted as a function of time after the decoding process. As can be observed from Figure 4.10, the desired user is successfully decoded so that the complementary delays (related to the encoder) introduce a cumulative delay for all chips (black curves within the red window decision). The interfering users, in turn, manifest themselves as a background signal (orange and olive curves).

Finally, the demodulation process is carried out by mixing the decoded signal (signal is added to the 90° optical hybrid) with a broadband pulse, replica of the auto-correlation signal, provided by the LO. The signal after demodulation is shown in Figure 4.11, where the normalized absolute value of power is plotted as a function of time. Note that the multiplication does not alter the waveform of the desired user signal nor the chip position at the auto-correlation peak. Moreover, the auto-correlation chip signal is maintained whereas the cross-correlation signals aside the decision window are suppressed by the LO signal. Once again, this type of MAI does not have influence over the errors because the bit decision is made by comparison with the signal within the window decision. Therefore, as in the previous section, the demodulation can be seen as a MAI mitigation method and, consequently, as a mechanism to increase the SIR.

Next we evaluate the performances of both OOK- and PSK-based FFH-OCDMA

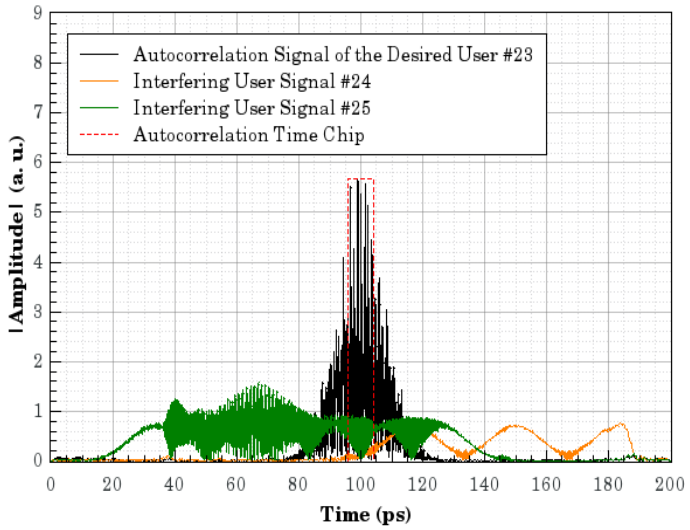

Figure 4.10: Time representation of the FFH decoder output showing the desired user autocorrelation (black curves) in the decision window (red curves) superposed by interfering users pulses (orange and olive curves).

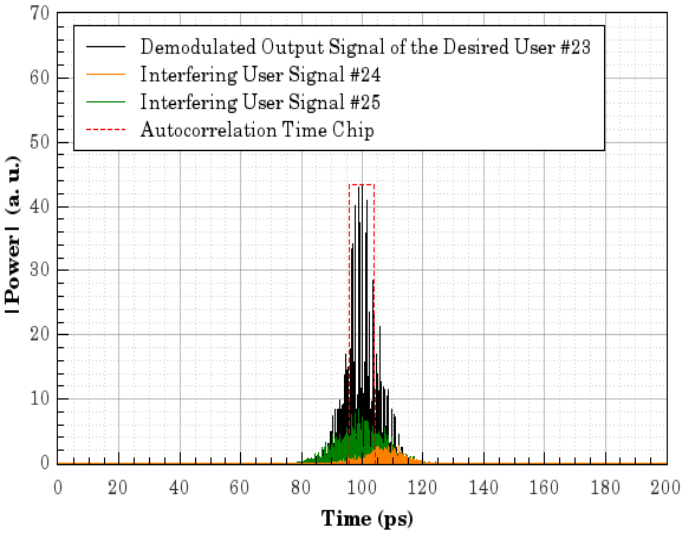

Figure 4.11: Time representation of the demodulation output showing the desired user autocorrelation (black curves) in the decision window (red curves) superposed by interfering users pulses (green and olive curves).

networks under nonideal scenario (regarding the waveforms shown along this section). Firstly, the BER as a function of the number of simultaneous users for OOK-based network is shown in Figure 4.12.

As can be observed, the BER performance is considerably penalized. This is due to the auto-correlation power set outside the window decision (the temporal width of the window decision is the same of one temporal chip) and also the cross-correlation power added at the window decision. In this case, the maximum number of simultaneous users that transmits in the error-free regime decreases to 11 and 15, respectively, when 19 and 29 wavelength slots are available for the code generation.

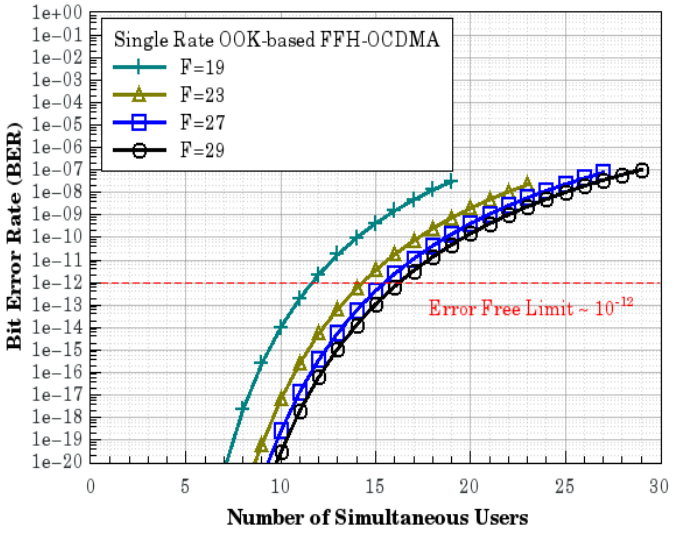

Figure 4.12: BER for the proposed FFH-OCDMA based on OOK modulation formats considering a nonideal scenario and using the following wavelength subbands: 19 (cross), 23 (triangles), 27 (squares) and 29 (circles).

Next, the performance of the PSK-based network over the nonideal scenario is investigated. The BER as a function of the number of simultaneous users is shown in Figure 4.13. As can be noticed, the BER levels are maintained below the error-free limit even when all users are present in the network, independently of the number of available wavelengths slots employed in the code design.

Finally, the multirate OCDMA performance based on both OOK and PSK modulation formats is analyzed under the nonideal encoding scenario. The results are shown in Figure 4.14. Initially, the performance results of the OOK-based multirate OCDMA (hollow symbols) is considered. As can be seen, the desired user performance at high rate transmission is unacceptable if error-free communication is desired. On the other hand, OOK

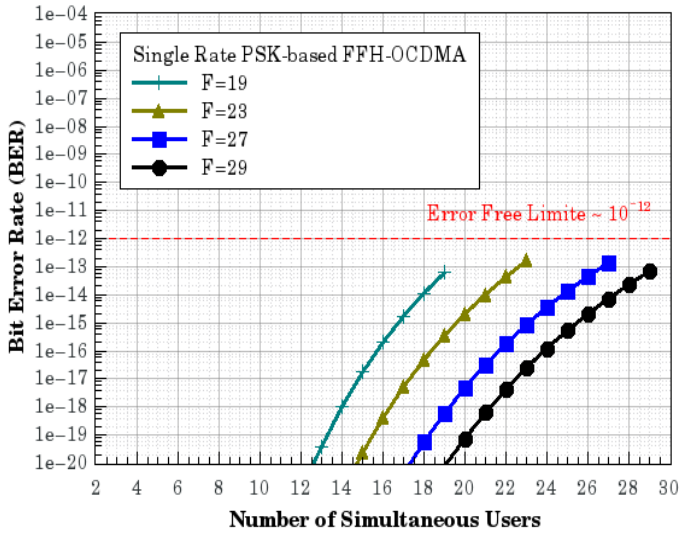

Figure 4.13: BER for the proposed FFH-OCDMA based on PSK modulation formats considering a nonideal scenario and using the following wavelength subbands: 19 (cross), 23 (triangles), 27 (squares) and 29 (circles).

can support up to 11 simultaneous users under an error-free environment when the desired user transmits at low rate. However, this small number of users does not satisfy the PON standard requirements. Fortunately, the proposed PSK-based multirate network supports a number of users far superior than that of legacy OOK-based multirate network. The performance results of PSK-based networks (solid symbols), also shown in Figure 4.14, clearly reveals that, independently of the desired user transmission rate, the BERs remain under the error-free region.

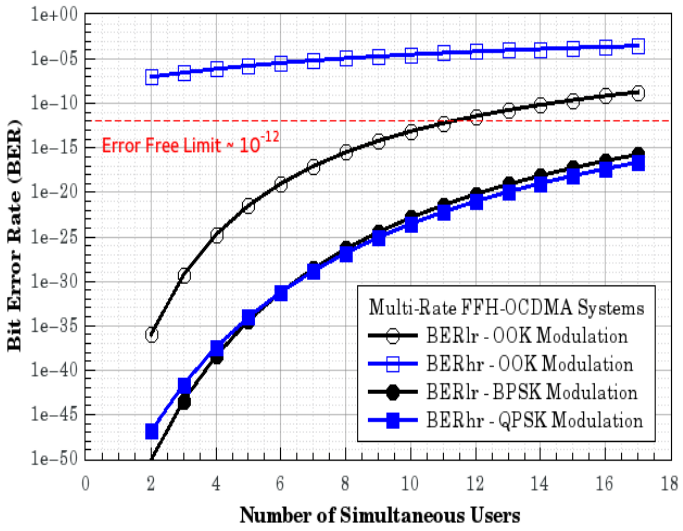

Figure 4.14: BER for the proposed multirate FFH-OCDMA based on PSK modulation formats (solid symbols) and legacy FFH-OCDMA based on OOK modulation format (hollow symbols). Circles refer to low-rate users and squares to high-rate users.

CHAPTER 5

5 CONCLUSIONS

In this thesis, the performances of single and multirate FFH-OCDMA networks based on coherent modulation formats were addressed. The proposed formalism accounted for the influence of MAI on the desired user's signal/receiver. It was shown that PSK modulation formats (BPSK or QPSK) can increase the SIR of the desired user's receiver when compared to legacy OOK-based networks. Consequently, the performance of the single rate PSK-based network indicated that users can transmit error-free even when the maximum number of users is simultaneously active in the network. This is true for any number of wavelength slots (i.e., 17, 23, 27 or 29 wavelengths) available for FFH code generation. In addition, it was also investigated the performance of a new PSK-based multirate network (which employs BPSK and QPSK modulation formats for low- and high-rate user classes, respectively). This network configuration offers the advantage of not requiring code length reduction of high-rate users by virtue of QPSK multiple bits per symbol transmission (two bits). The results show that when a maximum of 23 simultaneous users (17 low-rate users plus 6 high-rate users) are active in the PSK-based network and the SIR improvement is good enough to support error-free transmission of the desired user in both class. Furthermore, the users can surprisingly achieve similar BER performance for both low- and high-rate classes. Therefore, these advanced PSK formats are indeed potential candidates for NG-PON2 where higher data rates and vast amounts of users will be major network requirements.

5.1 FUTURE PERSPECTIVES

In this section, some suggestions on how this work can contribute to improve the performance of OCDMA network are presented. Although the results presented here have demonstrated the effectiveness of the BPSK and QPSK for increasing the performance, many opportunities for extending the scope of this thesis still remains. The results of this thesis point to several interesting directions for future work:

- ✓ Utilization of polarization multiplexing in order to double the spectral efficiency of phase modulation techniques;
- ✓ Moving to higher order modulation formats to provide more differentiated services in multirate networks;
- ✓ Employment of adaptive modulation techniques to improve the operational efficiency of networks.

REFERENCES

[1] M. Ilyas and H.T. Mouftah, *The handbook of optical communication networks.* Boca Raton, Fla; CRC Press, 2003.

[2] Crisp J. *Introduction to fiber optics*. 2nd ed. Oxford: Newnes Press; 2001.

[3] M. Bass and E. W. Van Stryland, *Fiber Optics Handbook*. New York: McGraw-Hill, 2002.

[4] P. R. Prucnal, *Optical Code Division Multiple Access: Fundamentals and Applications*. New York: Taylor & Francis, Dec. 2005.

[5] H. Yin and D. Richardson, *Optical code division multiple access communication networks: theory and applications*. Tsinghua University Press, Springer-Verlag, 2008.

[6] R. P. Scott, W. Cong, K. Li, V. J. Hernandez, B. H. Kolner, J. P. Heritage, and S. J. B. Yoo, "Demonstration of an error-free 4 × 10 Gb/s multiuser SPECTS O-CDMA network testbed," *IEEE Photon. Technol. Lett*., vol. 16, no. 9, pp. 2186–2188, Sep. 2004.

[7] R. Matsumoto, T. Kodama, S. Shimizu, R. Nomura, K. Omichi, N. Wadaand, and K. Kitayama, "40G-OCDMA-PON system with an asymmetric structure using a single multi-port and sampled SSFBG encoder/decoders," *IEEEJournal of Lightwave Technology*, vol.32, no. 6, pp. 1132–1143, March 2014.

[8] G. Kramer, M. D. Andrade, R. Roy, and P. Chowdhury, "Evolution of optical access networks: architectures and capacity upgrades," *Proc. of the IEEE*, vol. 100, no. 5, pp. 1188–1196, May 2012.

[9] L. G. Kazovsky, S.-W. Wong, V. Gudla, P.T. Afshar, S.-H. Yen, S. Yamashita, and Y. Yan, "Challenges in next-generation optical access networks: addressing reach extension and security weaknesses," *IET Optoelectronics*, vol. 5, no. 4, pp. 133-143, August 2011.

[10] Kitayama, K., "Rationale of OCDMA/OFDMA for NG-PON,", 2011 Int. Conf. on Inf. Photonics (ICO), vol., no., pp.1,2, 18-20 May 2011.

[11] A. L. Sanches, J. V. dos Reis, Jr., and B.-H. V. Borges, "Analysis of high-speed optical wavelength/time CDMA networks using pulse position modulation and forward error correction techniques," IEEE J. Lightwave Technol.., vol. 27, no. 22, pp. 5134–5144, Nov. 2009.

[12] K. Fouli and M. Maier, "OCDMA and Optical Coding: Principles, Applications, and Challenges," *IEEE Commun. Mag*., vol 45, no. 8, pp. 27-34, Aug. 2007.

[13] A. Stok and E. H. Sargent, "The role of optical CDMA in access networks," *IEEE Commun. Mag*., vol. 40, no. 9, pp. 83–87, Sep. 2002.

[14] R. Davey, J. Kani, F. Bourgart, and K.McCammon, "Options for future optical access networks," *IEEE Commun. Mag*., vol. 44, no. 10, pp. 50–56, Oct. 2006.

[15] T. H. Shake, "Security performance of optical CDMA against eaves-dropping," *J. Lightwave Technol*., vol. 23, no. 2, pp. 655–670, Feb. 2005.

[16] M. Y. Azizoglu, J. A. Salehi, and Y. Li, "Optical CDMA via temporal codes," *IEEE Trans. Commun*., vol. 40, no. 7, pp. 1162-1170, Jul. 1992.

[17] J. Salehi, "Code division multiple-access techniques in optical fiber networks - Part I: Fundamental principles," *IEEE Trans. Commun*., vol. 37, no. 8, pp. 824-833, Aug. 1989.

[18] J. Salehi and C. A. Brackett, "Code division multiple-access techniques in optical fiber networks - Part 2: Systems performance analysis," *IEEE Trans. Commun*., vol. 37, no. 8, pp. 834-842, Aug. 1989.

[19] W. Chung, J. Salehi, and V. Wei, "Optical orthogonal codes: Design, analysis, and applications," *IEEE Trans. Inform. Theory*, vol. 35, no. 3, pp. 595-604, May 1989.

[20] S. Maric, M. Hahm, and E. Titlebaum, "Construction and performance analysis of a new family of optical orthogonal codes for CDMA fiber-optic networks," *IEEE Trans. Commun*., vol. 43, no. 234, pp. 485-489, Feb. 1995.

[21] L. Tancevski and I. Andonovic, "Wavelength Hopping/Time Spreading Code Division Multiple Access Systems", *IEEE Electron. Lett*., vol. 30, No. 17, pp. 1388-1390, Aug. 1994.

[22] L. Tancevski and I. Andonovic, "Hybrid wavelength hopping/time spreading schemes for use in massive optical networks with increased security", *J. Lightwave Technol*., vol. 14, no. 12, pp. 2636-2647, Dec. 1996.

[23] G. C. Yang and W. C. Kwong, "Performance comparison of multiwavelength CDMA and WDMA+CDMA for fiber-optic networks", *IEEE Trans. Commun*., vol. 45, no. 11, pp. 1426-1434, Nov. 1997.

[24] W. C. Kwong, G. C. Yang, V. Baby, C. S. Bres and P. R. Prucnal, "Multiple-Wavelength Optical Orthogonal Codes Under Prime-Sequence Permutations for Optical CDMA", *IEEE Trans. Commun*., vol. 53, no. 1, pp. 117–123, Jan. 2005.

[25] K. Yu and N. Park, "Design of new family of two-dimensional wavelength-time spreading codes for optical code division multiple access networks." *Electron. Lett*.,vol 35, no. 10, pp. 830–831, 1999.

[26] T.M. Bazan, D. Harle, and I. Andonovic, Performance analysis of 2-D time-wavelength OCDMA systems with coherent light sources: Code design considerations, *J. Lightwave Technol*., vol. 24, no. 10, pp. 3583-3589, Oct. 2006.

[27] L. Tancevski , M. Tur , J. Budin and I. Andonovic "Hybrid wavelength hopping/time spreading code division multiple access systems," *Proc. Inst. Electr. Eng.—Optoelectronics*, vol. 143, pp. 161-166, Jun. 1996.

[28] Kwong, W.C., Yang, G.C., and Liu, Y.C.: "A new family of wavelength-time optical CDMA codes utilizing programmable arrayed waveguide gratings," *IEEE J. Sel. Areas Commun*., 2005, 23, pp. 1564–1571.

[29] S. Shurong, H. Yin, Z. Wang, "A New Family of 2-D Optical Orthogonal Codes and Analisys of Its Performance in Optical CDMA Access Networks," *J. Lightwave Technol*., vol. 24, no. 4, pp. 1646–1652, Apr. 2006.

[30] E. S. Shivaleela, A. Selvarajan, and T. Srinivas, "Two-dimensional optical orthogonal codes for fiber-optic CDMA networks," *J. Lightwave Technol*., vol. 23, no. 2, pp. 647–654, Feb. 2005.

[31] C. Yang, J. Huang and Y. Wang, "Multipulse-Per-Row Codes for High-Speed Optical Wavelength/Time CDMA Networks," *IEEE Photon. Technol. Lett*, vol. 19, no. 21, pp.1756-1758, Nov. 2007.

[32] R. M. H. Yim, L. R. Chen, and J. Bajcsy, "Design and performance of 2-D codes for wavelength-time optical CDMA," *IEEE Photon. Technol. Lett.*, vol. 14, no. 5, pp. 714–716, May 2002.

[33] C. C. Yang and J. F. Huang, "Two-dimensional m-matrices coding in spatial/frequency optical CDMA networks," *IEEE Photon. Technol. Lett.*, vol. 15, no. 1, pp. 168–170, Jan. 2003.

[34] A. J. Mendez, R. M. Gagliardi, V. J. Hernandez, C. V. Bennett, and W. J. Lennon, "Design and performance analysis of wavelength/time (W/T) matrix codes for optical CDMA," *J. Lightwave Technol*., vol. 21, no. 11, pp. 2524–2533, Nov. 2003.

[35] S. V. Maric, O. Moreno, and C. J. Corrada, "Multimedia transmission in fiber optical LANs using optical CDMA," *IEEE J. Lightwave Technol*., vol. 14, no. 10, pp. 2149-2153, Oct. 1996.

[36] N. G. Tarhuni and T. O. Korhonen, "Multi-weight multi-length strict optical orthogonal codes," in *Proc. 6th Nordic Signal Processing Symp. (NORSIG),* Espoo, Finland, Jun. 9–11, pp. 161–164, 2004.

[37] L. Bin, "One-Coincidence Sequences with Specified Distance Between Adjacent Symbols for Frequency-Hopping Multiple Access," *IEEE Transactions on Communications*, vol. 45, no. 4, pp. 408-410, April 1997.

[38] H. Fathallah, L. A. Rusch, and S. LaRochelle, "Passive optical fast wavelength-hop CDMA communications network," *IEEE J. Lightwave Technol*., vol. 17, no. 3, pp. 397-405, March 1999.

[39] E. Inaty, P. Fortier, and L. A. Rusch, "SIR performance evaluation of a multirate OFFH-CDMA system," *IEEE Commun. Lett*., vol. 5, no. 5, pp. 224–226, May 2001.

[40] E. Inaty, H. M. H. Shalaby, P. Fortier, and L. A. Rusch, "Multirate optical fast wavelength hopping CDMA system using power control," *IEEE J. Lightwave Technol*., vol. 20, no. 2, pp. 166–177, Feb. 2002.

[41] Infinera. “Coherent DWDMTechnologies”. (Whitepaper). 2012. Disponível em: <www.infinera.com/pdfs/whitepapers/Infinera_Coherent_Tech.pdf>. Acesso em: 5 fev. 2015

[42] Infinera. “Super-Channels: DWDM Transmission at100Gb/s and Beyond”. (Whitepaper). 2012. Disponível em: <www.infinera.com/pdfs/whitepapers/SuperChannel_WhitePaper.pdf>. Acesso em: 5 fev. 2015.

[43] G. Manzacca, A. M. Vegni, X. Wang, N. Wada, G. Cincotti, and K. Kitayama, "Performance Analysis of a Multiport Encoder/Decoder in OCDMA Scenario," IEEE J. Selected Topics in Quantum Electronics, vol. 13, no. 5, pp. 1415-1421, Sept./Oct. 2007.

[44] R. Matsumoto, T. Kodama, S. Shimizu, R. Nomura, K. Omichi, N. Wada, and K. Kitayama. "40G-OCDMA-PON Network with an Asymmetric Structure Using a Single Multi-Port and Sampled SSFBG Encoder/Decoders." *IEEE J. Lightwave. Technol*., vol. 32, no. 6, pp. 1132-1143, 2014.

[45] Y. Chen, R. Wang, T. Pu, P. Xiang, H. Zhu, T. Fang, and J. Zheng. "Novel Multiple Access Interference Elimination based on Mach-Zehnder Modulator for OCDMA Networks." *Asia Comm. and Photonics Conf*.. Optical Society of America, 2013.

[46] A. Srivastava, "Next generation PON evolution," In SPIE OPTO, *International Society for Optics and Photonics*, pp. 864509-864509, 2013.

[47] H. Choi, T. Tsuritani and I. Morita, "BER-adaptive flexible-format transmitter for elastic optical networks," *Opt. Express*, vol. 20, pp. 18652-18658, August 2002.

[48] G. Huang, Y. Miyoshi, A. Maruta, Y. Yoshida, and K. Kitayama, "All-Optical OOK to 16-QAM Modulation Format Conversion Employing Nonlinear Optical Loop Mirror," *IEEE J. Lightwave. Technol*., vol. 30, no. 9, pp. 1342-1350, May 2012.

[49] T. R. Raddo, A. L. Sanches, J. V. dos Reis, Jr., and B.-H. V. Borges, "A new approach for evaluating the BER of a multirate, multiclass OFFH-CDMA network," *IEEE Commun. Letters*, vol. 16, no. 2, pp. 259-261, February 2012.

[50] S. Zou, M.M. Karbassian and H. Ghafouri-Shiraz, “Extended 2D codes supporting multirate and QoS in optical CDMA networks with Poisson and binomial MAI models,” *J. Opt. Commun. Netw*, vol. 5, no. 5, pp. 524-531, 2013.

[51] T. R. Raddo, A. Sanches, J. V. dos Reis Jr., and B. V. Borges, “Influence of the MAI Distribution Over the BER Evaluation in a Multirate, Multiclass OOC-OCDMA System,” in *Proc ANIC*, paper ATuB5, 2011.

[52] J. Jiang, D. Wu and P. Fan, “General constructions of optimal variable-weight optical orthogonal codes,” *Trans. Inf. Theory*, vol. 57, pp. 4488-4496, July 2011.

[53] V. Baby, W.-C. Kwong, C.-Y. Chang, G.-C. Yang, and P. R. Prucnal, “Performance analysis of variable-weight multilength optical codes for wavelength–time O-CDMA multimedia systems,” *Trans. Commun*., vol. 55, no. 7, pp. 1325–1333, July 2007.

[54] P. R. Prucnal, M. A. Santoro and T. R. Fan, "Spread Spectrum Fiber-optic Local Area Network Using Optical Processing", *J. Lightwave Technol.*, vol. LT-4, No. 5, pp. 547-554, May. 1986.

[55] F. Coppinger, C. K. Madsen and B. Jalali, "Photonic Microwave Filtering Using Coherently Coupled Integrated Ring Resonators", *Microwave and Opt. Technol. Lett.*, vol. 21, No. 2, pp. 90-93, Apr. 1999.

[56] J. G. Zhang, Y. Wen, and P. Li, "Proposed OCDMA Encoders And Decoders Based Silica-On-Silicom Integrated Optics", *Microwave and Opt. Technol. Lett.*, vol. 40, No. 3, pp. 205-209, Feb. 2004.

[57] A. A. Shaar and P. A. Davies, "Prime Sequences: Quasi-Optimal Sequences for Channel Code Division Multiplexing", *IEEE Elect. Lett.*, Vol. 19, No. 21, pp. 888-889, 13 Oct. 1983.

[58] D. Zaccarin and M. Kavehrad, "An Optical CDMA System Based on Spectral Encoding of LED", *IEEE Phot. Techn. Lett.*, Vol. 4, No. 4, pp. 479-482, Apr. 1993.

[59] M. Kavehrad and D. Zaccarin, "Optical Code-Division-Multiplexed Systems Based on Spectral Encoding of Noncoherent Sources", *J. Lightwave. Technol.*, Vol. 13, No. 3, pp. 534-545, Mar. 1995.

[60] E. Park, A. J. Mendez and E. M. Garmire, "Temporal/Spatial Optical CDMA Networks-Design, Demonstration, and Comparison with Temporal Networks", *IEEE Photon. Technol. Lett.*, Vol. 4, No. 10, pp. 1160-1162, Oct. 1992.

[61] A. J. Mendez, J. L. Lambert, J. M. Morookian, and R. M. Gagliardi, "Synthesis and Demonstration of High Speed, Bandwidth Efficient Optical Code Division Multiple Access (CDMA) Tested at 1 Gb/s Throughput", *IEEE Photon. Technol. Lett.*, Vol. 6, No. 9, pp. 1146-1149, Sep. 1994.

[62] S. P. Wan and Y. Hu, "Two-dimensional optical CDMA differential system with prime/OOC codes," *IEEE Photon. Technol. Lett.*, vol. 13, pp. 1373–1375, Dec. 2001.

[63] L. Galdino, T. R. Raddo, A. L. Sanches, L. H. Bonani, and E. Moschim, "Performance Comparison of Hybrid 1-D WDM/OCDMA and 2-D OCDMA Towards Future Access Network Migration Scenario" in *IEEE International Conference on Transparent Optical Networks*, ICTON 2012, Coventry, England, July 2012.

[64] H. Fathallah, "Optical fast frequency hopping CDMA: principle, simulation and experiment," Thesis submitted to the degree of doctor philosophy at Universitè Laval, Facultè Des Sciences et de Gènie, 2002.

[65] H. Fathallah, L. A. Rusch, and S. LaRochelle, "Passive optical fast frequency-hop CDMA communications system," *J. Lightwave Technol.*, vol. 17, pp. 397–405, 1999.

[66] H. Fathallah and L. A. Rusch, “Robust optical FFH-CDMA communications: Coding in place of frequency and temperature controls,” *J. Lightwave Technol*., vol. 17, pp. 1284–1293, Aug. 1999.

[67] E. Inaty, H. M. H. Shalaby, and P. Fortier, “On the cutoff rate of a multiclass OFFH-CDMA system,” *IEEE Trans. Commun*., vol. 53, no. 2, pp. 323–334, Feb. 2005.

[68] A. A. Shaar and P. Davies, “A survey of one coincidence sequences for frequency-hopped spread spectrum systems,” *Inst. Elect. Eng. Proc*., vol. 131, no. 7, pp. 719–724, Apr. 1984.

[69] K. Yu, J. Shin, and N. Park, “Wavelength-time spreading optical CDMA systems using wavelength multiplexers and mirrored fiber delay lines,” *IEEE Photon. Technol. Lett*., vol. 12, no. 9, pp. 1278–1280, Sep. 2000.

[70] S. Min, H. Yoo, and Y. Won, “Time-wavelength hybrid optical CDMA system with tunable encoder/decoder using switch and fixed delay line,”*Opt. Commun*., vol. 216, no. 4–6, pp. 335–342, Feb. 2003.

[71] S. Ayotte, M. Rochette, J. Magné, L. A. Rusch, and S. LaRochelle, “Experimental verification and capacity prediction of FE-OCDMA using superimposed FBG*,” J. Lightw. Technol.*, vol. 25, no. 2, pp. 724–731, Feb. 2005.

[72] J. Mendez, R. M. Gagliardi, V. J. Hernandez, C. V. Bennett, and W. J. Lennon, “High-performance optical CDMA system based on 2-D optical orthogonal codes,” *J. Lightwave Technol*., vol. 22, no. 11, pp. 2409–2419, 2004.

[73] R.V. Santos-Filho, *Análise de Sistemas CDMA Ópticos*. Dissertação (Mestrado em Engenharia Elétrica) – Universidade de São Paulo, São Carlos, 2006.

[74] Walklin, S.; Conradi, J., "Effect of Mach-Zehnder modulator DC extinction ratio on residual chirp-induced dispersion in 10-Gb/s binary and AM-PSK duobinary lightwave systems," *Photonics Technology Letters, IEEE* , vol.9, no.10, pp.1400,1402, Oct. 1997.

[75] I. P. Kaminow and T. L. Koch, Eds., Optical Fiber Telecommunications III A, Academic Press, 1997.

[76] L. Xu, V. Baby and P. R. Prucnal, “Multiple access interference (MAI) noise reduction in a 2D optical cdma system ultrafast optical thresholding,” *Lasers and Electro-Optics Society*, 2004. LEOS 2004. The 17th Annual Meeting of the IEEE, vol.2, pp. 591-592, 7-11 Nov. 2004.

[77] A. L. Sanches, J. V. Reis Junior, S. M. Rossi, M. R.X. Barros, M. A. Romero, B.-H V. Borges, “Análise de Sistemas OCDMA Utilizando Códigos Bidimensionais com Limitadores Ópticos Abruptos e Código Corretor de Erro”. *MOMAG*, 2008, Florianópolis.

[78] P. J. Reyes-Iglesias, A. Ortega-Moñux, and I. Molina Fernández, “Enhanced monolithically integrated coherent 120° down converter with high fabrication yield,” *Opt. Express*. 20 (21), 23013–23018 (2012).

[79] P. Runge, S. Schubert, A. Seeger, K. Janiak, J. Stephan, D. Trommer, P. Domburg, and M. Nielsen. "Monolithic InP receiver chip with a 90° hybrid and 56GHz balanced photodiodes," *Opt. Express*. Vol. 20, B250-B255, 2012.

[80] P. Dong, C. Xie, and L. Buhl. "Monolithic polarization diversity coherent receiver based on 120-degree optical hybrids on silicon," *Opt. Express*. Vol. 22, pp. 2119-2125, 2014.

[81] J. A. Salehi, A. M. Weiner, and J. P. Heritage, "Coherent ultra short pulse code-division multiple access communication systems," *IEEE J. Lightwave Technol*., pp. 478–491, Mar. 1990.

[82] T. Erdogan, "Fiber grating spectra," *IEEE J. Lightwave Technol*., vol. 15, pp.1277–1294, 1997.

[83] V. Eramo, "Impact of the MAI and beat noise on the performance of OCDM/WDM optical packet switches using Gold codes," *Opt. Express*, vol. 18, pp. 17897-17912, 2010.

[84] R. Slavík and S. LaRochelle, "Large-band periodic filters for DWDM using multiple-superimposed fiber Bragg gratings," *IEEE Photon. Technol. Lett*., vol. 14, no. 12, pp. 1704–1706, Dec. 2002.

[85] Q. J. Wang, Y. Zhang and Y. C. Soh, "Efficient structure for optical interleavers using superimposed chirped fiber Bragg gratings," *IEEE Photon. Technol. Lett*., vol. 17, no. 2, pp. 387–389, Feb. 2005.

[86] J. L. Zheng, R. Wang, T. Pu, L. Lu, T. Fang, Y. Su, L. Li, and X. F. Chen, "Phase-controlled superimposed FBGs and their applications in spectral-phase en/decoding," *Opt. Express*, vol 19, no. 9, pp. 8580–8595, April. 2011.

[87] Nogueira, R. N., *Redes de Bragg em Fibra Óptica*. 2005. 343p. (Mestrado em Física) – Departamento de Física, Universidade de Aveiro, Aveiro, Portugal, 2005.

[88] A. W. Snyder and J. D. Love, ***Optical Waveguide Theory*** (Chapman & Hall, 1983).

[89] H. Kogelnik, "***Filter response of nonuniform almost-periodic structures***," Bell Sys.Tech. J. 55, 109—126 (1976).

[90] D. Marcuse, ***Theory of Dielectric Optical Waveguides*** (New York: Academic, 1991).

[91] L. Poladian, "Resonance Mode Expansions and Exact Solutions for Nonuniform Gratings," *Phys. Rev*. E 54, 2963—2975 (1996).

[92] J. Skaar. (2000) Synthesis and Characterization of Fiber Bragg Gratings. Norwegian Univ. of Sci. Technol., Trondheim, Norway.

[93] A. D. Neto, E. Moschim,"Some Optical Orthogonal Codes for asynchronous CDMA Systems", *Proccedings of IEEE GLOBECOM'*, 2002,vol.3, pp. 2065 - 2068, Taiwan,

Nov., 2002

[94] Neto, A. D., and E. Moschim. *Construção de Novos Códigos Ortogonais Ópticos por meio de Equações Diofantinas*. 2005. 117p. (Doutorado em Engenharia Elétrica) – Deparrtamento de Engenharia Elétrica e de Computação, Universidade de Campinas, Campinas, Brazil, 2005.

APPENDIX A – FIBER BRAGG GRATING MODELING

The fiber Bragg gratings are normally constructed in a short segment of optical fiber in order to reflect particular wavelengths. This is achieved based on a periodic variation of the refractive index of the optical fiber core. Then, in the generalized form, this variation can be represented by the combination of several functions as [87]

$$\delta n_{eff}(z) = \overline{\delta n}_{eff}(z) + A_p(z) f\left[\frac{\Lambda(z)}{\cos(\theta_b)}, z\right], \tag{A1}$$

where $\overline{\delta n}_{eff}(z)$ is the average value of the modulation index, $A_p(z)$ is the amplitude of the modulation along the grating (apodization), $f[\Lambda(z)/\cos(\theta_b), z]$ is the function that represents the modulation profile, $\Lambda(z)$ is the grating period, and θ_b is the inclined grating degree.

The writing technique process occurs via optical interference and increases the modulation amplitude (consequently, increasing the reflection index). Thus, $A_p(z)$ can be expressed as [87]

$$A_p(z) = \overline{\delta n}_{eff}(z) v(z), \tag{A2}$$

where $0 \leq v(z) \leq 1$ is the fringe visibily, which depends directly on the interference quality.

For example, the commonly adopted functions for the apodization profile are the following

a. Sinc profile

$$A_p(z) = \frac{\sin\left[\frac{2\pi\left(z-\frac{L}{2}\right)}{L}\right]}{\frac{2\pi\left(z-\frac{L}{2}\right)}{L}} \tag{A3}$$

b. Hiperbolic tangent

$$A_p(z) = \frac{\tanh\left\{\mathrm{P}\left[1 - 2\left|\frac{\mathrm{z}-\mathrm{L}/2}{\mathrm{L}}\right|\right]\right\}}{\tanh(\mathrm{P})} \tag{A4}$$

c. Raised cosine

$$A_p(z) = \frac{1}{2}\left\{1 + \cos\left[\frac{\pi(\mathrm{z} - \mathrm{L}/2)}{\mathrm{FWHM}}\right]\right\} \tag{A5}$$

d. Raised Gaussian

$$A_p(z) = \exp\left\{-\left[2(\ln 2)^{1/\mathrm{P}}\left(\frac{\mathrm{z} - \mathrm{L}/2}{\mathrm{FWHM}}\right)\right]^{\mathrm{P}}\right\} \tag{A6}$$

where FWHM is the full width at half maximum, L is the grating length and P is used to adjust the desired profile.

The writing of the Bragg gratings generates a modulation profile with sinusoidal characteristics. Thus, the z-dependence of the index perturbation is approximately quasi-sinusoidal in the sense that it can be written as [82]

$$\delta n_{eff}(z) = \overline{\delta n}_{eff}(z)\left\{1 + v(z)\cos\left[\frac{2\pi}{\Lambda}z + \phi(z)\right]\right\}, \tag{A7}$$

where $\phi(z)$ is the slowly varying grating phase.

The relation between the spectral dependence of a fiber grating and the corresponding grating structure is usually described by the coupled mode theory. Coupled mode theory is described in several works and detailed analysis can be found in [88]-[91]. Here, it is considered the fiber is lossless and single mode in the wavelength range of interest, i.e, it is considered only one forward and one backward propagating mode. Then, near the wavelength for which reflection of a mode of amplitude $A(z)$ into an identical counter-propagating mode of amplitude $B(z)$ is the dominant interaction in a Bragg grating, the coupled mode equations

may be simplified by retaining only terms that involve the amplitudes of the particular mode [82].

The forward and backward propagating field envelopes are mutually coupled by the coupled mode equations

$$\frac{dR(z)}{dz} = i\hat{\sigma}R(z) + i\kappa S(z), \tag{A8}$$

and

$$\frac{dS(z)}{dz} = -i\hat{\sigma}S(z) - i\kappa^{*}u(z), \tag{A9}$$

where the amplitudes $R(z) = A(z)e^{i(\delta z - \phi/2)}$ and $S(z) = B(z)e^{-i(\delta z + \phi/2)}$, κ is the "ac" coupling coefficient and $\hat{\sigma}$is a general"dc" self-coupling coefficient defined as

$$\hat{\sigma} = \delta + \sigma - \frac{1}{2}\frac{d\phi}{dz}, \tag{A10}$$

The detuning , which is independent for all gratings, is defined to be

$$\delta = \beta - \frac{\pi}{\Lambda} = 2\pi n_{eff}\left(\frac{1}{\lambda} - \frac{1}{\lambda_D}\right), \tag{A11}$$

where β is the mode propagation constant, $\lambda_D \equiv 2n_{eff}\Lambda$ is the "design wavelength" and n_{eff} is the effective index. Note that when $\delta = 0$, the Bragg condition $\lambda = 2n_{eff}\Lambda$ is found.

In addition, for a single-mode Bragg reflection grating, it is found the following simple relations

$$\sigma = \frac{2\pi}{\lambda}\overline{\delta n}_{eff} \tag{A12}$$

and

$$\kappa = \kappa^{*} = \frac{\pi}{\lambda}v\overline{\delta n}_{eff} \tag{A13}$$

If the grating is uniform, $\overline{\delta n}_{eff}$ is a constant, and $d\phi/dz = 0$, and κ, σ and $\hat{\sigma}$ are constants. Thus, (A8) and (A9) are coupled first-order ordinary differential equations with constant coefficients, for which closed-form solutions can be found when appropriate boundary conditions are specified.

Once the coupled mode formalism has been described, the numerical method utilized to model the encoders/decoders, known as transfer matrix method (TMM) [87], [92], is now presented.

In TMM, the grating is divided into a sufficient number N of sections so that each section can be approximately treated as uniform. Let the section length be $\Delta = L/N$. By applying in the appropriate boundary conditions and solving the coupled-mode equations, it is found that the transfer matrix relation between the fields at z and at $z + \Delta$ is

$$\begin{bmatrix} A_{k-1}^{+} \\ B_{k-1}^{+} \end{bmatrix} = T_k \begin{bmatrix} A_k^{+} \\ B_k^{+} \end{bmatrix} \tag{A14}$$

where$\varphi = \sqrt{\kappa^2 - \hat{\sigma}^2}$ and L_k is length of the k-th section of the gratting.

As a result, T_k is a 2 × 2 matrix with elements [87]

$$T_k = \begin{bmatrix} \cosh(\varphi L_k) - i\dfrac{\hat{\sigma}}{\varphi}\sinh(\varphi L_k) & -i\,\dfrac{\kappa}{\varphi}\sinh(\varphi L_k) \\ i\,\dfrac{\kappa^*}{\varphi}\sinh(\varphi L_k) & \cosh(\varphi L_k) + i\dfrac{\hat{\sigma}}{\varphi}\sinh(\varphi L_k) \end{bmatrix} \tag{A15}$$

Once given all transfer functions of the M sections, the full transfer function of the grating T is calculated via products of individual matrices T_k as

$$T = \prod_{k=1}^{M} T_k \tag{A16}$$

and, consequently

$$\begin{bmatrix} A^+(0) \\ B^+(0) \end{bmatrix} = T \begin{bmatrix} A^+(L) \\ B^+(L) \end{bmatrix} \tag{A17}$$

Finally, the coefficients of reflection and transmission can be calculated as

$$R = \left| \frac{T_{21}}{T_{11}} \right|^2 \tag{A18}$$

and

$$T^r = \left| \frac{1}{T_{11}} \right|^2, \tag{A19}$$

respectively.

The mathematical formalism necessary to simulate the behavior of Bragg gratings has been described in order to show the encoded desired user signal. In all simulations performed, the same parameters adopted for the nonideal scenario given in the beginning of this thesis were used. The main objective is to evaluate the side lobes suppression of apodized gratings.

Figure A.1 shows the transfer function of the desired user encoder employing uniform gratings. As can be seen, the side lobes are quite noticeable, which impact significantly in a negative manner on the encoding quality. Nonetheless, as mentioned above, the encoding quality can be improved when considering gratings with a specific apodization profile. In this case, it is adopted the *sinc* profile in order to also compare the results with those of Fathalah

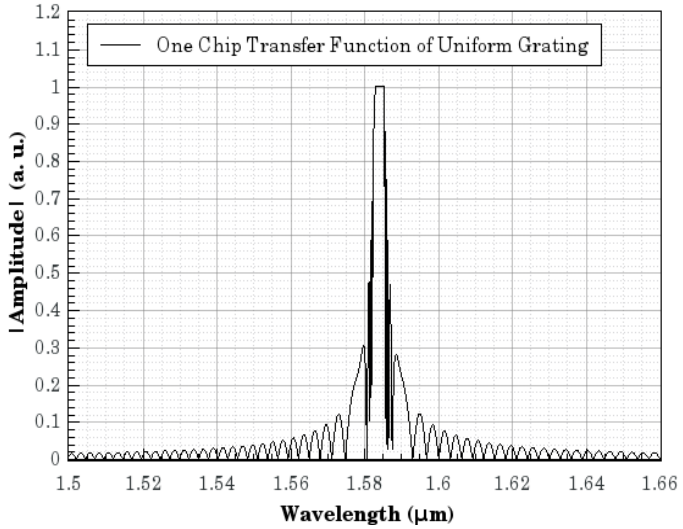

Figure A.1: Transfer Function of One Chip Encoder Using Uniform Grating.

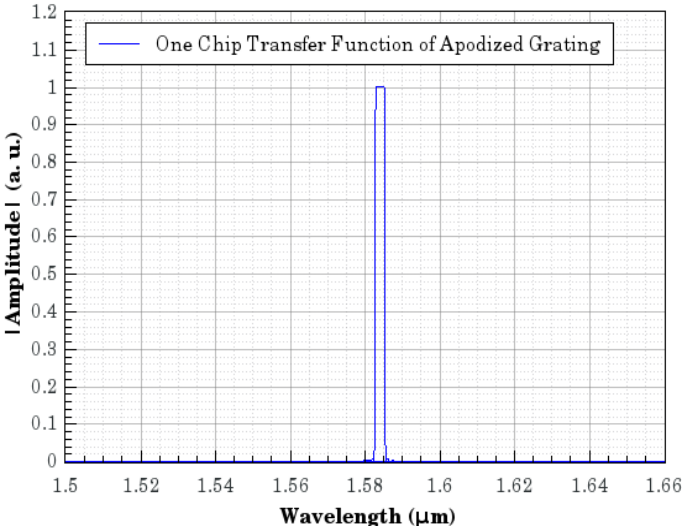

Figure A.2: Transfer Function of One Chip Encoder Using *Sinc* Apodized Grating.

et. all [65]. Finally, the transfer function of the desired user encoder when *sinc* apodized gratings are used is shown in Figure A2.

APPENDIX B - OPTIMUM THRESHOLD EVALUATION

The decision process influences directly in the network performances and, therefore, such stage should have utmost attention. In this sense, the threshold value has a critical impact on the bit decision and, therefore, it is a variable to be optimized. Here, it is obtained a threshold value that optimizes the general network performance in terms of BER, as demonstrated in [93], [94].

In order to illustrate the detection process of a Gaussian variable, the performance of the receptor is given by

$$Pe = P(Z = 1 \geq T_h/0)P(0) + P(Z = 0 < T_h/1)P(1) \quad \text{(B1)}$$

where Z is the decision variable, T_h is the threshold and, $P(0)$ and $P(1)$ are the probabilities of transmission of bits "0" and "1", respectively.

The decision variable Z, in the instant of sampling, has a Gaussian probability density function when the bit "1" is detected is given by

$$P(Z) = \frac{1}{\sqrt{2\pi}\sigma_1} e^{-\frac{(Z-\mu_1)^2}{2\sigma_1^2}}, \quad \text{(B2)}$$

where μ_1 and σ_1^2 are the mean and variances associated with the bit "1" transmission, respectively. Similarly, the decision variable Z when the "0" bit is detected has a Gaussian probability density function given by

$$P(Z) = \frac{1}{\sqrt{2\pi}\sigma_0} e^{-\frac{(Z-\mu_0)^2}{2\sigma_0^2}}, \quad \text{(B3)}$$

where μ_0 and σ_0^2 are the mean and variance associated to the bit "0" transmission, respectively.

Considering that both bits “0” and “1” are transmitted with equal probabilities, i.e, $P(0) = P(1) = {}^{1}/_{2}$, the error probability in the receptor can be expressed as

$$Pe = \frac{1}{2}\int_{-\infty}^{T_h} \frac{1}{\sqrt{2\pi}\sigma_1} e^{-\frac{(Z-\mu_1)^2}{2\sigma_1^2}} dZ + \frac{1}{2}\int_{T_h}^{\infty} \frac{1}{\sqrt{2\pi}\sigma_0} e^{-\frac{(Z-\mu_0)^2}{2\sigma_0^2}} dZ \tag{B4}$$

The optimum threshold can be obtained by equating the above equation to zero and, then, differentiating for T_h. After the differentiation it is obtained the ensuing equation

$$\frac{dPe}{Th} = P(Z = 0 < T_h/1)P(1) - P(Z = 1 \geq T_h/0)P(0) = 0$$

$$P(Z = 0 < T_h/1) = P(Z = 1 \geq T_h/0)$$

$$\frac{1}{\sigma_1} e^{-\frac{(Z-\mu_1)^2}{2\sigma_1^2}} = \frac{1}{\sigma_0} e^{-\frac{(Z-\mu_0)^2}{2\sigma_0^2}}$$

$$\frac{(T_h-\mu_0)^2}{2\sigma_0^2} - \frac{(\mu_1-T_h)^2}{2\sigma_1^2} = \ln\left(\frac{\sigma_1}{\sigma_0}\right), \tag{B5}$$

which can be substituted by the following equivalent quadratic equation

$$aT_h^2 + bT_h + c = 0, \tag{B6}$$

where $a = \sigma_1^2 - \sigma_0^2$, $b = 2(\mu_1\sigma_0^2 - \mu_0\sigma_1^2)$, and $c = \mu_0\sigma_1^2 - \mu_1\sigma_0^2 - 2\sigma_1^2\sigma_0^2 \ln\left(\frac{\sigma_1}{\sigma_0}\right)$. Thus, solving the quadratic equation for T_h, it is obtained that

$$T_h = \frac{-\mu_1\sigma_0^2 + \mu_0\sigma_1^2 + \sqrt{\sigma_1^2\sigma_0^2(\mu_1-\mu_0)^2 + 2(\sigma_1^2-\sigma_0^2)\ln\left(\frac{\sigma_1}{\sigma_0}\right)}}{\sigma_1^2 - \sigma_0^2} \tag{B7}$$

Further, if the signal is much larger than the noise, it can be considered that

$$(\mu_1 - \mu_0)^2 \gg \frac{2(\sigma_1^2-\sigma_0^2)\ln\left(\frac{\sigma_1}{\sigma_0}\right)}{\sigma_1^2\sigma_0^2} \tag{B8}$$

Therefore, the optimum decision threshold is given by

$$T_h = \frac{\mu_1\sigma_0 + \mu_0\sigma_1}{\sigma_1 + \sigma_0} \tag{B9}$$

Finally, under the condition $\sigma_1 = \sigma_0$, the optimum threshold can be expressed as

$$T_h = \frac{\mu_1 + \mu_0}{2} \tag{B10}$$

APPENDIX C – FFH CODES CONSTRUCTION

The FFH sequences can be constructed by means of two distinct theorems related if the number of available wavelengths is odd or even [37], [38]. Only for convenience sake, this appendix is restricted to odd wavelength number approach, which is used in the codes construction used in this thesis.

Firstly, let the number of available wavelengths q be an odd integer. In addition, consider $C = (c_0, c_1, \dots, c_{2k-1})$ a permutation of $D = (d+1, d+2, \dots, q-d-1)$, where d is the absolute value of the diference between two adjacent wavelengths and $2k = q - 2d - 1$. Further, let

$$D_n(j) = \left(\sum_{i=n}^{(n+j-1) mod\, \lfloor 2k \rfloor} c_i \right) mod \lfloor q \rfloor, \tag{C1}$$

where $0 \leq n \leq 2k-1$ and $2 \leq j \leq k$. Then, it is selected C among all possible permutations of D which satisfies

1. $c_i + c_{i+k} = q$, and $2 \leq j \leq k$;
2. For each j, $2 \leq j \leq k$, all $D_i(j)$ are different for $0 \leq i \leq 2k-1$;

If the vector C exists, it is called generator sequence, and a set of q FFH sequences are generated by

$$F_j = [D_0(1) + j, D_0(2) + j, \dots, D_0(2k) + j\,], \tag{C2}$$

where $0 \leq j \leq q-1$, and "+" is modulo q addition.

Even though the main steps of the FFH construction proposed in [37] have been revisited, it is interesting to provide the final sequences generated from 19, 23 and 27 available wavelengths (note that the codes sequences generated from 29 available wavelengths were presented in Table 1). The respective tables follow.

Codes	Chips / Wavelengths											
#1	2	3	16	9	18	10	8	7	13	1	11	0
#2	3	4	17	10	0	11	9	8	14	2	12	1
#3	4	5	18	11	1	12	10	9	15	3	13	2
#4	5	6	0	12	2	13	11	10	16	4	14	3
#5	6	7	1	13	3	14	12	11	17	5	15	4
#6	7	8	2	14	4	15	13	12	18	6	16	5
#7	8	9	3	15	5	16	14	13	0	7	17	6
#8	9	10	4	16	6	17	15	14	1	8	18	7
#9	10	11	5	17	7	18	16	15	2	9	0	8
#10	11	12	6	18	8	0	17	16	3	10	1	9
#11	12	13	7	0	9	1	18	17	4	11	2	10
#12	13	14	8	1	10	2	0	18	5	12	3	11
#13	14	15	9	2	11	3	1	0	6	13	4	12
#14	15	16	10	3	12	4	2	1	7	14	5	13
#15	16	17	11	4	13	5	3	2	8	15	6	14
#16	17	18	12	5	14	6	4	3	9	16	7	15
#17	18	0	13	6	15	7	5	4	10	17	8	16
#18	0	1	14	7	16	8	6	5	11	18	9	17
#19	1	2	15	8	17	9	7	6	12	0	10	18

TABLE C.1: FFH User codes generated from 19 available wavelengths

Codes	Chips / Wavelengths											
#1	10	2	21	18	12	17	7	15	19	22	5	0
#2	11	3	22	19	13	18	8	16	20	0	6	1
#3	12	4	0	20	14	19	9	17	21	1	7	2
#4	13	5	1	21	15	20	10	18	22	2	8	3
#5	14	6	2	22	16	21	11	19	0	3	9	4
#6	15	7	3	0	17	22	12	20	1	4	10	5
#7	16	8	4	1	18	0	13	21	2	5	11	6
#8	17	9	5	2	19	1	14	22	3	6	12	7
#9	18	10	6	3	20	2	15	0	4	7	13	8
#10	19	11	7	4	21	3	16	1	5	8	14	9
#11	20	12	8	5	22	4	17	2	6	9	15	10
#12	21	13	9	6	0	5	18	3	7	10	16	11
#13	22	14	10	7	1	6	19	4	8	11	17	12
#14	0	15	11	8	2	7	20	5	9	12	18	13
#15	1	16	12	9	3	8	21	6	10	13	19	14
#16	2	17	13	10	4	9	22	7	11	14	20	15
#17	3	18	14	11	5	10	0	8	12	15	21	16
#18	4	19	15	12	6	11	1	9	13	16	22	17
#19	5	20	16	13	7	12	2	10	14	17	0	18
#20	6	21	17	14	8	13	3	11	15	18	1	19
#21	7	22	18	15	9	14	4	12	16	19	2	20
#22	8	0	19	16	10	15	5	13	17	20	3	21
#23	9	1	20	17	11	16	6	14	18	21	4	22

TABLE C.2: FFH User codes generated from 23 available wavelengths

Codes	Chips / Wavelengths											
#1	13	9	19	10	26	24	11	15	5	14	25	0
#2	14	10	20	11	0	25	12	16	6	15	26	1
#3	15	11	21	12	1	26	13	17	7	16	0	2
#4	16	12	22	13	2	0	14	18	8	17	1	3
#5	17	13	23	14	3	1	15	19	9	18	2	4
#6	18	14	24	15	4	2	16	20	10	19	3	5
#7	19	15	25	16	5	3	17	21	11	20	4	6
#8	20	16	26	17	6	4	18	22	12	21	5	7
#9	21	17	0	18	7	5	19	23	13	22	6	8
#10	22	18	1	19	8	6	20	24	14	23	7	9
#11	23	19	2	20	9	7	21	25	15	24	8	10
#12	24	20	3	21	10	8	22	26	16	25	9	11
#13	25	21	4	22	11	9	23	0	17	26	10	12
#14	26	22	5	23	12	10	24	1	18	0	11	13
#15	0	23	6	24	13	11	25	2	19	1	12	14
#16	1	24	7	25	14	12	26	3	20	2	13	15
#17	2	25	8	26	15	13	0	4	21	3	14	16
#18	3	26	9	0	16	14	1	5	22	4	15	17
#19	4	0	10	1	17	15	2	6	23	5	16	18
#20	5	1	11	2	18	16	3	7	24	6	17	19
#21	6	2	12	3	19	17	4	8	25	7	18	20
#22	7	3	13	4	20	18	5	9	26	8	19	21
#23	8	4	14	5	21	19	6	10	0	9	20	22
#24	9	5	15	6	22	20	7	11	1	10	21	23
#25	10	6	16	7	23	21	8	12	2	11	22	24
#26	11	7	17	8	24	22	9	13	3	12	23	25
#27	12	8	18	9	25	23	10	14	4	13	24	26

TABLE C.3: FFH User codes generated from 27 available wavelengths